SPECTROPHOTOMETRY OF SUPERNOVAE AND THEIR REMNANTS

Thesis by

Robert Paul Kirshner

In Partial Fulfillment of the Requirements

for the Degree of

Doctor of Philosophy

California Institute of Technology

Pasadena, California

1975

(Submitted July 26, 1974)

For Lucy

ACKNOWLEDGEMENT

I would like to thank my advisor, J.B. Oke, for the encouragement, useful advice, and infectious enthusiasm that helped make my years at Caltech interesting, productive, and educational. I would also like to thank John Kwan for his expert help in the analysis of Type II spectra, the determination of their distances, and for his detailed criticism of this manuscript. Bruce Woodgate provided a great deal of energy, money, and fun during our investigation of the Cygnus Loop.

For their generosity with data, ideas, and encouragement, Leonard Searle, J.E. Gunn, J.L. Greenstein, and R.E. Schild deserve special thanks along with H.C. Arp, M. Schmidt, A. Sandage, and W.L.W. Sargent.

To Richard Gott, Gus Oemler, Steve Schectman, Paul Schechter, Ed Turner, and Barry Turnrose, thanks for a gift more precious than a spectrogram: friendship.

Thanks to the technical staff, especially Larry Blakée, Earle Emery, Martin Olsiewski, Dennis Palm, and Bud Smith.

I was supported for 3 years by an NSF Fellowship

and for one by a Virginia Steele Scott Fellowship, for which I am very grateful.

My thanks to Elsa Titchenell, and to Lucy Kirshner for their help in preparing the manuscript.

Chapter 2 will appear in the November, 1974 Astrophysical Journal, Chapter 3 was Ap.J.(Letters)188,L79 (1973), parts of Chapter 4 are from Ap.J. 185,303(1973), Chapter 5 will appear in the October, 1974, Ap.J., Chapter 6 contains parts of Ap.J.(Letters) 180,L97(1973), and all of them appear here with the permission of the University Chicago Press for the American Astronomical Society.

ABSTRACT

Spectrophotometry of extragalactic supernovae shortly after discovery, and of galactic supernova remnants has been used to derive the masses, temeratures, compositions, and distances of supernovae.

The Crab Nebula is shown to have a mass of ionized hydrogen in excess of 0.3 $M_{\odot}$, but no enrichment of oxygen, nitrogen, or sulfur. The Cygnus Loop is shown to emit [Fe XIV], indicating gas at 2 x 10^6 °K: this establishes the thermal nature of the x-ray emission, and casts doubt on the Loop's size and distance.

Type II supernovae are shown to be consistent with a few solar masses of material at cosmic abundance. Their distances are found without reference to any other astronomical distance through a model of the expansion. Type I supernovae are shown to consist of about 1 solar mass of matter that may be 20 times enriched in iron, if the identification of [Fe II] lines at late stages is correct.

TABLE OF CONTENTS

Chapter 1

Parents, Elements, and Remnants

I NEW RESULTS

This thesis reports the results of investigations into the spectra of supernovae and their remnants. It includes spectroscopic and spectrophotometric studies of several supernovae of Types I and II beginning shortly after discovery and continuing for many months. It includes spectrophotometry of the Crab Nebula, and the discovery of faint [Fe XIV] emission from the Cygnus Loop. The emphasis in this paper is on the presentation of the new data, empirical models of the supernova envelopes and on attempts to understand the parents of supernovae, the elements they produce, and the remnants they form.

The new results from these observations include: accurate line strengths in the Crab Nebula, and a lower bound to its mass of 0.3 $M_\odot$; the proof that x-rays from the Cygnus Loop are emitted thermally, and new doubts about its size and energy; a consistent model of Type II supernovae as expanding envelopes containing about 3 $M_\odot$ of gas at normal elemental abundances; a method for determining the distances to extragalactic supernovae without reference to any other astronomically determined distance; and a model for Type I supernovae in which 1 $M_\odot$ of matter with greatly enriched iron abundance creates the observed spectrum. The purpose of this introductory chapter is to describe

some of the ways in which these observations help clarify the overall understanding of supernovae.

II WHAT STARS BECOME SUPERNOVAE?

Supernovae are supposed to be the result of a cataclysmic collapse, which separates the long path of nuclear energy production from the condensed dead stellar phases of white dwarf, neutron star, black hole, or utter disruption (Baade and Zwicky 1934, Zwicky 1938). One important question is, at what point in stellar evolution does this catastrophe take place?

Most observational evidence on this question is indirect, as no pre-supernova star has ever knowingly been observed. Further, the observational evidence is strongly in favor of at least two kinds of supernovae, as determined from their spectra, and these two classes require two kinds of parents.

These two classes are well defined empirically: Type I by the long series of spectra taken by Minkowski (Minkowski 1939, Greenstein and Minkowski 1973) and by the long series of spectrophotometry presented in Chapter 6 for 1972e; Type II are well defined by the series of spectra and scans presented in Chapter 4.

The evidence on progenitors of supernova derives partly from the galaxies in which they are found. Not one of the 14 SN II's whose spectrum has been published (Oke and Searle 1974) has been discovered in an elliptical galaxy. By contrast, SN I's have been observed in galaxies of all kinds. The

traditional view of this difference has been that the SN II's come from young massive stars of Population I, while SN I's arise from the old low mass stellar population that dominates elliptical galaxies and is present in both spirals and ellipticals. One difficulty with this simple picture is that 4 SN I's have been identified from spectra in irregular galaxies, while no SN II's have been seen, despite the fact that young, massive stars dominate the light from irregulars.

Furthermore, it is not impossible that elliptical galaxies might contain some Population I objects, so the identification of SN I's with old low mass stars is not ironclad. Tammann (1973) argues on many grounds, including their presence in irregulars, their spatial distribution in spirals, and from galactic supernova remnants that SN I's come from young, massive stars. Thus, the indirect evidence from statistics is equivocal.

However, the evidence presented in Chapter 4 shows that roughly 3 $M_\odot$ of material is ejected in a Type II explosion, while the evidence from Chapter 6 is that about 1 $M_\odot$ is ejected by Type I supernovae. Thus the direct evidence is consistent with the idea that SN II's may arise from massive stars, while SN I's arise from low mass stars.

a. Theories for Type II

Theorists have concentrated on models for massive stars, which may correspond to SN II's. The aim of the

theorist has been to follow the evolution of stars of various masses through the turn-off from the main sequence, up the giant branch, and through the era of core and shell burning to the brink of the supernova disaster. His work is made difficult by physical and numerical instabilities which appear in stars and in models which are burning fuels in thin shells.

The currently fashionable way to avoid dealing with these intractable problems explicitly is to ignore the details of the unstable phases, while calculating their gross effects on composition and the subsequent structure, then skipping to the next stable phase. This trick has enabled Paczynski and others (Paczynski 1970) to follow the evolution of stars of various initial masses to late stages, just preceding the supernova event.

The conclusion of this kind of investigation makes the theoretical parents of SN II's rather clear. For stars less than 3.5 $M_{\odot}$ no catastrophe occurs as the star is able to shed much of its mass, presumably into a planetary nebula, and the remnant is safely able to settle down as a white dwarf, somewhat under the Chandrasekhar limit.

For stars in the range 4 to 10 solar masses, supernova detonation by explosive carbon ignition seems inevitable. For this mass range, the evolution of the core and envelope are almost separate: all the cores are nearly identical, independent of the star's total mass, and they all appear

to ignite carbon after they have become thoroughly degenerate in the core. This appears to create a rapid thermal runaway, and violent disruption of the star (Arnett 1969). The curious fact is that, although SN II's are thought to be the origin of pulsars, the models leave no stellar remnant (despite considerable effort by their creators!)

These are the stars which correspond best to the supernova rates inferred from historical supernovae, pulsars, and radio remnants of 1 per 50 ±25 years (Tammann 1973). That is, the death rate of stars from 4-10 $M_{\odot}$ is about equal to the rate of production of supernovae. Despite the annoying absence of a remnant in carbon detonation models, the statistical arguments together with the observations of Chapter 4 seem to provide reasonable evidence that they are the parents of Type II supernova.

b. Theories for Type I

Theoretical models for Type I supernovae have been based on the assumption that they must come from the low mass objects that predominate in elliptical galaxies. One is based on a metastable white dwarf which becomes unstable following a long stellar lifetime, due to the effects of electron capture (Finzi and Wolf 1967). A second theory considers the production of the naked core of a solar mass star in a binary system by mass transfer. The subsequent quick evolution of its companion and the

return mass transfer might send the degenerate core over the Chandrasekhar limit, and on to detonation (Hartwick 1972).

The circumstantial evidence from statistics of extragalactic supernovae is unclear, although the dominance of SN I's in irregulars could be taken as evidence that they are not from low mass stars. The observational fact that the SN I's form a very distinct and homogeneous class whose photometric and spectroscopic properties are closely reproduced in every individual case argues that some unique set of circumstances is necessary for every SN I.

The direct evidence from Chapter 6 does not distinguish the two models discussed here, but does seem to confirm that they are low mass objects, and that they may well be highly evolved.

III DO SUPERNOVAE PRODUCE THE HEAVY ELEMENTS?

One of the great efforts of modern astrophysics has been the attempt to understand the origin of the chemical elements in terms of astronomical events. The current idea is that hydrogen is the only primeval element and that its isotopes, helium, and a few traces of other light elements were manufactured during the hot dense phase of the universe. This leaves about 100 elements and 10^{10} years unaccounted for!

The systematics of abundances of other elements and the detailed nuclear physics of their manufacture point to

a brief, hot, dense state that might take place in a supernova.

Following this idea, tremendous effort has been lavished on calculating the effect of rapid heating, which might be due to a shock running through the innards of a supernova, on the abundances of the elements (Woosley, Arnett, and Clayton 1973). It is important to emphasize that the condition of rapid heating and subsequent cooling employed in these calculations is not associated with any particular model of a supernova explosion.

The observations in this thesis show that some abundances associated with supernovae may be extraordinary. In the Crab Nebula, the results of Chapter 2 indicate that the ejecta have normal abundances of oxygen, nitrogen, and sulfur relative to hydrogen, but that the helium abundance may be very high, unless a great deal of hydrogen is hidden.

The observations of Type II supernova, in Chapter 4, indicate no abundances that differ greatly from normal: presumably this is because the stellar evolution of the star is arrested at carbon burning, and because the matter we see comes from the outer layers of the star. If a hot shock does create new elements in the core of the star, it may have no profound effect on the abundances at the outside.

The observations of Type I supernovae, in Chapter 6, indicate the presence of about 0.02 $M_{\odot}$ of iron, as evidenced

by the great strength of [Fe II] lines at late epochs. If the star also ejects the indicated 1 $M_{\odot}$ of hydrogen, the abundance would be about 20 times the cosmic ratio. Presumably this is the result of rapid nucleosynthesis in the explosion, although it might be that the exploding object was the enriched core of a massive, highly evolved star.

The discovery of this overabundance of iron in Type I supernovae probably constitutes the best evidence to date that elements really are produced in supernovae.

IV SUPERNOVAE AND THEIR REMNANTS

Because the gas dynamics of supernova ejecta plowing into the interstellar medium are reasonably well understood (see for example Chevalier 1974), the study of remnants provides a convenient way to measure the energy output of a supernova. Also, statistical efforts to link galactic remnants with supernovae of a given type provide an important link in establishing the paternity of supernovae.

In Chapter 3 of this thesis, the temperature of the Cygnus Loop is shown to be more than 2×10^6 °K. This requires shock velocities of 400 km s^{-1}. Because the radial velocity of the Cygnus Loop has been assumed to be only 100 km s^{-1} (Minkowski 1958), it may be that the distance and energy of the Cygnus Loop have been seriously overestimated,

and its current stage of evolution badly misunderstood. This may have important effects on the links between supernovae and their remnants.

The observations of the Crab Nebula, reported in Chapter 2 do not establish clearly whether the Crab is the result of a SN I or an SN II. With a suitable twist of the observed facts, either hypothesis can be accommodated. However, the arguments that the Crab and its pulsar might result from a fairly massive SN II are not weakened by the observations of the Crab, and seem strengthened by the abundance determinations and velocity distributions for Type II supernovae that are derived in Chapters 4 and 5.

REFERENCES

Arnett, W.D. 1969, Ap. and Space Sci., 5, 180.

Baade, W. and Zwicky, F. 1934, Proc. Nat. Acad. Sci. U.S. 20, 254.

Chevalier, R.A. 1974, Ap. J., 188, 501.

Finzi, A. and Wolf, R.A. 1967, Ap. J., 150, 115.

Greenstein, J.L. and Minkowski , R. 1973, Ap. J., 182, 225.

Hartwick, F.D.A. 1972, Nature Phys. Sci., 237, 137.

Minkowski, R. 1939, Ap. J., 89, 143.

1958, Rev. Mod. Phys., 30, 1048.

Oke, J.B. and Searle, L. 1974, Ann. Rev. Astron. Astrophys., (to be published).

Paczynski, B.E. 1970, Acta. Astron. 20, 47.

Tammann, G. 1973, in Lecce Symposium on Supernovae (to be published).

Woosley, S.E., Arnett, W.D. and Clayton, D.D. 1973, Ap J. Supp., 26, 231.

Zwicky, F. 1938, Ap. J., 88 522.

Chapter 2

Spectrophotometry of the Crab Nebula

I INTRODUCTION

The Crab Nebula, the remnant of the 1054 A.D. supernova, is of special interest because the stellar remnant is visible, because a strong continuum of non-thermal emission extends from the radio region up to X-rays, and because the striking optical filaments possess unusual spectra (for numerous references, see Davies and Smith 1971). The object of this paper is to report observations of the integrated optical emission from the entire nebula, from 3400 Å to 7800 Å, with special emphasis on the continuum slope and on emission line strengths. The continuum is compared with measurements in other spectral regions, while the line strengths provide an estimate of the mass in the filaments.

II OBSERVATIONS

Observations were obtained in 1968 and 1974 with the Palomar Ten Centimeter Telescope, an *f*/3.3 Newtonian reflector, and the 200-inch (508 cm) prime focus photoelectric spectrum scanner, with entrance apertures of 8′. Observations alternated 15 times per second between an aperture centered on the Crab, and another, 33′ away, which measured sky brightness. Absolute flux densities were obtained at 23 wavelengths selected either to measure strong emission lines, or to avoid them. The calibration was based on the observations of Vega, ε Ori, and other stars obtained with the same telescope (Oke and Schild 1970).

Table 1 details the observed flux densities, and the error estimated from repeated measurements. All the measurements, except those at 6724 Å and 7780 Å were obtained on more than one night.

Figure 1 illustrates the observations, and compares the results of O'Dell (1962) where the Oke and Schild (1970) calibration of ε Ori has been substituted for that assumed by O'Dell. The slight systematic decrease in flux density from O'Dell's result, averaging -0.007 in log f_ν, is not explained. His observations were made with interference filters, did not have simultaneous sky measures, and involved the use of several telescopes, which makes it unlikely that the observed difference represents a real change in the Crab.

III CONTINUUM

We can represent the continuum data in Figure 1 by a least squares fit to a power law: $f_\nu = c\nu^\alpha$, where α=-2.32. This slope is slightly steeper than measurements made a few seconds of arc from the pulsar by Oke (1969). It is somewhat less steep than α = -2.56 observed by Scargle (1969) 1 minute NW of the center of the nebula, or the region about 70″ SSE observed by Miller (1973). The fact that the slope observed for the entire nebula corresponds to the slope near the center only shows that the bulk of the continuum emission in the observed spectral range comes from the central region of the nebula.

The interstellar reddening between the Crab and Earth

TABLE 1

CRAB NEBULA OBSERVATIONS

λ	$\Delta\lambda$	log ν	log f_ν	σ(log f_ν)	Remarks
3390	100	14.947	-23.466	0.016	Continuum
3509	100	14.932	-23.434	0.032	Continuum
3727	50	14.906	-22.870	0.008	[O II] 3727+3729
3980	100	14.877	-23.302	0.024	Continuum + slight [Ne III]
4101	100	14.864	-23.282	0.036	Continuum + slight Hδ, [S II]
4255	100	14.848	-23.286	0.040	Continuum
4566	100	14.818	-23.242	0.028	Continuum
4810	50	14.795	-23.170	0.021	Continuum
4860	50	14.790	-23.044	0.012	Hβ
4910	50	14.786	-23.146	0.022	Continuum
4960	50	14.782	-22.777	0.012	[O III] 4959
5010	50	14.777	-22.491	0.004	[O III] 5007
5060	50	14.773	-23.074	0.024	Continuum
5236	100	14.758	-23.026	0.008	Continuum
5556	100	14.732	-22.982	0.012	Continuum
5840	100	14.711	-22.886	0.012	Continuum
6050	100	14.695	-22.874	0.024	Continuum
6370	100	14.673	-22.830	0.012	Continuum
6560	100	14.660	-22.299	0.012	Hα+[N II] 6548+6584
6724	100	14.649	-22.438	0.022	[S II] 6717+6731
7100	100	14.626	-22.738	0.048	Continuum
7550	100	14.599	-22.740	0.024	Continuum
7780	100	14.586	-22.749	0.108	Continuum

has been investigated recently by Miller (1973). From line ratios of [SII] observed in filaments, he deduced an extinction $A_V = 1^m.6 \pm 0.2$, in reasonable accord with the work of O'Dell (1962) and Brodskaya (1963), given a distance to the Crab of about 2 kpc (Trimble 1973). Although, as Miller points out, the result is sensitive to errors in absolute calibration and in atomic parameters, it does provide a sound basis for interpreting the continuum data. Figure 2 shows the continuum points, corrected for various values of interstellar absorption, where the Whitford relation has been used (Whitford 1958, Miller and Mathews 1972). Table 2 summarizes the least squares fits to the continua.

The relation of the optical results to radio data (Baldwin 1971, Montgomery et al 1971), infrared data (Becklin and Kleinmann 1968, Ney and Stein 1968), and X-rays (Peterson and Jacobsen, 1970) is demonstrated in Figure 3.

Some interesting features emerge. First, the spectrum has power laws of increasing slope toward higher frequency (as long as $A_V \lesssim 1.8$). This is presumably due to the spectrum of relativistic electrons generated in the Crab, and their diffusion through its magnetic field structure.

Second, the extrapolation of the optical spectrum $\alpha = -0.41$ passes through the near infrared points, not too far below the 3μ and 5μ points, and intersects the radio continuum near 10^9 Hz. Although the

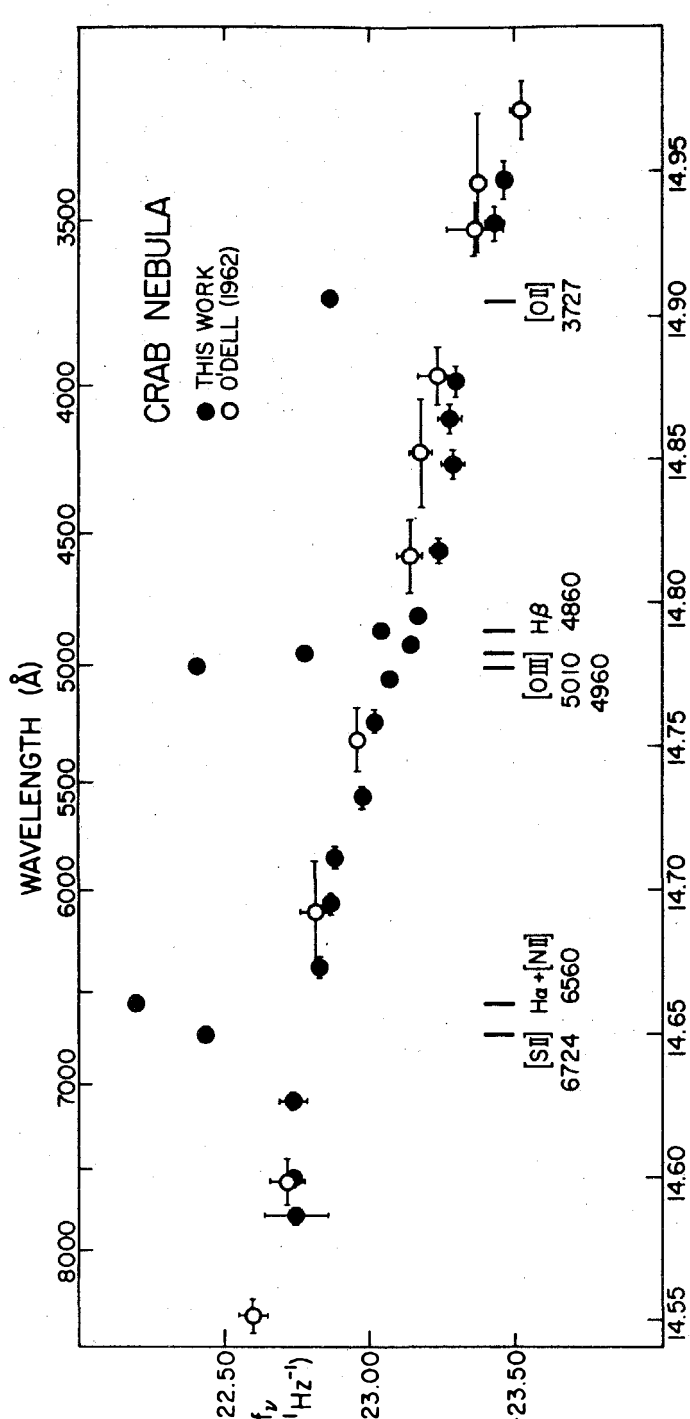

Fig. 1 -- Observed log flux density (erg cm^{-2} s^{-1} Hz^{-1}) versus log frequency (Hz). The filled circles (●) indicate the measurements in this paper, the open circles (○) the measurements of O'Dell (1962). The vertical error bars show the standard deviation when it is larger than the circle; the horizontal bars show the bandwidths.

conventional wisdom (Baldwin 1971) holds that the radio continuum is flat to 10^{11} Hz, there is some evidence that the radio emission may show a steepening slope beginning near 15 GHz. The very careful measurement at 16 GHz by Wrixton et al (1972) lies more than 3σ below the extrapolation from the 13.6 GHz measurement of Medd (1972). Wrixton et al suggest that the spectrum may have steepened over that frequency interval. The millimeter measurements summarized by Montgomery et al (1971) are confusing because of poor signal-to-noise and serious aperture correction problems. Only three sets of measurement in that summary had good signal-to-noise and were derived from maps: those are the points plotted on Figure 3. While there may be difficulties with absolute calibration at millimeter wavelengths, it is suggestive that these points lie below the extrapolated radio continuum and near the extrapolated optical continuum.

The extrapolation of the optical continuum into the ultraviolet is of considerable importance in understanding the ionization structure of the filaments. Figure 3 suggests that the extrapolation of the X-rays intersects the optical continuum just beyond the observed wavelength range. Then a good estimate for the ultraviolet continuum might be the extrapolated X-ray continuum.

TABLE 2

Least Squares Power Law Fit: $f_\nu = C\left(\frac{\nu}{10^{15}\,\mathrm{Hz}}\right)^{\alpha}$

A_V	log C	α
0.0	-23.60	-2.32
1.4	-22.59	-0.65
1.6	-22.44	-0.41
1.8	-22.30	-0.17

III LINE STRENGTHS

The absolute flux in an emission line can be determined by subtracting the continuum's contribution from the total observed flux. Because of the large number of continuum measurements, the linear interpolation to the flux at a line is quite accurate. Because the bandpasses are accurately known, the flux can be readily determined from the flux density. The results are shown in Table 3. The Hβ flux of $1.31 \pm 0.4 \times 10^{-11}$ erg cm^{-2} sec^{-1} agrees surprisingly well with the value 1.21×10^{-11} reported by O'Dell (1962) despite important differences in technique.

The Hβ flux permits an estimate of the contribution to the continuum from hydrogen recombination. From the calculations of Brown and Mathews (1970) and $T_e = 15{,}000°K$ (Woltjer 1958), it is easy to show that the recombination continuum for the entire Crab lies at least an order of magnitude below the observed flux densities, even at the Balmer jump.

The line ratios of Table 3 are in good accord with Woltjer's (1958) work on bright filaments for [N II], [O II], and [O III]. The [S II] is about twice as strong as Woltjer's estimate. The ratios at the Crab are tabulated for $A_V = 1^m.6$: the Hβ flux for that reddening is 7.5×10^{-11} erg cm^{-2}sec^{-1}.

If the reddening is really correct, then the blend at 6560 can be divided into Hα/Hβ = 3 and [N II]/Hβ = 7, which is roughly consistent with the Hα/[N II] ratio of 0.3-0.4 observed in filaments by Trimble (1970). If the [O II],

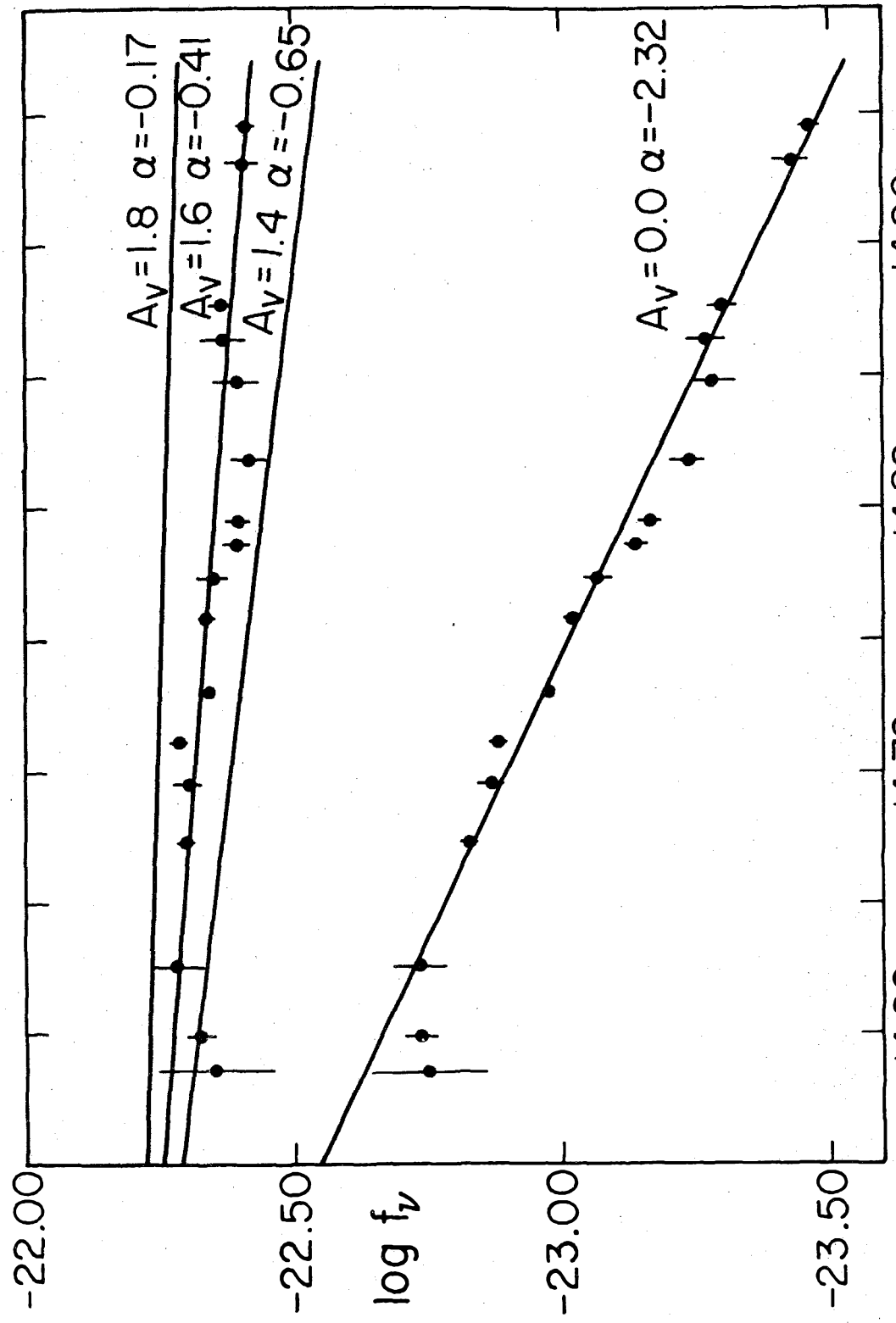

Fig. 2 -- Effects of reddening on the continuum. Continuum measurements are shown, with standard deviations, for reddenings A_V = 0.0 and 1.6. Least squares fits to the continuum points are shown for A_V = 0.0, 1.4, 1.6, and 1.8.

[N II], and [S II] lines are formed by collisions, in roughly the same region as the H recombination, approximate abundances can be estimated from Table 3. If T_o = 15,000 °K, using the N^+ and O^+ collision cross-sections from Czyzak et al (1968) and the S^+ cross-section from Saraph and Seaton (1970), the required abundances are $O^+/H^+ = 1.2 \times 10^{-4}$, $N^+/H^+ \approx 1.7 \times 10^{-5}$, $S^+/H^+ = 8.3 \times 10^{-6}$, all of which are somewhat lower than "cosmic" abundances. Although lowering the temperature brings these abundances into better agreement, real understanding can come only from detailed theoretical studies such as those of Davidson and Tucker (1970) and Davidson (1973).

The absolute flux of Hβ is directly related to the number of hydrogen recombinations, and thus to the mass of ionized hydrogen.

$$M_{H\ II} = 0.43\ \mathfrak{M}_\odot \frac{\left(\frac{D}{2kpc}\right)^2 \left(\frac{f_{H\beta}}{1.3 \times 10^{-11} erg\ cm^{-2} sec^{-1}}\right) \left(10^{0.472(A_V - 1.6)}\right)}{\left(\frac{N_e}{10^3 cm^{-3}}\right) \left(\frac{\varepsilon}{7.0 \times 10^{-26} erg\ sec^{-1} cm^3}\right)}$$

Here D is the distance to the Crab (Trimble 1973), $f_{H\beta}$ is the measured flux in Hβ, A_V is the absorption in the V band (Miller 1973), N_e is the electron density of a typical filament (Osterbrock 1957), and ε is the Hβ emissivity in erg sec^{-1} cm^3. Here ε is from recombination theory at $T_e \approx$ 15,000 °K (Brocklehurst 1971). The value of T_e and N_e refer to bright filaments where spectroscopy has been most detailed. Careful study of individual filaments is necessary to show whether these assumptions hold for most filaments.

TABLE 3

Line Strengths

Line	f (erg cm^{-2} s^{-1})	$\frac{[Ion]}{H\beta}$ $A_V=0.0$	$\frac{[Ion]}{H\beta}$ $A_V=1.6$
[O II] 3729+3729	$9.9\pm0.5\times10^{-11}$	8 ± 2	13 ± 3
Hβ 4861	$1.3\pm0.4\times10^{-11}$	1 ± 0.4	1 ± 0.4
[O III] 4959	$5.6\pm0.5\times10^{-11}$	4 ± 1	4 ± 1
[O III] 5007	$14.5\pm0.4\times10^{-11}$	11 ± 3	10 ± 3
Hα 6563+ [N II] 6548+6584	$24 \pm 2 \times10^{-11}$	18 ± 4	10 ± 3
[S II] 6717+6731	$13 \pm 2 \times10^{-11}$	10 ± 3	6 ± 2

The conclusion that 0.43 $\mathfrak{M}_\odot$ of ionized hydrogen must be present is only a lower bound to the mass of the filaments. If Woltjer's (1958) line strengths for He^{++} 4686/Hβ and He^{+} 4471/Hβ measured in bright filaments are assumed to apply to the whole nebula, then the Hβ flux measured here can be combined with the recombination theory of Brocklehurst (1971) and Robbins (1968) to estimate the ratios $M(He^{++})/M(H^{+})$ and $M(He^{+})/M(H^{+})$. The results are $M(He^{++}) = 0.1\ \mathfrak{M}_\odot$ and $M(He^{+}) = 0.9\ \mathfrak{M}_\odot$ for $T_e = 15{,}000$ °K and $N_e = 10^3$. Although better measurements of the line strengths, densities and temperatures are needed for more precise estimates, it seems probable that the filaments have a combined mass of about 1.4 $\mathfrak{M}_\odot$, and that helium is unusually abundant relative to hydrogen.

Can this picture be reconciled with observations of extragalactic supernovae? Type I supernovae are surely underabundant in hydrogen (Kirshner et al 1973) and the light curve of the Crab corresponded well to the Type I prototype (Minkowski 1968). The velocity of 1000 km s^{-1} observed in the filaments is comparable to that observed in Kepler's supernova (van den Bergh et al. 1973) which was almost certainly a Type I (Minkowski 1966). So it does not seem incredible that the Crab might have come from a Type I supernova, with a mass of about 2 $\mathfrak{M}_\odot$, including the mass of the envelope and a small neutron star of 0.5 $\mathfrak{M}_\odot$.

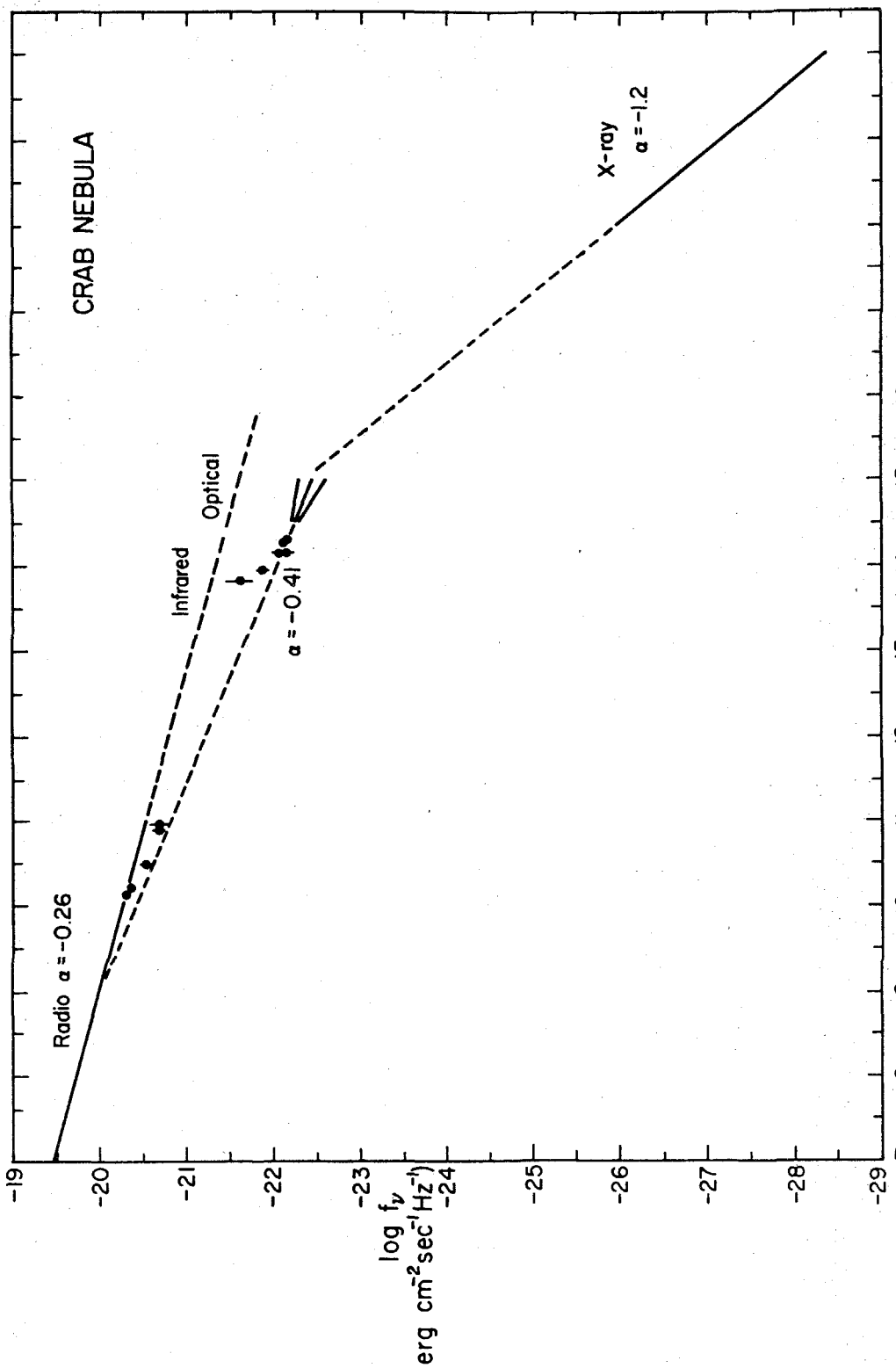

Fig. 3 -- Log f_ν versus log ν. Optical slopes are shown for A_V = 1.4, 1.6, and 1.8, as determined from the measurements of this paper.

On the other hand, if the Crab were the product of a Type II explosion, for example the carbon detonation (Arnett 1969) of a 4-8 $\mathfrak{M}_\odot$ star, we would expect a nearly normal hydrogen-to-helium ratio in the envelope. Then the 1.0 $\mathfrak{M}_\odot$ of He^+ and He^{++} (to say nothing of He^0) requires at least 4.0 $\mathfrak{M}_\odot$ of hydrogen. Since we see only 0.4 $\mathfrak{M}_\odot$ of H^+, 3.6 $\mathfrak{M}_\odot$ of neutral hydrogen must be hidden - presumably in the cores of filaments. This is roughly consistent with the estimates of Trimble (1970) based on [O I] emission. Then the total mass of the pre-supernova star might be 5 $\mathfrak{M}_\odot$ in the envelope plus at least 0.5 $\mathfrak{M}_\odot$ in the neutron star, for 5.5 $\mathfrak{M}_\odot$. Although velocities of 10,000 km s^{-1} are observed at the violet edges of P-Cygni profiles in Type II supernovae, the indications are that most of the mass is at much lower velocities (Kirshner and Kwan 1974). It does not seem unreasonable that a 6 $\mathfrak{M}_\odot$ star could explode from carbon ignition, eject 5 $\mathfrak{M}_\odot$ at less than 1500 km s^{-1} and leave a neutron star remnant.

In short, the evidence presented here is not sufficient to reject either the Type I or Type II identifications or even the hypothesis that the Crab belongs to neither class.

REFERENCES

Arnett, W.D. 1969, Ap. and Sp. Sci., 5, 180.

Baldwin, J.E. 1971 in Davies and Smith op.cit., p.22.

Becklin, E.E. and Kleinmann D.E. 1968, Ap.J.(Letters), 152, L25.

Bergh, S. van den, Marscher, A.P., and Terzian 1973, Ap.J. Suppl. No. 227, 26, 19.

Brocklehurst, M. 1971, MNRAS, 153, 471.

Brodskaya, E.S. 1963, Bull. Crimean Ap. Obs., 30, 126.

Brown, R.L. and Mathews W.G. 1970, Ap.J., 160, 939.

Czyzak, S.J., Kruegar, T.K., Martins, P. de A.P., Saraph, H.E., Seaton, M.J. and Shemming, J. 1968. IAU Symposium No. 34, Planetary Nebulae, ed. D. E. Osterbrock and C.R. O'Dell (Dordrecht: Reidel) p. 143.

Davidson K. 1973 Ap.J., 186, 223.

Davidson, K. and Tucker, W. 1970, Ap.J., 161, 437.

Davies, R.D. and Smith F.G. (eds.) 1971, The Crab Nebula (New York: Springer-Verlag).

Kirshner, R.P., Oke, J.B., Penston, M.V., and Searle, L. 1973, Ap.J., 185, 303

Kirshner, R.P. and Kwan, J. 1974, Ap.J. (in press).

Medd, W.J. 1972, Ap.J., 171, 41.

Miller, J.S. 1973, Ap.J. (Letters), 180, L83.

Miller, J.S. and Mathews, W.G. 1972, Ap.J., 172, 593.

Minkowski, R. 1966, A.J. 71, 371

Minkowski, R. 1968 in Nebulae and Interstellar Matter, ed. B.M.Middlehurst and L.H.Aller (Chicago: University of Chicago Press) p. 623.

Montgomery, J.W., Epstein, E.E., Oliver, J.P., Dworetsky M.M., and Fogarty, W.G. 1971, Ap.J., 167, 77.

Ney, E.P. and Stein W.A. 1968 Ap.J. (Letters), 152, L21.

O'Dell, C.R. 1962, Ap.J., 136, 809.

Oke, J.B. 1969, Ap.J. (Letters), 156, L49.

Oke, J.B. and Schild, R.E. 1970, Ap.J., 161, 1015.

Osterbrock, D.E. 1957, Pub.A.S.P., 69, 227.

Peterson, L.E. and Jacobsen A.S. 1970, Pub.A.S.P., 82, 412.

Robbins, R.R. 1968, Ap.J. 151, 497.

Saraph, H.E. and Seaton M.J. 1970, MNRAS, 148, 367.

Scargle, J.D. 1969, Ap.J., 156, 401.

Trimble, V. 1970, A.J., 75,926.

Trimble, V. 1973, Pub.A.S.P., 85, 579.

Whitford, A.E. 1958, A.J. 63, 201.

Woltjer, L. 1958, B.A.N., 14, 39.

Wrixton, G.T., Gott, J.R., and Penzias A.A. 1972, Ap.J., 174, 399.

Chapter 3

[Fe XIV] Emission from the Cygnus Loop

I. INTRODUCTION

Since X-rays from the Cygnus Loop were first detected by Grader, Hill, and Stoering (1970), several groups have made X-ray observations and have fitted model spectra. There is general agreement that the emission is thermal with a characteristic temperature of a few million degrees. Gorenstein *et al.* (1971) find that their data are fitted by a bremsstrahlung continuum at 4×10^6 ° K, with a line which they suggest is the O VIII Lα line at 19.0 Å, while Stevens, Riegler, and Garmire (1973) require a 2.8×10^6 ° K plasma with a line feature which may be the O VII lines at 21.6–22.2 Å or the O VIII line. Using data from similar instrumentation, Bleeker *et al.* (1972) obtained a good fit to their spectra from bremsstrahlung alone with a temperature $T = (2.7 \pm 0.4) \times 10^6$ ° K. Theoretical models of optically thin plasmas with solar abundance by Tucker and Koren (1971) and Mewe (1972) show that most of the X-ray flux comes from spectral lines for temperatures below 30×10^6 ° K. Tucker (1971) has used these models to reinterpret the data of Gorenstein *et al.* and estimates a temperature of 2×10^6 ° K. All the data obtained so far are limited by the poor spectral resolution of proportional counters in the 20–100 Å range, which does not permit clear distinction between line and continuum spectra, nor does it permit the separation of individual lines.

Although suggestive of a thermal plasma, the X-ray data could be fitted by nonthermal models, with appropriate choice of model parameters and interstellar absorption. Unambiguous detection of spectral lines is required to demonstrate the thermal nature of the X-ray emitting plasma.

As pointed out by Shklovskii (1967), those supernova remnants which emit thermal X-rays from hot plasma at a few million degrees will also emit optical coronal lines. Kurtz, Vanden Bout, and Angel (1972) estimate that at a temperature of 2×10^6 ° K the power in the [Fe XIV] λ5303 Å line is 5×10^{-3} of the total X-ray power, and at 3×10^6 ° K it is 2.2×10^{-3} of the total X-ray power. Kurtz *et al.* searched for the [Fe XIV] λ5303 Å line in various regions of the Cygnus Loop but without an X-ray map to guide the search area. No positive detection of the line was made.

II. OBSERVATIONS

We have used the interference filter photometer described by Kurtz *et al.* to search for the [Fe XIV] λ5303 Å line in the Cygnus Loop, Puppis A, and IC 443. For these new observations we used a filter of wider bandpass (5.9 Å FWHM) and higher transmission (50 percent), and used the X-ray map of Stevens and Garmire (1973) as a guide. The instrument consisted of an f/5 objective lens 15 cm in diameter with a 59′ diameter field stop at the focal plane. The beam was collimated, passed through the 5.1-cm-diameter interference filter, and refocused by a camera lens onto a cooled photomultiplier. The filter was rocked by an electromagnet so that for the ON-band position the filter was normal to the beam, and for the OFF-band position the filter was rotated 6.5°, which shifted the central wavelength 16 Å to the blue. This shift ensures that there is no overlap of the OFF-band bandpass with the iron line emission even

if there is broadening up to ± 8 Å. High turbulent velocities causing such broadening are possible if the heating to the observed X-ray temperature is by shock waves (Woltjer 1972). As the filter was tilted periodically (1 Hz) to the ON-band and OFF-band positions, the photomultiplier pulses were gated synchronously into two scalers. In order to keep the transmission in the ON-band close to the coronal line wavelength, the filter temperature was kept in the range 5°–20° C, where it passed an average central wavelength of 5303.4 Å for the center of the field of view and an average central wavelength of 5302.2 Å for the 1° field. For normal operation and with the 1° diameter field, the temperature shift and field shift were small compared with the filter bandwidth. The filter could be heated to over 50° C to move the bandpass off the 5303 Å line by 6 Å to the red. The filter efficiency and bandpass were measured at the coudé scanner at McDonald Observatory by Dr. P. Vanden Bout, who used the Sun as a source. The instrument sensitivity was calibrated by measuring the counting rate from α Lyr and α Cyg, using the α Lyr fluxes from Oke and Schild (1970) and correcting for absorption variations with zenith angle.

The principle of the measurement is to determine the ratio of counting rates in the ON and OFF wavelength bands for the regions of interest in the remnant and the nearby field. Coronal line emission then appears as a small increase in this ratio, the brightness of the [Fe XIV] line emission being much less than the nightsky light from airglow, faint stars, and city lights. Because of variations in the airglow, it was found to be necessary to make frequent comparisons with the adjacent sky, and in these observations integration of 2–3 minutes were made alternately on the same region and surrounding sky. Several adjacent sky regions were chosen outside of the remnant to obtain the best average of the spectral slope of the nearby sky.

The counting rate from the line in the source is given by

$$R = \left[N_{BS} - N_{BK} \frac{N_{AS}}{N_{AK}} \right] T^{-1} , \qquad (1)$$

where N_{BS} is the number of counts in the ON-band in time T on the source; N_{BK} is the number of counts in the ON-band on the adjacent sky; N_{AS} is the number of counts in the OFF-band on the source; N_{AK} is the number of counts in the OFF-band on the adjacent sky. The line brightness calculated in this way is insensitive to changes in absolute brightness of the night sky and is sensitive only to differences in the spectral ratio ON-band/OFF-band between the source and sky.

For the Cygnus Loop, the observed fields are shown as circles in figure 1, superposed on the 8–60 Å X-ray map of Stevens and Garmire (1973). For Puppis A and IC 443, the whole source was in the field of view. The results are presented in table 1.

For area 1, the observed flux of $(7.1 \pm 1.2) \times 10^{-12}$ ergs $(\text{cm}^2\ \text{s})^{-1}$ is significant at 6.0 standard deviations above zero, and the flux for area 3 of $(3.8 \pm 1.1) \times 10^{-12}$ ergs $(\text{cm}^2\ \text{s})^{-1}$ is significant at 3.4 standard deviations above zero. This significance is not affected by a possible uncertainty of about 10 percent in the absolute calibration. The values for the brightness of the line relative to the night sky in the 6 Å bandpass were about 0.7 and 0.4 percent for areas 1 and 3. The two regions of enhanced X-ray emission shown as areas 1A and 3A were observed by using a 0°6 diameter field, and optical line radiation was positively detected in both these regions. Also, the line surface brightness was higher in both these regions than the average surface brightness over the largely overlapping 1° diameter fields. Each result in table 1 is a weighted mean of observations from several nights, the weights and the final quoted error being obtained from the internal scatter of each night's observations. The scatter is generally about 1.5 to 2 times worse than would be expected from photon sta-

TABLE 1

[Fe XIV] 5303 Å RESULTS FOR THE CYGNUS LOOP, PUPPIS A, AND IC 443

Source	Field Diameter (°)	Energy in Line [10^{-12} ergs $(\text{cm}^2\ \text{s})^{-1}$]	Line Surface Brightness [10^{-8} ergs $(\text{cm}^2\ \text{s sr})^{-1}$]	Statistical Significance (σ)	X-Ray Flux* [10^{-9} ergs $(\text{cm}^2\ \text{s})^{-1}$]	Number of Nights Observed
Cygnus Loop:						
Area 1	1.0	+7.1±1.2	+3.1±0.5	+6.0	2.9	7
Area 1, wavelength shifted to 5309 Å	1.0	−2.1±1.8	−0.9±0.8	−1.2	...	3
Area 2	1.0	−0.4±1.5	−0.2±0.7	−0.3	1.2	4
Area 3	1.0	+3.8±1.1	+1.6±0.5	+3.4	1.8	3
Area 1A	0.6	+4.1±0.7	+4.8±0.8	+6.0	1.6	2
Area 1A, wavelength shifted to 5309 Å	0.6	−0.2±1.0	−0.2±1.2	−0.2	...	1
Area 3A	0.6	+2.9±0.9	+3.4±1.0	+3.3	0.9	3
Puppis A	1.0	−2.6±4.1	−1.1±1.8	−0.7	...	2
IC 443	1.0	+8.2±4.5	+3.6±2.0	+1.8	...	3

* Stevens and Garmire 1973.

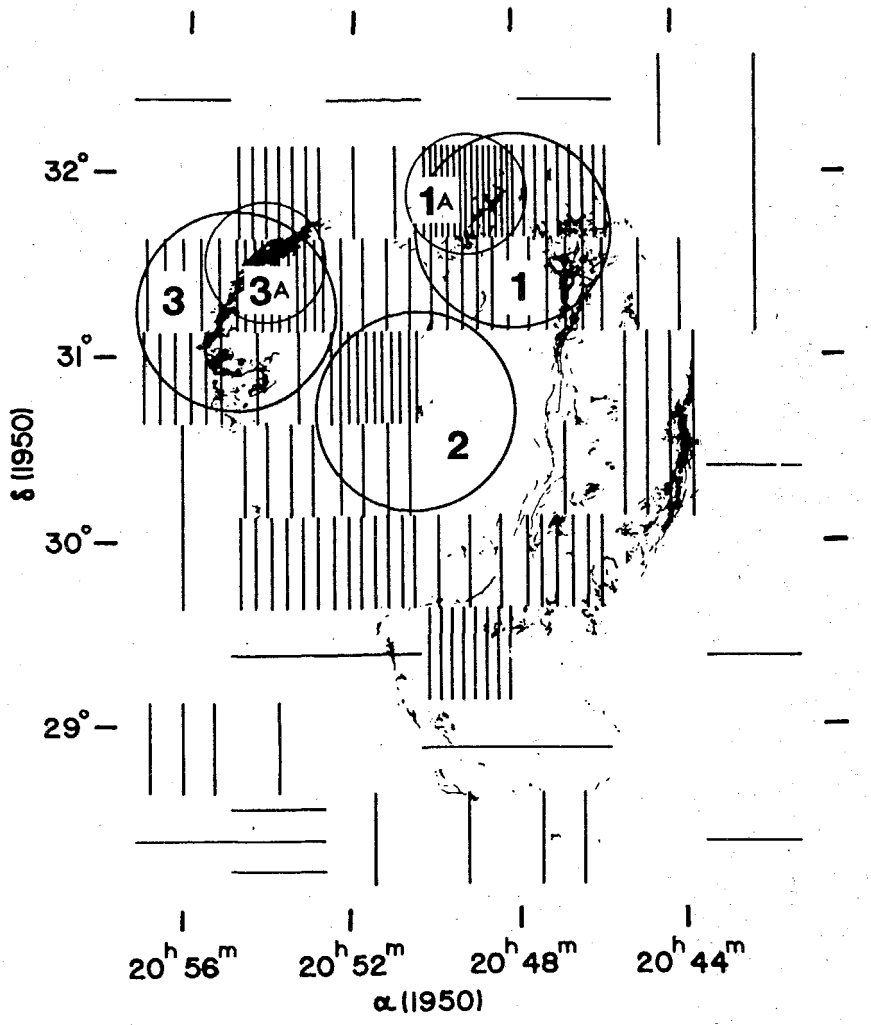

FIG. 1.—Reproduction of the Stevens and Garmire (1973) X-ray map, superposed on the Palomar *Sky Survey* photograph. The fields of view for which observations have been made are shown by the circles, numbered as in the table. The density of vertical lines is proportional to the X-ray flux.

tistics alone. The remainder was probably contributed by nightsky variations, as the scatter increased considerably if the chopping on and off the source was done more slowly than every 2 or 3 min.

III. DISCUSSION

Contributions to the line flux by starlight, continuum from the Cygnus Loop, and other known lines have been investigated and found to be negligible. In particular the heated filter results show that the [Ca V] 5309 Å line is not present.

Comparing our data with the results of Kurtz *et al.* for area 1, we find that the average surface brightness of the line in the field observed is $(3.1 \pm 0.5) \times 10^{-8}$ ergs $(\text{cm}^2\ \text{s sr})^{-1}$. This is just over 4 times brighter than the 3 σ upper limit given by Kurtz *et al.* for a field region which partly overlaps area 1. However, using the Stevens and Garmire X-ray map on Kurtz *et al.*'s region, we see that its X-ray surface brightness was about 0.25 of that of area 1.[1]

From the X-ray map of Stevens and Garmire we see that 20 percent of the X-rays from the Cygnus Loop come from our area 1 so that the X-ray power from the same field is $(2.9 \pm 0.4) \times 10^{-9}$ ergs $(\text{cm}^2\ \text{s})^{-1}$. Then the observed ratio of [Fe XIV] coronal-line power to total X-ray power is $(2.4 \pm 0.6) \times 10^{-3}$. This ratio fits the prediction of Kurtz *et al.* for a temperature of $(2.8 \pm 0.3) \times 10^{6}$ ° K if all the X-ray flux is of thermal origin, assuming an iron abundance of 2.6×10^{-5} of the hydrogen abundance. This temperature agrees very well

[1] Burginyon (1973) has pointed out that in the annular model assumed by Kurtz *et al.* to obtain an X-ray surface brightness, an error of a factor 4 was made. This does not affect the optical upper limits quoted there but only the ratio to the X-ray flux.

with those calculated from the X-ray spectra, suggesting that all the X-ray flux is thermal. Even if the optimum temperature for [Fe XIV] formation, 2.0×10^6 ° K, were assumed, the coronal-line strength would require that half the X-ray flux be thermal.

Similarly, the Stevens and Garmire map shows a flux of 1.2×10^{-9} ergs $(cm^2\ s)^{-1}$ and 1.8×10^{-9} ergs $(cm^2\ s)^{-1}$ from our areas 2 and 3. The ratios of [Fe XIV] line power to X-ray power are $(2.1 \pm 0.8) \times 10^{-3}$ for area 3 and a 3σ upper limit of 3.7×10^{-3} for area 2. The positive result for area 3 again demonstrates the thermal nature of the X-ray emitting plasma with a temperature of $(2.8 \pm 0.4) \times 10^6$ ° K if all the X-ray flux is thermal. The upper limit for area 2 does allow the X-ray flux to be thermal in the range $(2\text{–}3) \times 10^6$ ° K, although the recent rocket observations of Rappaport *et al.* (1973) indicate a harder X-ray spectrum for this region than for most of the Cygnus Loop.

The results from areas 1A and 3A with 0°.6 diameter field show that the correlation of [Fe XIV] line power to X-ray power continues to exist at this smaller field, giving some confidence in the brighter parts of the X-ray map down to its half-degree resolution. The ratios of [Fe XIV] line power to X-ray power are $(2.6 \pm 0.6) \times 10^{-3}$ for area 1A and $(3.8 \pm 1.3) \times 10^{-3}$ for area 3A, giving temperatures of $(2.8 \pm 0.3) \times 10^6$ ° K and $(2.5 \pm 0.4) \times 10^6$ ° K, respectively.

For areas 1 and 1A, the absence of the line when the wavelength was shifted by heating the filter suggests that the line is not broadened by as much as about 8 Å FWHM, which would be the predicted effect if a shock of velocity 450 km s^{-1} were fully converted into mass motions. Minkowski's (1958) measurement of a radial velocity of 116 km s^{-1} has been used with proper motion measures to derive the distance and diameter. If the X-rays are produced immediately behind the present shock and are not fossil radiation, then Minkowski's radial velocity does not measure the shock velocity, and its use for comparison with proper motions is not straightforward.

The agreement between the temperatures derived from the ratios of [Fe XIV] line to X-ray flux and from the X-ray spectra using a normal iron abundance (2.6×10^{-5} of hydrogen) supports the assumption of this normal abundance. Observations of interstellar ultraviolet lines using the *Copernicus* satellite have shown that iron is depleted by up to a factor 100 (Jenkins 1973). Field (1973) has explained this by the condensation of heavy elements into grains. If the observed underabundances are general in the interstellar medium, then our observations show that the shock wave has destroyed the grains and released the iron back into the gas.

In conclusion, a spectral feature has been discovered at 5303 Å in the regions of the Cygnus Loop brightest in X-rays. We attribute it to the coronal line of [Fe XIV]. The observed intensity agrees very well with the hypothesis that the X-rays are emitted from an optically thin thermal plasma at $(2.8 \pm 0.3) \times 10^6$ ° K.

This work was supported by the National Aeronautics and Space Administration under contract NAS8-29703, by the Research Corporation, and by the National Science Foundation under grant GP 31356X. We thank Professor R. Novick and Professor L. Woltjer for advice and encouragement. We are grateful to Professor G. Garmire for permission to reproduce the X-ray map, to Dr. P. Vanden Bout for calibrating the filters, to C. Janes, G. Hansen, and D. Doss of McDonald Observatory for assistance with the apparatus, to Dr. J. Miller for providing data on the filament spectra prior to publication, and to McDonald Observatory and the Hale Observatories for the use of their facilities. This *Letter* is Columbia Astrophysics Laboratory Contribution No. 90.

REFERENCES

Bleeker, J. A. M., Deerenberg, A. J. M., Yamashita, K., Hayakawa, S., and Tanaka, Y. 1972, *Ap. J.*, **178**, 377.
Burginyon, G. 1973, private communication.
Field, G. 1973, Annual Divisional Meeting of the AAS, High-Energy Astrophysics Division, and APS, Division of Cosmic Physics, Tucson, Arizona, December 6–8.
Gorenstein, P., Harris, B., Gursky, H., Giacconi, R., Novick, R., and Vanden Bout, P. 1971, *Science*, **172**, 369.
Grader, R. J., Hill, R. W., and Stoering, J. P. 1970, *Ap. J. (Letters)*, **161**, L45.
Jenkins, E. B. 1973, Annual Divisional Meeting of the AAS, High-Energy Astrophysics Division, and APS, Division of Cosmic Physics, Tucson, Arizona, December 6–8.
Kurtz, D. W., Vanden Bout, P. A., and Angel, J. R. P. 1972, *Ap. J.* **178**, 701.
Mewe, R. 1972, *Solar Phys.*, **22**, 459.
Minkowski, R. 1958, *Rev. Mod. Phys.*, **30**, 1048.
Oke, J. B., and Schild, R. E. 1970, *Ap. J.*, **161**, 1018.
Rappaport, S., Cash, W., Doxsey, R., Moore, G., and Borken, R. 1973, private communication.
Shklovskii, I. S. 1967, *Soviet Astr.—AJ*, **10**, 594.
Stevens, J. C., and Garmire, G. 1973, *Ap. J. (Letters)*, **180**, L19.
Stevens, J. C., Riegler, G. R., and Garmire, G. P. 1973, *Ap. J.*, **183**, 61.
Tucker, W. 1971, *Science*, **172**, 372.
Tucker, W., and Koren, M. 1971, *Ap. J.*, **168**, 283.
Woltjer, L. 1972, *Ann. Rev. Astr. and Ap.*, **10**, 129.

Chapter 4

The Atmospheres of Type II Supernovae

I INTRODUCTION

Since 1969, the multichannel spectrometer (MCSP, Oke 1969) attached to the 5-m Hale reflector has been used to obtain photometric scans of supernovae. In this chapter, the observations are described, and a rough analysis of the supernova envelope is presented. The general picture is of a differentially expanding gas, with mass above 1 $M_{\odot}$, and abundances similar to those in the sun. Some unusual problems in the recombination of hydrogen are considered, and the peculiar line ratios in Ca II are accounted for. Line identifications with Na I, Mg I, Fe II and [OI] are substantiated, and other possible identifications are dealt with in a systematic way.

II OBSERVATIONS

Two kinds of observations have been obtained for SN II's: photometric scans with the multichannel spectrometer and image tube spectra. The spectra provide much better wavelength information, but do not give quantitative data over a wide range of frequencies. In this chapter where the physical properties of supernova envelopes are discussed, such as the densities, temperatures, and abundances of elements, the MCSP data are the most useful and are presented here. The image tube spectra are presented in Chapter 5, where more exact line positions and shapes are used to determine expansion velocities in the envelope, which are used to derive the distances to extragalactic supernovae. The results of Chapter 5 will be

TABLE 1

Date (UT)	Julian Date- 2,440,000	Plate	Observer	Dispersion or Channel width	Useful Wavelength range
			SN 1969ℓ		
1969 Dec.13	568	Q1591	Schmidt	190 Å mm^{-1}	3400-6500 Å
1970 Jan. 3	589	Q1640	Schmidt	190	3400-6500
Jan. 5	591	MCSP	Oke	40/80 *	3300-10600
Jan.14	600	MCSP	Oke	40/80	3300-10600
Jan.30	616	Q1713	Sargent	190	3900-6700
Jan.31	617	Q1745	Sargent	190	3900-6700
Feb. 1	618	Q1773	Sargent	90	4100-6000
Feb. 1	618	Q1774	Sargent	90	3700-4400
Feb. 3	620	Q1811	Schmidt	190	3600-6700
Aug. 8	806	Q2158	Gunn	190	3800-6700
Aug. 8	806	Q2159	Gunn	190	3800-6700
Sept.7	836	Q2244	Schmidt	190	3800-6700
Sept24	853	MCSP	Gunn	80/160	3600-10600
1971 Feb.21	1003	MCSP	Gunn	80/160	4000-8000
			SN 1970g		
1970 Aug. 4	802	MCSP	Oke	40/80	3300-10600
Aug. 5	803	Q2133	Arp	190	3800-6700
Aug. 5	803	Q2134	Arp	190	3800-6700
Aug. 6	804	Q2140	Arp	190	3800-6700
Aug. 6	804	Q2141	Arp	190	3800-6700
Aug. 9	807	Q2161	Gunn	190	3800-6700
Aug.11	809	Q2178	Gunn	190	3800-6700
Aug.11	809	Q2179	Gunn	190	3800-6700
Sept.8	837	MCSP	Searle	40/80	3300-10600
1971 Apr.15	1056	MCSP	Penston	80/160	3800-9000
July 3	1135	MCSP	Penston	80/160	3800-8500

assumed here, namely, a distance of 6 Mpc to M101, 12 Mpc to NGC 1058, and 12 Mpc to NGC 3627.

The MCSP provides quantitative spectra over the wavelength range λ3200 to 11000, with a resolution of 20 to 160 Å. This modest resolution is well suited to the broad, indistinct and sometimes hopelessly blended features of supernova spectra. With the MCSP, observations at about 19th magnitude are practical, which permits long series of spectra to be obtained.

The photometric nature of the scans permits quantitative understanding of the continuum shape and flux, absorption line shapes and emission line strengths-- all of which figure importantly in the understanding of supernova envelopes. Most of the data presented here have been recently published by Kirshner et al (1973).

Three Type II supernovae have been extensively observed: SN 1969ℓ in NGC 1058, SN 1970g in M101 (NGC 5457), and SN 1973r in NGC 3627. Table 1 details the observations of SN 1969ℓ and SN 1970g, while table 2 gives the observations of SN 1973r.

MCSP observations were made so that no gaps occurred and the entire wavelength range was covered. Observations between λ8900 and λ9700 are somewhat uncertain because of strong water vapor absorption in the Earth's atmosphere. In particularly bad cases, the observations were completely deleted over this wavelength range. The spectral energy distributions are based on the absolute calibration of α Lyrae given by Oke and Schild (1970).

TABLE 2

Date (UT)	Julian Date -2,440,000	Plate	Observer	Dispersion or Channel Width	Useful Wavelength Range
1973 Dec. 31	2046	Q4685	Sandage	190 Å mm^{-1}	3900-6100 Å
		Q4686	Sandage	190	3900-6100
		Q4687	Sandage	190	3900-6100
1974 Jan. 15	2061	MCSP	Oke	40/80 Å	3500-11000
1974 Jan. 18	2064	Q4723	Sandage	190	4400-6600
		Q4724	Sandage	190	4000-6700
		Q4725	Sandage	190	4000-6700
1974 April 26	2163	MCSP	Oke	40/80	3800-9000

Figure 1 shows the MCSP scans for NGC 1058. As with all the scan data, log f_ν, the logarithm of the flux density (erg cm^{-2} s^{-1} Hz^{-1}) is plotted against log ν, where ν is the observed frequency. Individual points are joined by straight lines; when observations have small errors and are closely spaced in wavelength, the adjacent line segments form a smooth curve. In the central part of the spectrum, from logν 14.6-14.9, no error bars are shown if the errors are smaller than ± 0.02 in log f_ν.

On the left side of each energy distribution is a tick, with the corresponding value of log f_ν. This tick is repeated on the right. The last three digits of the Julian Day number appear on the right side of each plot. Possible line identifications are indicated along the bottom of the figures, along with corresponding marks at the top of the diagram. Finally, a wavelength scale is plotted across the top of the figure.

As for 1969ℓ, the scans of 1970g are presented in figure 2. Two scans of SN1973r are presented in figure 3. The first was made one month after discovery, and the second about four months after discovery. Because of improvements in the performance of the MCSP, the second scan is at the same resolution as the first despite the decrease in flux density, and a large number of features is visible.

The aim of this chapter is to infer from these observations and the identifications of lines, reasonable estimates of abundances and ionization, and the electron density in

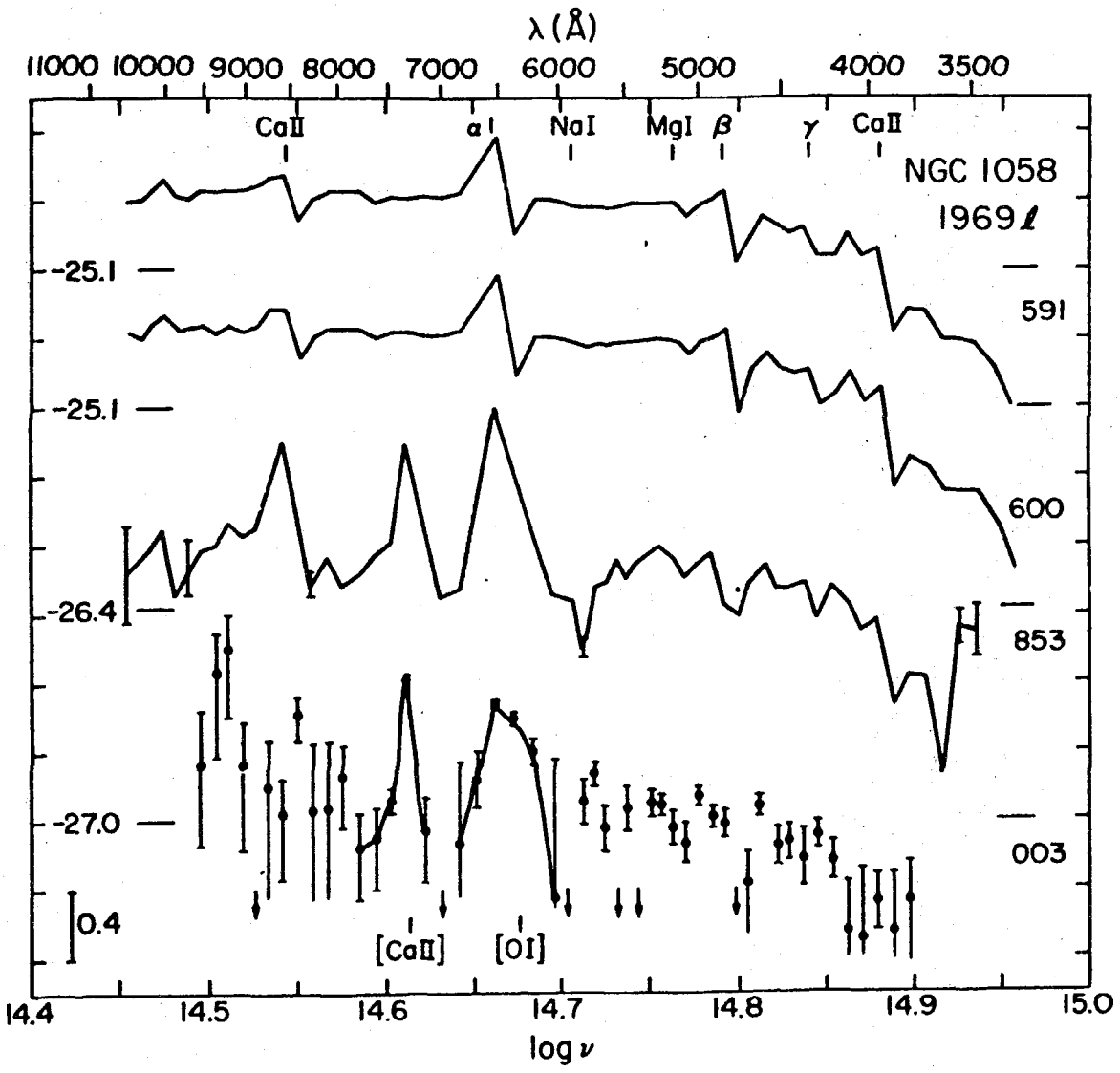

Fig. 1-- Scans of the Type II SN 1969ℓ in NGC 1058. The last three digits of the Julian Date are at the right of each scan. See text for detailed explanation.

the expanding supernova envelope. This is done through determination of the photospheric radius and temperature, the study of hydrogen recombination, and of the formation of lines in the envelope.

The results must be consistent with the lines that are seen, should explain the absence of others, and lead to the identification of still other lines.

For example, the identification of the Hα emission provides information about the electron density, and the population of the n=2 level. This result must be consistent with the observed Balmer decrement. Similarly, the electron density, together with the proposed identification of the CaII λ7300 line must be consistent with the observed ratios of CaII H and K, λ8600, and λ7300 lines. These problems and others leading to a consistent picture of the physical conditions in the envelopes of SN II's are discussed in the following sections.

III CONTINUUM MEASURES

The scans show that a continuum is present throughout the first year of expansion: the continua are supposed to be blackbodies. In view of the uncertainties in the distribution of the temperature and continuous opacity in the ejected gas, no more detailed model seems justified. However, the blackbody which fits best over the interval λ10 000 - 5000 lies well above the observed flux from the supernova shortward of λ4000. Table 3 shows the best fits to the

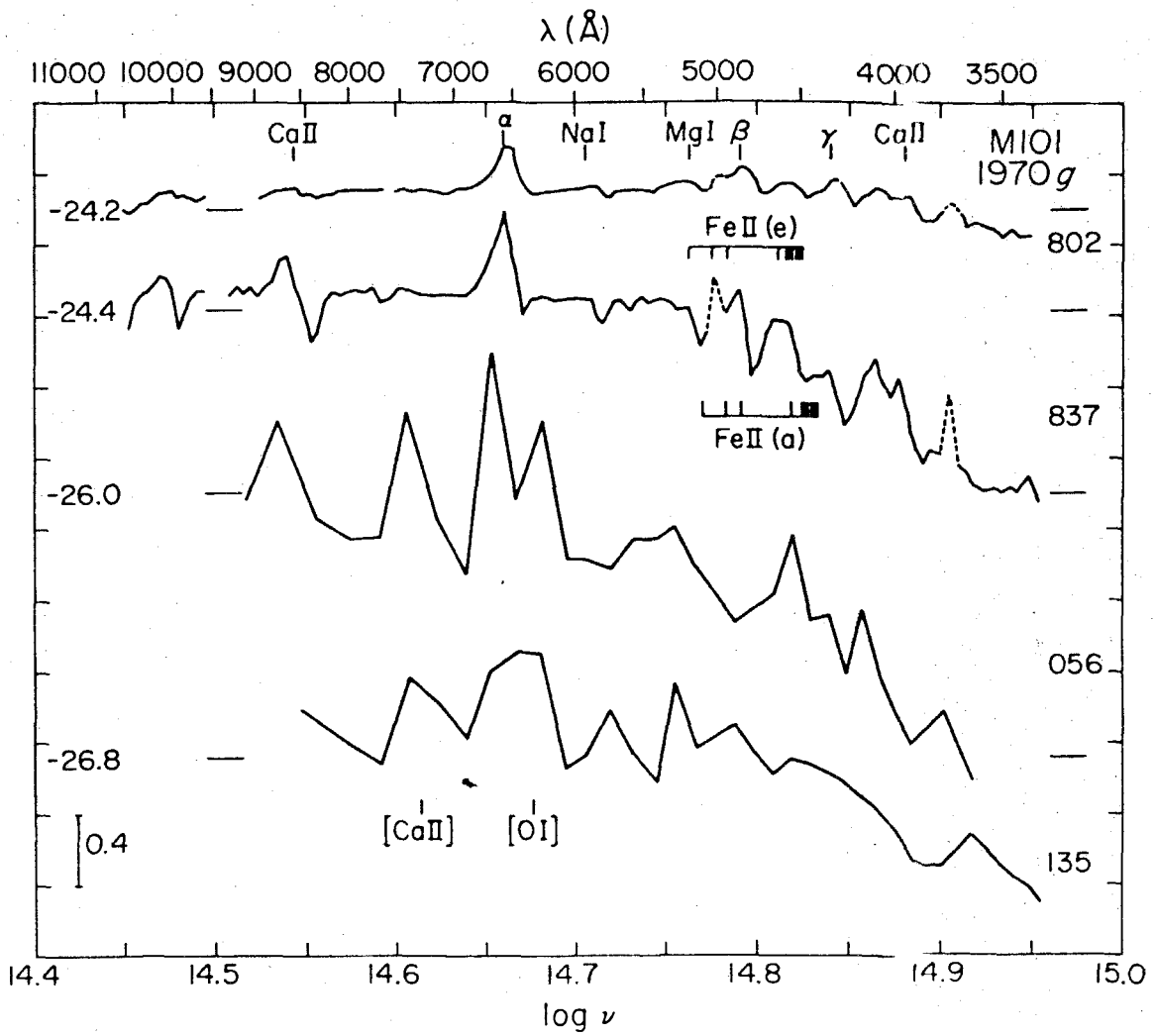

Fig.2-- Scans of the Type II SN 1970g in M 101. The positions of the strongest expected Fe II lines are shown: the emissions are at their rest wavelengths, the absorptions displaced 0.008 in logν to the violet.

temperatures, and the radii required to give the observed flux density. Reddening has been included in the temperature estimates for 1970g and 1973r.

The notable fact is that, after initial expansion and cooling, the temperature at the photosphere seems to remain very nearly constant from age one month to 14 months. The observed decrease in flux density is attributed to shrinkage of the photosphere. This shrinkage is the inevitable result of a finite mass: as the envelope continues to expand, the outer layers become transparent in the continuum and eventually the photosphere retreats, despite the outward motion of the gas.

IV LINE IDENTIFICATION

a. General Considerations

Before discussing the detailed line identifications, it is important to establish the kinematics of the envelope. As is evident from figures 1, 2, 3 and 4, the shapes of several lines exhibit a definite P Cygni character: blue-shifted absorptions balanced by nearly equal emissions centered near the rest wavelength.

This result, in the presence of a strong continuum, suggests that the supernova envelope consists of a photosphere with an expanding atmosphere above it. P Cygni lines are formed by resonant scattering of the photospheric photons by atoms of the expanding gas.

We suppose that all the matter ejected from the supernova

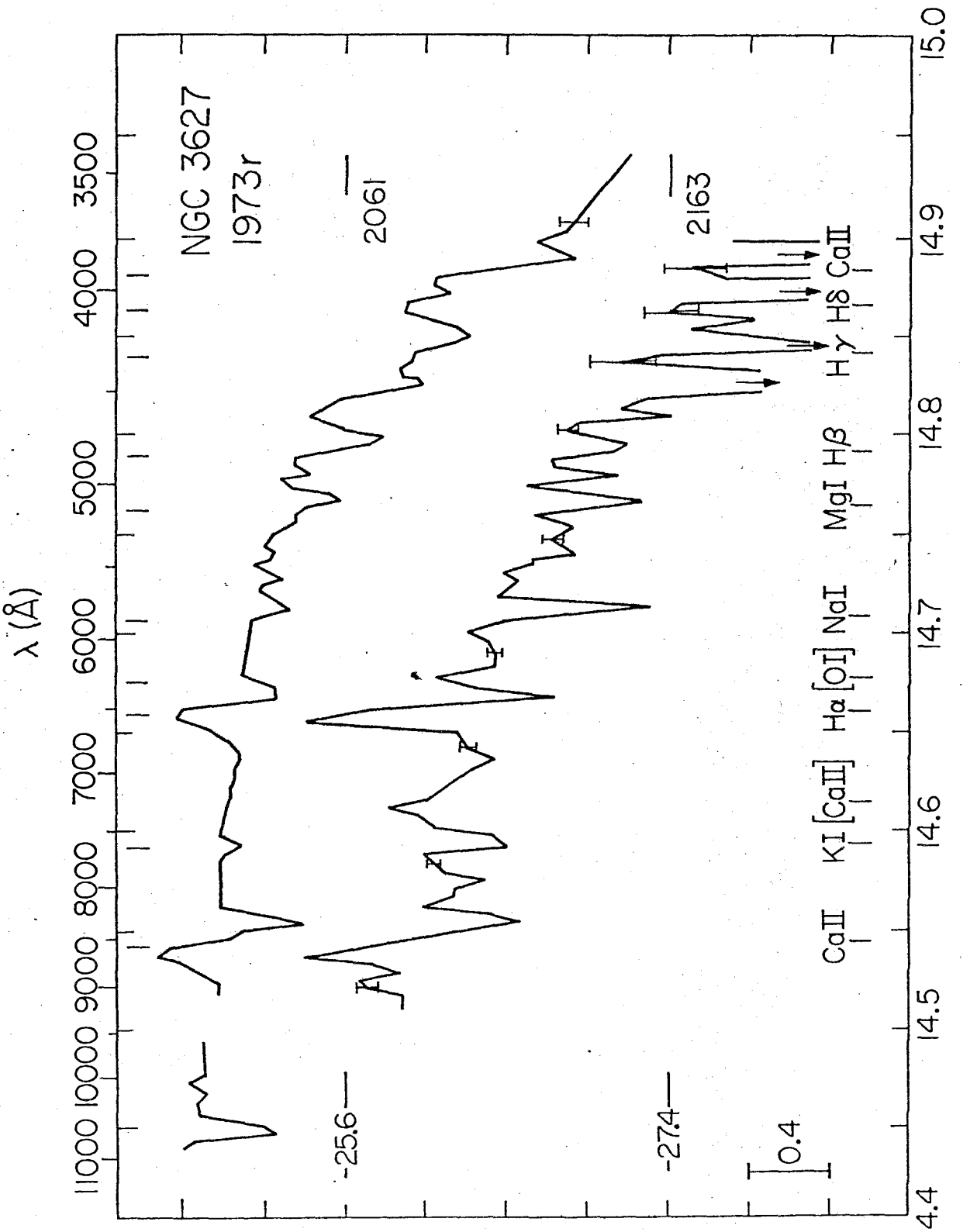

Fig. 3 -- Scans of the Type II SN 1973r in NGC 3627.

expands radially and freely from a central point of explosion. Then the matter at velocity v is a distance r=vt from the center, where t is the time since the explosion. At each point in the envelope, the line opacity is the same along any path and is given by:

$$\tau = \frac{hc}{4\pi} BN \left(\frac{r}{v}\right) . \qquad (1)$$

Here B is the Einstein absorption coefficient and N is the number density of atoms in the lower state of the line at the particular point in space. The number density in the upper state of the transition is much smaller and can be neglected. Equation (1) depends on the assumptions that the thermal widths are much smaller than the widths due to mass motions (Castor 1970) and that N varies slowly over a velocity range of the order of the thermal velocity. The escape probability for a photon emitted at a point is:

$$\beta = (1-e^{-\tau})/\tau . \qquad (2)$$

These results permit a quantitative evaluation of line identifications.

b. Balmer Lines

As shown in figure 4, the emission component of the line at Hα far outweighs the absorption. This net line flux should be due only to recombination in the envelope, as we expect the scattering to have about zero equivalent width and the collisional excitation of Hα is

TABLE 3

Supernova	Julian Date -2,440,000	Age (days)	Age (s)	T (°K)	r(ph) (cm)	Remarks
1969ℓ NGC 1058	591 } 600 }	35	3.0+6	6000	1.6+15	
	853	293	2.5+7	6000?	3.5+14	
	1003	443	3.8+7	6000??	1.0+14	
1970g M101 (NGC 5457)	802	2?	1.7+5	9500	8.6+14	A_v = 0.44
	837	37	3.2+6	5000	1.7+15	
	1056	256	2.2+7	5000?	2 +14	H II region subtracted
	1135	335	2.9+7	5000?	1 +14	
1973r NGC 3627	2061	26	2.3+6	5000	1.6+15	A_v = 0.5
	2163	128	1.1+7	5000	3 +14	

unimportant.

As we will demonstrate, the electron density is 10^{10}-10^{7} cm^{-3}, so that most electrons come from hydrogen, and $n_e = n_{H^+}$. Given the recombination coefficient α (T) from Brocklehurst (1971), we can easily derive $\int n_e^2 dV$ from the number of Hα photons emitted. The volume emitting the hydrogen line, $\int dV$, can be estimated from the velocity of the gas, as measured on the red wing of the emission feature, and the time. The results are summarized in table 4, which also gives the r.m.s. electron density, $\bar{n}_e$. The uncertainties in these estimates should not amount to more than a factor of two, except possibly at the late epochs (8 months or more) when the volume is not very well determined. We note that the recombining gas requires a minimum mass of 0.3 $M_\odot$, for the protons alone.

As shown in table 5, the recombination time $1/\bar{n}_e\alpha$ is always the age of the supernova envelope. This implies that the hydrogen in the envelope should have recombined far more rapidly than it is observed to do. This subsection shows that re-ionization from the n = 2 level is a plausible mechanism for replenishing the electrons.

Several mechanisms could prevent the electron density from decreasing as fast as Hα photons are produced. Under some circumstances, photoionization from the ground state is effective, but the dilute radiation from a 5000° K photosphere is far too weak a source of ultraviolet photons. Collisions are even more feeble in maintaining the electron density over long times.

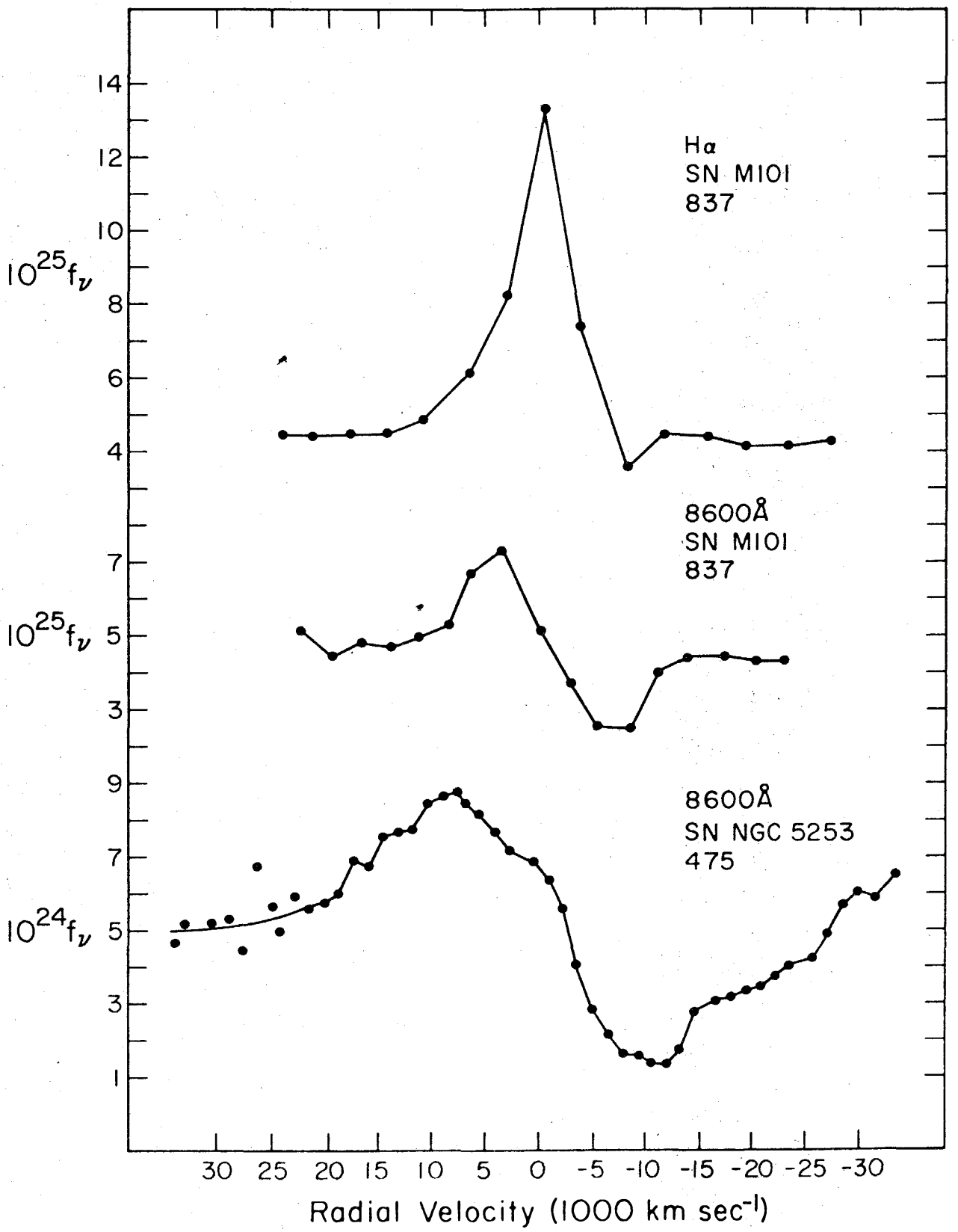

Fig. 4-- Line profiles from selected scans.

As illustrated in table 5, a computation of the rate of photons emitted shortward of the Balmer limit at λ3648 shows that at early times, this photon flux Q(Balmer) exceeds the recombination rate, and at late times is nearly equal to it. Given the uncertainties in the continuum flux near λ3648, it seems likely that enough photons are produced shortward of the Balmer limit to re-ionize the hydrogen, and decrease the rate at which electrons are lost. Under these circumstances, the destruction of a free electron does not occur when it is captured by a proton and cascades to n=2, but only when recombination is followed by de-excitation of the n=2 state. That is:

$$\frac{d\, n_e(r)}{dt} = -n_e^{\,2}(r)\alpha\left(\frac{A_{21}}{\frac{\pi r^2(ph)}{r^2}\int_{\nu_o}\frac{B(\nu)}{h\nu}\sigma(\nu)d\nu + A_{21}}\right) = -n_2(r)A_{21}\ , \qquad (3)$$

where A_{21} is the effective de-excitation rate from n=2 to the ground state, r(ph) is the photospheric radius, r the radius of the point in consideration, B(ν) the Planck function at the photospheric temperature, and σ(ν) the photoionization cross section from n=2. In this equation we have neglected the effect of expansion on the electron density. We shall denote the integral in equation (3) by $WP\sigma(\nu_o)$, where $\sigma(\nu_o)$ is the threshold photoionization cross-section from n=2, W is the geometrical dilution factor $\frac{r^2(ph)}{r^2}$, and $P = \pi\int_{\nu_o}^{\infty}(B(\nu)/h\nu)(\sigma(\nu)/\sigma(\nu_o))d\nu$ is equal to the number of photospheric photons emitted beyond the Balmer limit per second per unit area of the photosphere.

TABLE 4

SN	JD	v(atm) (cm s^{-1})	R(atm) (cm)	V(atm) (cm^3)	Q(Hα) (s^{-1})	α(T)	n_e
1969ℓ	600	1+9	3.0+15	1.1+47	2+52	5-14	2+9
	853	5+8	1.3+16	9.2+48	5+51	5-14	1+8
	1003	(4+8)	1.5+16	1.4+49	5+50	5-14	3+7
1970g	802	-	1 +15	4.2+45	9+51	2-14	1+10
	837	1+9	3.2+15	1.4+47	2+52	5-14	2+9
	1056	5+8	1.1+16	5.6+48	1+51	5-14	7+7
	1135	5+8	1.5+16	1.4+49	2+50	5-14	2+7
1973r	2061	1+9	2.3+15	5.1+46	6+51	5-14	2+9
	2163	5+8	5.5+15	7.0+47	1+51	5-14	2+8

Equation (3) also assumes that the continuum opacity through the envelope is less than about one. We expect this to be true because, through the era under consideration, we find $W\bar{P}\sigma >> A_{21}$ in the region where Hα is formed. Thus from equation (3), n_2 will be determined by the balance of recombination and re-ionization. In the early times of expansion, the total number of photons beyond the Balmer limit exceeds the number of Hα photons emitted, so that only a small optical depth in the continuum is required to balance the recombinations with re-ionizations. At later times, when the number of ionizing photospheric photons decreases, recombinations increase the population of the n=2 level until the continuum depth is large enough that reionizations balance the recombinations.

Three possible routes for de-excitation of the n=2 state have been considered: first, collisional de-excitations from 2p to 1s via electrons; second, 2p-1s radiative transitions that result in an escaped Lyman α photon; third, 2s-1p two-photon decays.

The collisional de-excitation rate can be estimated from the measurements of the excitation cross-section made at low energy by Fite (1962). Integrating that cross section with the electron velocity distribution at 5000°K gives an effective rate $C(2p\text{-}1s) = 1.58 \times 10^{-10}\ n_e n_2\ \text{sec}^{-1}$. The escape of Lyman α is more interesting; the Einstein A is about $6.25 \times 10^8\ \text{s}^{-1}$, but due to the very large optical depth in Lyman α, the net rate of decays by means of Lyman α escape is $n_{2p} A_{L\alpha} / \tau_{L\alpha}$.

TABLE 5

SN	1969ℓ			1970g				1973r	
JD	600	853	1003	802	837	1056	1135	2061	2163
t(s)	3.0+6	2.5+7	3.8+7	(1.7+5)	3.2+6	2.2+7	2.9+7	2.3+6	1.1+7
$1/\bar{n}_e \alpha$(s)	1+4	2+5	7+5	5+3	1+4	3+5	1+6	1+4	1+5
$\frac{Q(\text{Balmer})}{Q(H\alpha)}$	2.0	0.4	0.6	44	1.8	0.3	0.9	2.9	0.6
T(s)	2.1+7	3.3+7	2.0+7	1.7+7	2.1+7	2.0+7	1.2+7	9+6	1.6+7
$\bar{n}_2$	50	6	5		48	7	5	100	14
n_1	-	9+7	6+7			7+8	8+7		
$M_H(M_\odot)$		1.4	1.1			0.8	1.1		
τ_α	300	300	380		300	300	300	460	300
τ_β	44	44	56		44	44	44	68	44
τ_γ	15	15	19		15	15	15	23	15

From equation (1) this becomes

$$n_2 A_{L\alpha} / \tau_{L\alpha} = \frac{8\pi\nu^3}{c^3} \frac{g_1}{g_2} \frac{1}{t} \left(\frac{n_2}{n_1}\right) = 4.7 \left(\frac{10^7}{t}\right)\left(\frac{n_2}{10}\right)\left(\frac{10^9}{n_1}\right). \quad (4)$$

Here the g's are the statistical weights of the states.

Two-photon decays from the 2s to the 1s level have an Einstein A of about 8 s^{-1} (Spitzer and Greenstein 1951). Because 2p-2s collisions are much more rapid than this decay (Seaton 1955) about 1/4 of the total n=2 population will be in the 2s state at any moment. Then, since the emitted photons are not reabsorbed, the net escape rate is about $n_2(A_{2s-1s}/4)$ or $2n_2$ s^{-1}.

From the values of the electron density listed in table 4, we find that collisional de-excitation is always unimportant compared to two-photon decay. Because we do not know n_1, we cannot compare the two-photon decay rate with the Lyman α decay rate. However, an upper limit on the Lyman α decay rate permits an estimate of n_1, and hence an estimate of the supernova's mass.

If the picture of re-ionization from n=2 is correct, the decrease of the electron density and the observed Hα emission must be consistent. From equation (3) we find the effective decay time of the electrons is

$$T = -\frac{1}{n_e \alpha} \frac{WP\sigma + A_{21}}{A_{21}} \quad (5)$$

For the reionization process to operate, we require $WP\sigma >> A_{21}$ in the region where Hα is formed. As an example, with the

photosphere at a radius of 10^{15}cm and at a blackbody temperature of 5000°K, WPσ is about 30 at r = 10^{16}cm. With this approximation, we find that a uniform electron decay time throughout the envelope requires $n_e \propto W \propto r^{-2}$. We believe this to be the actual electron distribution. The density distribution of other matter is likely to be steeper than r^{-2}: only the delaying mechanism described here keeps $n_e \propto r^{-2}$.

The density of hydrogen atoms in the n=2 state, n_2, also is proportional to r^{-2}. With this dependence on radius, the number of Hα photons emitted, Q(Hα), the opacity in the Balmer continuum $\tau_{2c}(\nu)$, and the decay time of the electrons, T, are given by:

$$Q(H\alpha) = (4\pi\, n_e^2(R)\, R^4)\, (1/r(ph) - 1/R)\ ; \qquad (6)$$

$$\tau_{2c}(\nu) = \frac{\sigma(\nu)\, n_e^2(R)\, R^4}{\sigma(\nu_o)\, P\, r^2(ph)} \left(\frac{1}{r(ph)} - \frac{1}{R}\right);$$

$$\tau_{2c}(\nu) = \frac{\sigma(\nu)\, Q(H\alpha)}{\sigma(\nu_o)\, 4\pi\, r^2(ph)\, P}\ ; \qquad (7)$$

$$T = (1/n_e(R)\alpha)\ (P\sigma(\nu_o) r^2(ph)/A_{21}R^2). \qquad (8)$$

Here R denotes the outer radius of the envelope. With the estimates of Q(Hα), r(ph), R, and Q(Balmer) from tables 4 and 5, τ_{2c} and T can be inferred. Even though the input quantities are not very well determined, the estimate for T may be quite good. If at late times we require that $\tau_{2c}(\nu_o)=1$, so that Q(Balmer) = Q(Hα), then the electron decay time is given by:

$$T = \frac{1}{A_{21}} \frac{\sigma(\nu_o)}{\sqrt{4\pi\alpha}} \sqrt{Q(H\alpha)\left(\frac{1}{r_{ph}} - \frac{1}{R}\right)} \qquad (9)$$

The calculated values of T using $A_{21} = 2\ s^{-1}$ are presented in table 5. T is comparable to the age of the envelope. If we require that the Lyman α escape rate not exceed A_{21}, then we can estimate n_1 from equation (3), and thus derive a minimum mass for the supernova envelope. These results are also presented in table 5.

Using $n_2 = \int n_2 dr/(R-r_{ph})$ and equation (1) it is straightforward to find the effective optical depth in the Balmer lines. As shown in table 5, Hα is quite thick, but the fact that Lyman β is much thicker (τ of order 10^7) means that Hα photons are not converted to Lyman β despite numerous scatterings.

The situation is different for Hβ. Appreciable optical depth in Hβ permits many atoms to re-absorb an Hβ photon and return to n=4. There they can either re-emit the Hβ, or they can make the 4-3 transition, emitting an optically thin Paschen α, and eventually an Hα. Then the ratio of Hβ photons escaping to Paschen α photons escaping is just $(A_{42}/\tau_{24})/A_{43}$. Since the Einstein A's are nearly equal, and τ_{24} is estimated to be in the range 30-70, we expect very little Hβ to result from recombination. That explains the very large ratio of Hα/Hβ observed in all the scans. It

also has the effect of a modest (30%) increase in the Hα strength at a given electron density, and a two-fold increase in the Pα strength.

c. Lines of Ca II

Apart from the Balmer lines, the strongest features in the spectra of Type II supernovae about one month after maximum light are the features at λ3950 and λ8600. At times four months or more after maximum light, a strong emission feature appears at λ7300. The proposal (Kirshner et al, 1973) that all of these lines arise from Ca II is explored here in more detail. With the use of an explicit 3-level calculation for the calcium ion, the line strengths and line ratios observed are shown to be consistent with the physical conditions of the envelope inferred from Balmer line observations, and with a normal calcium abundance.

Figure 5 illustrates the three lowest energy levels of Ca II. The resonance lines, H and K, share the same $4p^2P$ upper state with the infrared triplet near λ8600. The lower level of the infrared line is the strongly metastable $3d^2D$ level. The forbidden transition $3d^2D$-$4s^2S$ violates the angular momentum selection rule, and has an Einstein A of about 1 s^{-1} (Osterbrock 1951, Warner 1968). It produces the lines at λ7300: the only other astronomical observation of these lines is in ν Sge (Greenstein and Merrill 1946).

It is easy to see why these lines could be important features in supernova envelopes. The interpretation of the

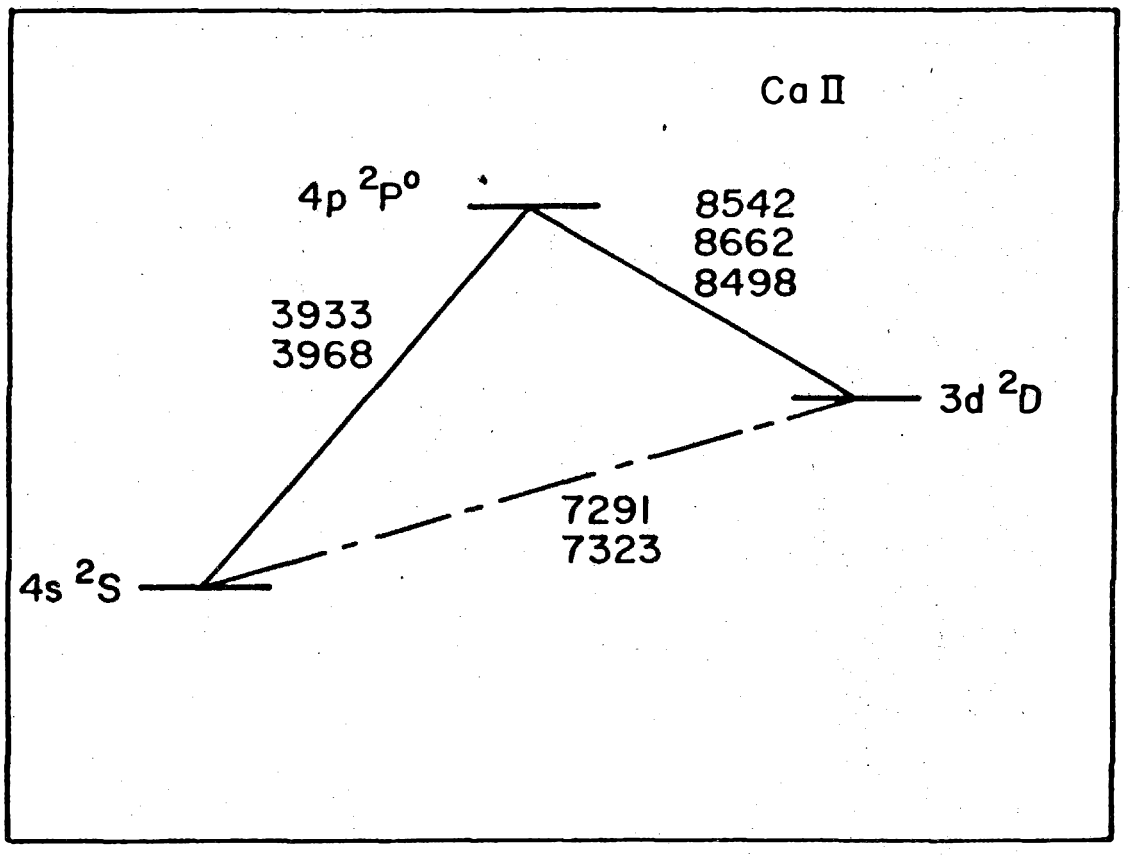

Fig. 5-- Partial Grotrian diagram for ionized calcium showing the three lowest levels.

continuum and the Balmer lines leads to a possible reversing layer consisting of a differentially expanding tenuous mass greater than $1M_{\odot}$ in which the electron density ranges from 10^{10} at early times, to 10^{7} at the last observations. The gas is irradiated by dilute photospheric flux, with $W=(r_{ph}/R)^2$ from 10^{-1} to 10^{-4} and T=10 000-5000°K.

Although the ionization conditions are quite feeble, they are adequate to keep nearly all calcium once ionized, but too weak to ionize it further. Because of the relatively high cosmic abundance of calcium (1.66×10^{-6} of hydrogen), and the large populations in the lower levels, large optical depths are present in strong lines. Thus it is not surprising that H and K and the infrared triplet are strong lines at early times. It is also not surprising to see the forbidden line appear after the continuum level has fallen by a factor of 50, with the electron density near 10^{7}.

We note that as the λ7300 line appears, the λ8600 line loses its absorption trough, and that the number of λ8600 photons produced is about equal to the number of λ7300 photons (table 6). While it is tempting to suppose along with Kirshner et al (1973) that, under the proper conditions, absorptions in H and K feed a cascade from 4p-3d-4s, which would produce equal numbers of λ8600 and λ7300 photons, this cannot be the correct explanation. The largest possible rate at which photons could be fed into this cascade would be the rate at which H and K photons are removed from the continuum.

It is clear from inspecting figures 1, 2 and 3 that the photons absorbed at H and K fall far short of the number produced at λ8600 and λ7300.

We propose here the following explanation for the peculiar ratios of the three Ca II lines. We believe that the 8600 and 7300 emission lines are formed by collisional excitation. The lines H and K are not observed in emission because collisions from the 4s to the 4p are more often followed by an emission of an λ8600 photon than by an H+K photon, due to the large optical depth in H+K. The effective rate of H+K emissions is $A(HK)\,\beta(HK)$ while for 8600, it is $A(8600)\,\beta(8600)$. For large optical depths, the branching ratio can be written $A(HK)\,\tau(8600)/A(8600)\,\tau(HK)$. As an example, if the ratio of population in the 3d to that in 4s is Boltzmann at 5000°K, the branching ratio is 0.2.

This argument holds only if the resulting increase in the population of the metastable state is drained away. This condition is met at late times when collisions from the 4s to the 3d are fast compared to collisions from the 4s to the 4p, and when the spontaneous decay rate from the metastable state becomes comparable to the rate of collisional de-excitations. We believe the absence of H+K emission at late times is explained by this model.

The nearly equal photon flux from λ8600 and λ7300 shown in figures 1 and 2 on JD 853 and JD 056 would then be a coincidence. At later times we expect the photon flux from

λ7300 to exceed that from λ8600, as the radiative decays from the metastable state greatly exceed the collisional de-excitations.

While both an λ8600 photon and a λ7300 photon are produced by a collision from 4s to 4p, only a λ7300 photon is produced by a collision from 4s to 3d. While collisions from the metastable 3d to 4p would create λ8600 photons without creating λ7300 photons, at late times the population in the 3d and the collision rate from 3d-4p are so small that very few λ8600 photons are produced this way.

At early times the situation is quite different. Then C(3d-4s) > A(3d-4s) and the population of the metastable state is fixed at the Boltzmann ratio to the ground 4s state. The number of λ7300 photons is fixed, regardless of how much larger the electron density might become. On the other hand, the process of producing λ8600 photons by collisions from 3d-4p becomes more important at increasing electron densities. At early times, we expect the number of λ8600 photons to be greater than the number of λ7300 photons.

These general predictions are borne out by comparison of figure 3 JD 2163, at age 4 months, figure 2 JD 135, at age 11 months, and figure 1 JD 003 at age 14 months. At very early times, net emission of λ7300 and of λ8600 is not observed because the strong continuum, and the resultant resonant scattering masks the contribution from collisions.

To model the processes described above, a numerical solution of the three level problem has been performed. The

TABLE 6

JD	Observed			Predicted			Best Fit	
	$\varepsilon(8600)$	$\varepsilon(7300)$	$\frac{Q(8600)}{Q(7300)}$	$\varepsilon(8600)$	$\varepsilon(7300)$	$\frac{Q(8600)}{Q(7300)}$	n_{CaII}	N_{CaII}
1969ℓ:								
600	4+3	-	>10	3+3	1+2	35	1+3	1+50
853	3+2	2+2	1.2	2+2	9+1	2.0	1+3	9+51
1003	-	5+1	-	3+1	4+1	0.7	6+2	8+51
1970g:								
837	3+3		>10	3+3	1+2	30	1+3	1+50
1056	6+1	8+1	0.8	6+1	5+1	1.2	6+2	3+51
1135		3	-	2	3	0.6	6+1	8+50
1973r:								
2061	2+4	-	>10	2+4	1+2	170	5+3	3+50
2163	3+2	2+2	1.8	3+2	1+2	2.2	2+3	2+51

differential expansion of the supernova envelope makes this problem particularly easy, as the radiative transfer problem becomes a local one. We use the escape probability formalism of Sobolev (1960) and Castor (1970), and the procedure of Goldreich and Kwan (1974). To illustrate, the rate of population change for the metastable level is:

$$\frac{dn_2}{dt} = -n_2(A_{21} + n_e(\gamma_{21} + \gamma_{23})) + n_3(A_{32}\beta_{23} + n_e\gamma_{32}) + n_1 n_e \gamma_{12}$$

The electron collision cross-sections from Burke and Moores (1968) and Petrini (1965) are integrated with the electron energy distribution to obtain excitation and de-excitation rates.

The system of equations is non-linear because of the dependence of β on the level populations. The equations were solved approximately by an iterative scheme until the accuracy of the solution was adequate. In general, it required only a few steps to produce solutions in which the net flow from one level to another was less than 1% of the smallest rate from one level to another by any particular route.

The aim of the calculation was to see whether the observed net rates of photon production in λ8600 and in λ7300 could be reproduced. In practice, it was always possible to match the emissivity (photons cm^{-3} s^{-1}) for one of the lines by adjusting the calcium density. Then the test of whether the model made sense was whether the corresponding emissivity for the other line matched the observations.

The five scans in which the two lines appear, along with the three scans in which only the λ8600 line is significant are listed in table 6 where the emissivity is tabulated. The calcium density that gives a rough fit to the λ8600 line is shown in the table. The corresponding λ7300 emissivity is gratifyingly close to the observed values. In the cases where the λ7300 line is much weaker than the λ8600 line, the predictions show the ratio 8600/7300 to be 30 or more. In the one intermediate case where the λ8600 line is significantly stronger than the λ7300, but both are observed (1973r, JD 2163), the prediction matches the observations very nicely. At late times, the λ7300 line is about as strong as the λ8600 line, and this behavior is reasonably well reproduced by the models. The total number of calcium atoms involved, $\int n(\text{Ca II})dV$, is also tabulated. Since one solar mass at cosmic abundance contains about 2.0×10^{51} calcium atoms, we see that the results are consistent with a normal calcium abundance and an envelope of a few solar masses. The relatively small numbers of calcium ions required for the scans at age one month (1969ℓ on JD 600, 1970g on JD 837, 1973r on JD 2061) may reflect the fact that considerable mass is still inside the photosphere at those epochs.

Overall, the understanding of the calcium emission seems satisfactory: the line ratios, which are mostly a function

of electron density, are consistent with the electron densities derived from the Hα emission. The line fluxes are consistent with a total amount of calcium that corresponds to a few solar masses at normal calcium abundance.

In the preceding calculation, it was tacitly assumed that all calcium was Ca^+. In this section the ionization state of calcium is roughly calculated, and the framework for calculating the ionization of other possible identifications is established.

The photoionization rate from a given level can be computed from the integral:

$$\gamma = \pi \int_{\nu_0}^{\infty} \sigma(\nu) \frac{B\nu(T)}{h\nu} \, d\nu \qquad (10)$$

Taking a sum over the relevant levels provides an estimate of the total photoionization rate, when the geometric dilution of the radiation field is included. Equating the recombination rate to the photoionization rate gives the ionization:

$$\frac{n^+}{n^\circ} = \frac{\gamma W}{\alpha n_e} \qquad (11)$$

Here α is the total recombination rate to all levels, and W is the dilution factor. Using values from Seaton (1951), the resulting ratios n^+/n° are calculated from the observed values for W and $\bar{n}_e$ given in tables 3 and 4, the results are displayed in table 7.

These calculations must underestimate

the true amount of ionization because they ignore ionization from upper states, and because the dilution factor used is the smallest possible: the value for the outer radius of the atmosphere.

The table shows that most calcium will be ionized at least once in the envelope. A similar calculation shows that the ions are not ionized again, despite a second ionization potential of 11.9 ev. Although most of the ionization of Ca^{+} to Ca^{++} takes place from the excited states that give rise to the infrared triplet and the forbidden line, consideration of the recombination rate shows that the photoionization does not significantly affect the level calculations of the previous section.

d. Lines of Na I, Mg I, Ca I

The identification of the Balmer lines and the three strong Ca II lines accounts for most of the strong features of Type II spectra. No other Ca II or hydrogen lines are expected to be present. The identification of other lines is helped considerably by the physical picture of the envelope developed in the previous sections through the analysis of those lines. Since the electron density, ionizing flux, mass, and total path length are known, it is possible to test guesses about further identifications by calculating the expected optical depth.

After the Balmer lines and the Ca II lines, the next strongest unblended features in the Type II spectra are at

λ5890 and at λ5180. The first could be either He I λ5876, or Na I λ5890 (the D-lines). The helium identification seems unlikely because none of the other strong triplet lines of He I is seen, and because the lower level ($2p^3P$) for that line lies 21 ev above the ground state. As for any line, we can estimate the optical depth:

$$\tau(5876) = \frac{n(2p)}{n(HeI)} \frac{n(HeI)}{n(He)} \frac{n(He)}{n(H)} \sigma \lambda n_H t$$

As in all the estimates to follow, if we assume "cosmic" abundance, and a hydrogen density that corresponds to 3 $M_\odot$ in the envelope, we are only required to estimate the ionization and excitation. In the absence of helium ionization, we expect all helium to be He I, and the 2p level to be populated no more than the Boltzmann level corresponding to the kinetic temperature. If T = 5000°K, the resulting optical depth in λ5876 is astoundingly small--at best 10^{-10}. No other helium lines, except λ10830 would be stronger, and λ10830 would still be negligible as long as there is no population from above.

We can do a similar calculation for Na I, except that the changes in ionization have to be considered explicitly. The result is shown in table 7: the D-lines have a large optical depth at all times, and should be a strong feature through the entire interval under consideration. In fact, the decrease in the ionization of the sodium as the radiation grows more dilute more than balances the decreasing column

TABLE 7

SN	1969ℓ			1970g			1973r	
JD	600	853	1003	837	1056	1135	2061	2163
W	3-1	7-4	4-5	3-1	4-4	9-5	5-1	6-3
W/n_e	2-10	8-12	2-12	8-11	4-12	4-12	2-10	2-11
$n_H t$	1+17	1+16	1+16	8+16	1+16	7+15	1+17	6+16
$Ca^+/Ca°$	7+3	3+2	7+1	8+3	3+2	2+2	1+4	1+3
τ(4226)	4+1	1+2	4+2	3+1	1+2	1+2	1+1	3+1
$Na^+/Na°$	1+3	6	1	1+3	5	4	3+3	2+1
τ(5890)	2+2	4+3	1+4	2+2	6+3	4+3	3+1	1+3
$Mg^+/Mg°$	2	7-2	2-2	2	6-2	5-2	2	2-1
τ(5171)	6+3	1+3	1+3	5+3	2+3	1+3	1+3	2+3

density: we expect the D-lines to grow stronger with time. The spectra of 1969ℓ and the scans of 1973r seem to show the D-lines to be of growing importance during the evolution of the spectrum. Thus we conclude that the feature near λ5890 is not He I, but rather Na I. No other Na I lines are expected.

Similarly, the feature at λ5180 is likely to be the b-lines of Mg I. They arise from a metastable level which for electron densities of 10^7 or more will surely be populated at the Boltzmann level for the electron temperature. As shown in table 7, the optical depths for Mg I are comparable to those for the D-lines, with a somewhat smaller variation due to ionization effects. As seen in the scans and spectra, the Mg I lines remain a strong and distinct feature throughout the entire period of observation. No other Mg I lines are predicted.

We can use the same method to check whether Ca I at λ4226 should be an important line. As shown in table 7, Ca I could be a line of modest strength at late times, but the uncertainties in the calculation are too large for a definite prediction. The spectra show no clear evidence for the line, although it could be related to feature 9 of figure 2 in Chapter 5.

In these simple cases, where the atomic physics is straightforward, it appears that the method used here is quite successful. It permits a choice between alternative

identifications that is based on the physical situation. The lines which are predicted to be strong are strong, and the lines which are expected to be weak are weak.

e. The Feature at λ4600

The strongest feature which has not been identified is the line whose emission peak and absorption trough correspond to a wavelength of λ4600. One possible identification is with the resonance line of Sr I at λ4607. If all strontium were neutral, and the abundance cosmic, this line could have an optical depth of about 10. However, strontium is calcium-like, with an ionization potential of 5.7 ev, so most strontium should be Sr^+. Then the optical depth of the 4607 line should be much less than one. The optical depths of the Sr II resonance lines at λ4078 and λ4216 should be of order unity, so it is not surprising that they do not form distinct features. In any event, the Sr II lines would be blended with Hγ and Hδ.

Another possibility for the λ4600 feature is suggested by analogy to other stars with similar physical settings: A supergiants, shells around late B stars, and novae near maximum light. The spectrum of Nova Herculis 1934 obtained on the evening of December 13 is illustrated in Stratton's monograph (1936). The line features are much weaker relative to the continuum and are much narrower than in SN II's, but the general character of the spectrum is quite similar to that of 1970g on JD 837. In this spectrum of Nova Herculis,

one strong feature is a complex emission band between λ4500 and λ4600, which is produced by transitions in multiplets 37 and 38 of Fe II. These lines, which arise from metastable levels 2.6 ev above the ground state are also among the strongest features in shell stars. Three other very strong Fe II lines that arise from metastable states about the same height above the ground state are λλ4923, 5018, and 5169 of multiplet 42. Rough estimates of the ionization and populations in these levels show that optical depths of order 100 should be expected. Then it seems very likely that Fe II lines from these multiplets account for the P Cygni features at λ4600, and at λ5000, as illustrated in figures 2. A similar conclusion based on the absorption features has been reached by Patchett and Branch (1972).

f. Lines of [O I]

In figures 1, 2 and 3, all the observations made 4 months or more after maximum light show some evidence of an emission feature at λ6300. The spectrum of 1969ℓ taken on 1970 August 8 (figure 2 of Chapter 5) shows this feature distinctly, while the corresponding scan shows it blended with Hα.

A reasonable proposal (Kirshner et al, 1973) is that the feature is the [O I] doublet at λ6300 and λ6330. We can test whether this identification is sensible by comparing the observed flux with that expected from an envelope of a few solar masses at 5000°K, with a cosmic oxygen abundance.

Because the densities of table 4 imply collision rates which are much faster than the radiative rates, the flux we expect to see is given by:

$$Q(6300+6363) = \frac{n(^1D)}{n(OI)} \frac{n(OI)}{n(O)} \frac{n(O)}{n(H)} A(^1D-^3P) n_H V$$

$$= \frac{g(^1D)}{g(^3P)} \frac{n(O)}{n(H)} \frac{M}{m_H} A(^1D-^3P) \exp(-2.27 \times 10^4/T)$$

For $T = 5000°K$, and $\frac{n(O)}{n(H)} = 6.76 \times 10^{-4}$

$$Q(6300+6363) = 4.3 \times 10^{+49} \frac{M}{M_\odot} \text{ photon } s^{-1}$$

We note that this is an upper limit to the photon flux: unless there is some means of population from above, the population in the ^1D level cannot exceed the assumed amount. Also, the photon flux should remain roughly constant, as long as the electron density is high enough ($n_e > 10^5$).

The scans show that about 1×10^{50} photons are emitted by 1973r on JD 2163, and about the same values for 1969ℓ on JD 1003, and 1970g on JD 1135. This photon flux corresponds to the emission from about 2 or 3 solar masses at the usual oxygen abundance. It is interesting that the photon flux for 1973r, only five months after maximum light, is comparable to the flux from 1969ℓ almost 15 months after maximum. This seems to support the idea that emission at both early times and late is proceeding at the maximum allowable rate.

The largest photon flux at λ6300 comes from the scan of 1970g in M101 on JD 1056. There we see about 5×10^{50} photons per second, corresponding to about 10 solar masses. Although the supernova in M101 erupted in an H II region, the O I flux from the surrounding gas has been subtracted from the supernova observations.

g. Other Lines

With a knowledge of the ionization conditions and the mechanism of line formation, it is possible to check systematically for other possible line identifications, both in emission and in absorption.

Some possibilities in emission include C I, λ8727, and S I, λ7726. Both of these are low lying forbidden lines of abundant elements that would be neutral. The photon flux from carbon probably could not exceed 1×10^{50} photons s^{-1}. This is comparable to the strength of O I, and could be significant at late epochs, although it would appear blended with λ8600 from Ca II at low resolution. The photon flux from the sulfur line might attain 2×10^{49} s^{-1}, and may be related to the very small emission seen in 1973r on JD 2163 (figure 3).

Potassium has two lines which can arise from the ground state, at λ7677 and at λ4045. Potassium is ionized at early epochs, but the line could attain τ of 100 after a few months. The scan of 1973r (JD 2163) shows two features at the correct wavelengths, however the atmospheric A-band of O_2 introduces some uncertainty at λ7677, while the blueshifted absorption

from Hδ would blend with λ4045. Thus the presence of potassium is not proven, but seems a good possibility.

V SUMMARY

Most of the features of Type II spectra can be understood in terms of an expanding atmosphere of 2-5 solar masses with cosmic abundance. Hydrogen recombination is slowed by reionization from the n=2 level by photospheric photons in the Balmer continuum. The net leakage from n=2 is probably by means of two-photon decay, if the supernova envelope has at least a few solar masses to prevent the easy escape of Lyman α. The opacity in Hβ accounts for the large Hα/Hβ ratio.

The interesting behavior of the Ca II emission lines can be understood in some detail, if the electron densities derived from the hydrogen recombination are correct, and if the envelope has a mass of about $3M_{\odot}$ with a cosmic calcium abundance.

Under the same assumptions, the strong lines of Na I and Mg I can be easily accounted for. The features at λ5000, and at λ4600 can probably be attributed to Fe II, and the [O I] line has the expected strength.

These threads of evidence seem so consistent, that one can have considerable confidence that this simple view of the overall situation is correct.

REFERENCES

Burke, P.G. and Moores, D.L. 1968, Proc. Phys. Soc. (London) B 1, 575.

Brocklehurst, M. 1971, MNRAS, 153, 471.

Castor, J.I. 1970, MNRAS, 149, 111.

Fite, W.L. 1962, in Atomic and Molecular Processes (D.R. Bates,ed.) Chapter 12. (Academic Press, New York).

Goldreich, P. and Kwan, J. 1974, Ap.J., 189, 441.

Greenstein, J.L. and Merrill, P.W. 1946, Ap.J., 104, 177.

Kirshner, R.P., Oke, J.B., Penston, M., and Searle, L. 1973, Ap.J., 185, 303.

Oke, J.B. 1969, Pub. A.S.P., 81,11.

Oke, J.B. and Schild, R.E. 1970 Ap.J., 161, 1015.

Osterbrock, D.E. 1951, Ap.J., 114, 469.

Patchett, B. and Branch, D. 1972, MNRAS, 158, 375.

Petrini, D. 1965, Comptes Rendus , 260, 4929.

Seaton, M.J. 1951, MNRAS, 111, 368.

Seaton, M.J. 1955, Proc. Phys. Soc. (London) A, 68, 457.

Sobolev, V.V. 1960, Moving Atmospheres of Stars (Harvard University Press, Cambridge).

Spitzer, L. and Greenstein, J.L. 1951, Ap.J., 114, 407.

Stratton, F.J.M. 1936, Ann. Solar Phys. Obs. Cambridge, Vol.4, Pt.4.

Warner, B. 1968, MNRAS, 139, 115.

Chapter 5

An Astrophysical Distance to Supernovae

I INTRODUCTION

The extragalactic distance scale depends on distances established within the Local Group, and within our own galaxy through variable stars and main sequence fitting. Ultimately, the stellar distance scale is tied to locally determined parallaxes, and in particular to the distance to the Hyades (Sandage 1956).

This paper outlines a method for determining extragalactic distances from observations of supernovae. It is independent of all distances determined in our galaxy, or in the Local Group, and it does not even assume that the observed events are of the same absolute magnitude.

On inspection of recent photometric scans of supernovae (Kirshner, Oke, Penston, and Searle 1973, hereafter referred to as KOPS), L. Searle suggested that the expansion of the photosphere, as determined from the temperature and apparent magnitude, could be linked to the expansion velocities observed in lines to estimate the distance to a supernova through Baade's (1926) method for variable stars.

When the energy distribution of the continuum is accurately characterized by a temperature T, the received flux density, f_ν, determines the angular size of the emitter, $\Theta = R/D$, through equation (1)

$$\Theta = [f_\nu / \pi\, B_\nu(T)]^{\frac{1}{2}} \quad . \tag{1}$$

Here R is the radius of the photosphere, D is the distance

to the supernova, and $B_\nu(T)$ is the Planck function. Thus the distance is determined by measurements of f_ν, T, and R. Both f_ν and T can be estimated directly. R is estimated by the following method.

In the simplest kinematic assumption the envelope undergoes free expansion once the shock emerges from the surface of the star. Gravitational deceleration and radiation pressure both produce velocity changes much smaller than the initial velocities imparted by the shock (Sakurai 1960, Grassberg et al. 1971). The pressure due to the interstellar medium is negligible because the amount of matter swept up by the supernova in a few months is very small, perhaps 10^{25} gm. If at some instant, t, the velocity of the material at the photosphere, v, is determined, and the time, t_o, at which the envelope started expanding is known, then given free expansion, the radius of the photosphere is

$$R = v(t - t_o) + R_o \ . \qquad (2)$$

The initial radius of the envelope is denoted by R_o, and it is assumed that when the envelope begins to expand, most of the material is located near R_o.

Usually, the photospheric radius becomes greater than the initial radius R_o after a relatively short time (cf. § II) and R_o can be ignored in the distance determination. The time of initial expansion t_o, however, is crucial to the distance determination. If a good estimate of t_o cannot be obtained, then two sets of values of v, T, and f_ν must be used, separated by a sufficient span of time.

It is easily shown, in this case, that the distance is

$$D = [v_2 (t_2-t_1) + R_o(1-v_2/v_1)] / [\theta_2-(\theta_1 v_2/v_1)] \qquad (3)$$

The difficulties of this method occur in estimating the temperature in eq. (1), and the velocity in eq. (2). In Section II of this paper the temperatures for the supernovae 1969ℓ and 1970g are derived directly from spectrophotometric scans when they are available, and otherwise indirectly from broadband photometry. The velocities are inferred from the observed line profiles in Section III. The distances to NGC 1058 and M 101 are derived in Section IV. Finally, in Section V the accuracy of the results is discussed and a summary is presented of appropriate procedures to be undertaken in future applications of this method.

II DATA

a. The Supernovae

This paper estimates the distances to two recent Type II supernovae: 1969ℓ in NGC 1058 and 1970g in M 101 (NGC5457). The supernova in the Sc galaxy NGC 1058 reached a maximum of B ≃ 13 on about 1969 December 3 (Ciatti et al 1971) and was very favorably located for observation, about 227" from the center of the galaxy. The observed recession velocity for NGC 1058 is +521 km sec^{-1} (de Vaucouleurs 1967), which corresponds to a velocity of 665 km sec^{-1} as viewed from the center of our galaxy.

TABLE 1

Date (UT)	Julian Date - 2,440,000	Plate	Observer	Dispersion or Channel width	Useful Wavelength range
			SN 1969ℓ		
1969 Dec.13	568	Q1591	Schmidt	190 Å mm^{-1}	3400-6500 Å
1970 Jan. 3	589	Q1640	Schmidt	190	3400-6500
Jan. 5	591	MCSP	Oke	40/80 *	3300-10600
Jan.14	600	MCSP	Oke	40/80	3300-10600
Jan.30	616	Q1713	Sargent	190	3900-6700
Jan.31	617	Q1745	Sargent	190	3900-6700
Feb. 1	618	Q1773	Sargent	90	4100-6000
Feb. 1	618	Q1774	Sargent	90	3700-4400
Feb. 3	620	Q1811	Schmidt	190	3600-6700
Aug. 8	806	Q2158	Gunn	190	3800-6700
Aug. 8	806	Q2159	Gunn	190	3800-6700
Sept.7	836	Q2244	Schmidt	190	3800-6700
Sept24	853	MCSP	Gunn	80/160	3600-10600
1971 Feb.21	1003	MCSP	Gunn	80/160	4000-8000
			SN 1970g		
1970 Aug. 4	802	MCSP	Oke	40/80	3300-10600
Aug. 5	803	Q2133	Arp	190	3800-6700
Aug. 5	803	Q2134	Arp	190	3800-6700
Aug. 6	804	Q2140	Arp	190	3800-6700
Aug. 6	804	Q2141	Arp	190	3800-6700
Aug. 9	807	Q2161	Gunn	190	3800-6700
Aug.11	809	Q2178	Gunn	190	3800-6700
Aug.11	809	Q2179	Gunn	190	3800-6700
Sept.8	837	MCSP	Searle	40/80	3300-10600
1971 Apr.15	1056	MCSP	Penston	80/160	3800-9000
July 3	1135	MCSP	Penston	80/160	3800-8500

The supernova in M 101, also an Sc galaxy, was brighter, reaching B ≃ 11 on about 1970 August 6 [IAU circulars 2269, 2271, 2282], but it was not so conveniently located, as it erupted in a large H II region, about 380″ from the galaxy's center. The observed recession is +300 km sec^{-1} (Humason et al. 1956), which corresponds to +415 km sec^{-1} in our galaxy's rest frame.

b. Spectra and Scans

Table 1 lists the observational material gathered at the Hale Observatories: all the slit spectra were obtained with the Cassegrain image tube spectrograph at the 200-inch (508 cm) Hale reflector. As described in KOPS, photometric scans were obtained at the Hale telescope with the multichannel spectrometer (MCSP).

Figure 1 illustrates the evolution of the spectrum of SN 1969ℓ with microphotometer density tracings, and shows 31 numbered features whose wavelengths are given in Table 2. The wavelengths listed are for the minimum or maximum of the feature as measured either with a Grant measuring engine, or directly on the tracings. In either case, the uncertainty due to the width of the lines exceeds the measuring errors of a few angstroms. Table 2 also suggests identifications for some of the most prominent features. These are in accord with those of KOPS, but differ from those of Ciatti et al (1971). Those authors identify a large number of N II, He I, and He II lines, which we exclude principally on the grounds that they

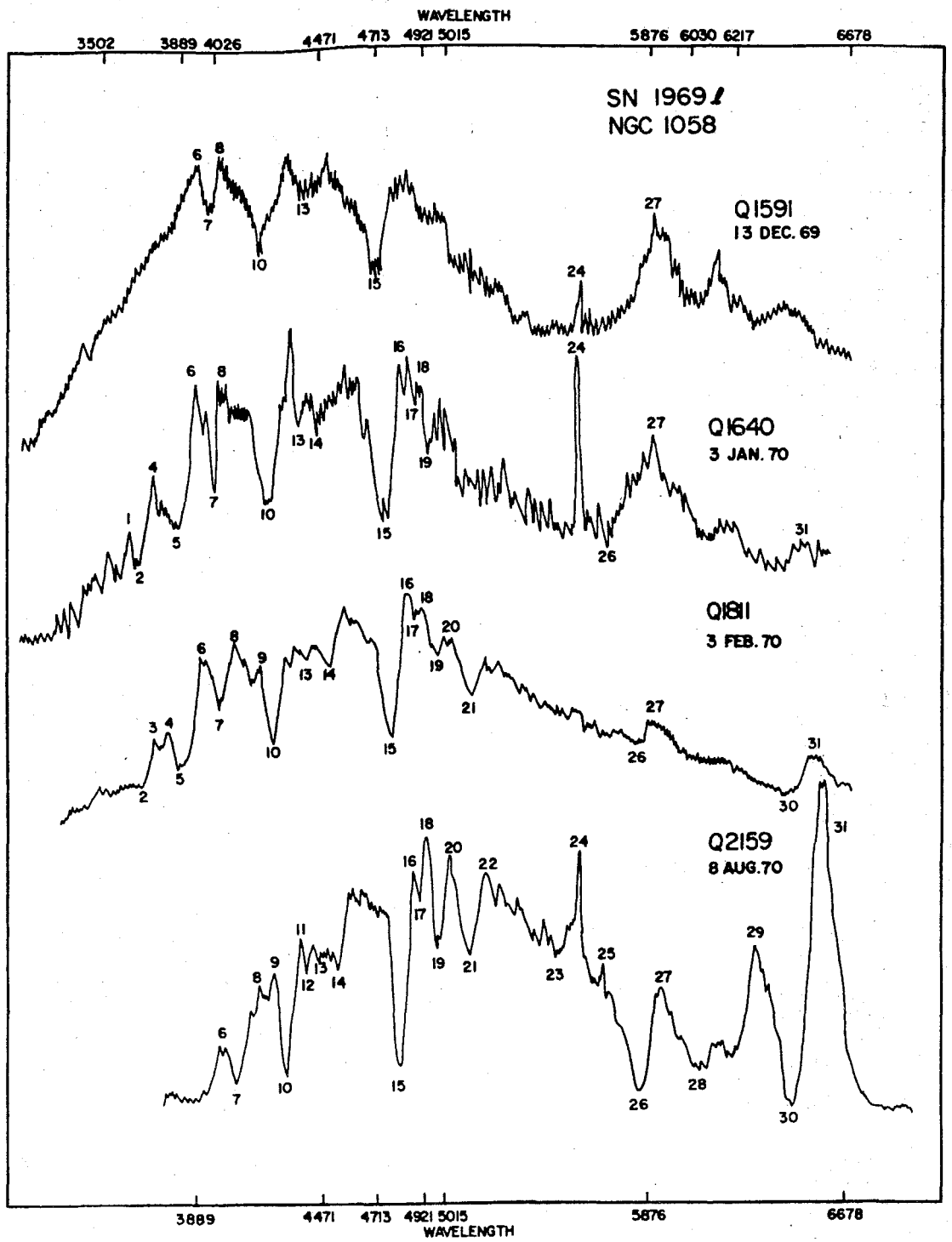

Fig. 1 -- Microphotometer density tracings of SN 1969ℓ in NGC 1058. The numbers near each tracing identify features whose wavelengths are listed in Table 2. Tracing Q2159 shows distinct [OI] emission at λ6300 (feature 29).

arise from atomic levels high above the ground state which would be populated only under conditions very different from those inferred by KOPS from the continuum temperatures. The trace for 1970 August 8 shows plainly the presence of [OI] 6300, which is the first clear evidence for this line in Type II supernovae. In KOPS, this line is present, but blended with Hα due to the large bandwidth of the observations.

Figure 2 indicates the numbered features for SN 1970g, while Table 3 gives the wavelengths. Since all the spectra were obtained at about the same time, the individual spectra are not listed. Because that time was near maximum light, the continuum was especially strong, and few lines were visible, just as on 1969 December 13 for SN 1969ℓ. The feature "7A" is seen in 1970g, but not in SN 1969ℓ.

c. Temperatures

The two scans in 1970 January of 1969ℓ (KOPS 1973) each exhibit a smooth continuum, which can be reasonably well approximated by a blackbody of T = 6000° ± 500° K. In each scan, the continuum flux falls more rapidly than the blackbody shortward of about 4000 Å, which may be the combined effect of line blanketing and the Balmer jump. Thus, the temperatures refer principally to the region 10,000 - 5000 Å, where the fit is very good. When used with appropriate caution, the UBV photographic photometry of Ciatti et al (1971) provides a measure of the temperature and luminosity at earlier times, where no scan is available.

The B and V colors for blackbodies derived by Matthews and Sandage (1963) can be described by the following equation.

TABLE 2

Feature	Proposed ID	Emission or Absorption	λ rest	Q2244 836	Q2159 806	Q2158 806	Q1811 620	Q1774 618	Q1773 618	Q1745 617	Q1713 616	Q1640 589	Q1591 568
1...	...	+	...	...	...	...	...	...	...	...	...	3539	...
2...	...	-	...	...	...	...	3679	...	...	...	...	3690	...
3...	...	+	...	...	...	...	3753	3751	...	...	...	...	...
4...	...	+	...	...	...	...	3805	3810	...	...	...	3778	...
5...	Ca II	-	3950	...	...	...	3875	3872	...	...	...	3853	...
6...	Ca II	+	3950	...	3987	4003	3977	3966	...	...	3981	3929	...
7...	Hδ	-	4101	...	4063	4068	4032	4046	...	...	4041	4022	3993
8...	Hδ	+	4101	...	4170	4171	4092	4097	...	...	...	4047	...
9...	...	+	...	4253	4241	4235	4220	4217	4214	4219	4219	...	...
10...	Hγ	-	4340	4296	4290	4296	4269	4274	4259	4260	4270	4252	4211
11...	Hγ	+	4340	4355	4355	4358	...	...	...	4350	...	...	...
12...	...	-	...	4397	4387	4388	4357	...	4341	4367	...	...	...
13...	...	-	...	...	4452	4440	4414	...	...	...	...	4390	4333
14...	...	-	...	4541	4527	4531	4505	...	4501	4499	4504	4498	...
15...	Hβ	-	4861	4805	4802	4801	4775	...	4777	4774	4776	4752	4712
16...	Hβ	+	4861	...	4864	4863	4841	...	...	4837	...	4846	...
17...	...	-	...	...	4888	4886	...	...	...	4876	...	4881	...
18...	...	+	...	4930	4931	4928	...	...	...	4905	...	4902	...
19...	...	-	...	4979	4982	4984	...	...	4963	4964	4965	4932	...
20...	...	+	...	5028	5031	5033	...	...	...	5047	...	...	...
21...	Mg I	-	5175	5120	5116	5117	5117	...	5109	5112	5111	...	...
22...	Mg I	+	5175	...	5186	5181	...	...	...	5182	...	...	...
23...	...	-	...	...	5485	5488	...	...	...	...	...	...	...
24...	night sky	+	5577	5578	5578	5576	...	....	...	5575	...	5572	...
25...	...	+	...	5702	5675	5679	...	...	...	...	...	...	...
26...	Na I	-	5890	5822	5825	5836	5837	...	...	5817	5786	...	...
27...	Na I	+	5890	5894	5916	5901	5881	...	...	...	...	5894	5913
28...	...	-	...	6060	6061	6125	...	...	...	...	...	...	...
29...	[O I]	+	6300	6300	6300	6300	...	...	...	...	...	...	...
30...	Hα	-	6563	6445	6450	6442	6426	...	...	6430	6422	...	...
31...	Hα	+	6563	6567	6564	6563	6546	...	...	6525	6523	6504	...

$$\frac{10{,}000\ ^\circ K}{T} = 1.59\ (B-V) + C\ , \qquad (4)$$

where T is the temperature of the blackbody, B and V the usual blue and visual magnitudes, and C is a constant which depends on the exact color system employed. For the Matthews and Sandage calibration, C = 0.70. Here, another calibration is established for the supernova in question. Using Ciatti et al's B-V = +0.75 on January 7, and T = 6000°K from the scans on January 5 and January 14, C is found to be 0.48 from equation (4). This new constant takes into account the color system used by Ciatti et al, and the deviations from a blackbody introduced by lines in this particular supernova, especially in the B-band.

With this calibrated value of C and equation (4) the B-V magnitudes observed by Ciatti et al are used to derive the photospheric temperature for each day of observation from 1969 December 3 to 1970 January 27. Using this derived blackbody temperature and the observed flux in the V-band, the angular size Θ is computed from eq. (1). The results are shown in Table 4 and in Figure 3 where the expansion of the photosphere is manifest. For the purpose of determining D, the values of $\Theta = R/D$ are, with R in units of 10^{15} cm and D in Mpc: JD 568, $\Theta = 0.039$ and JD 589, $\Theta = 0.115$.

This method of determining Θ is far from ideal: it would be better to determine all the Θ from scans. Some change in B-V could be due to changes in line intensity

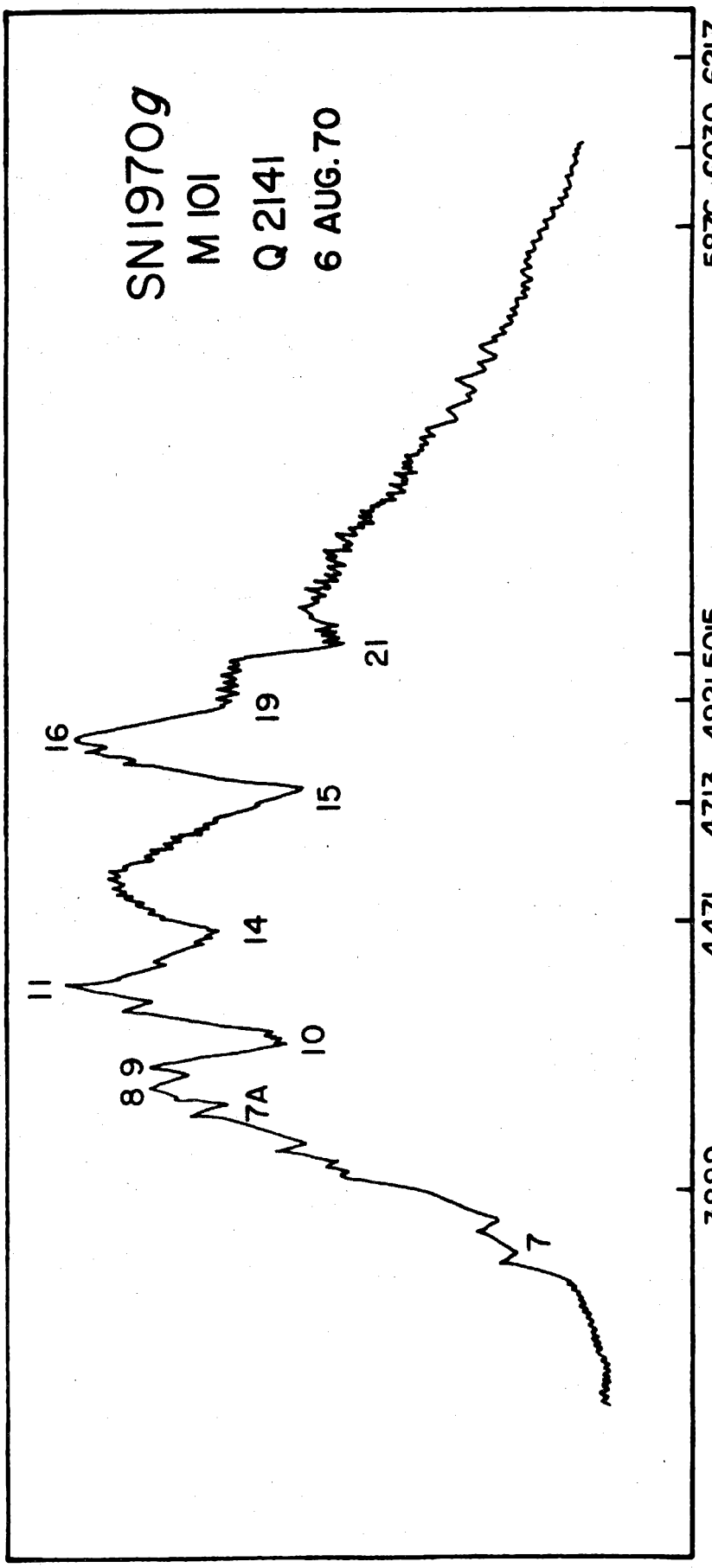

Fig. 2 -- Microphotometer density tracings of SN 1970g in M 101. The numbers refer to features whose wavelengths are listed in Table 3.

rather than to changes in the continuum; the extrapolation of equation (4) from 6000°K to 20,000°K in the early days of the supernova may not be justified. However, the evidence from spectra of this supernova is that the line intensities do not change radically at λ4400, near the peak sensitivity of the B-band or at λ5550 near the peak of the V-band. Also, when equation (4) is actually utilized in the distance determination, the extrapolation extends only to about 13,000°K.

The supernova 1970g appeared in a large H II region of M 101, which had previously been studied by Searle (1971), who determined its intrinsic reddening to be about $A_V = 0.44$ mag. In the absence of any more specific information, this value is adopted, and the scans of August 4 and September 8 are compared to blackbodies which have been reddened by the Whitford relation (Miller and Mathews 1972). The temperatures are found to be 9500°K ± 500°K for 1970 August 4, and 5000°K ± 500°K for 1970 September 8. As for 1969ℓ, the observed flux in the ultraviolet falls more rapidly than the blackbody curve, even when reddening is included. Photographic photometry by Kristian and Tammann (private communication) indicates B-V ≃ -0.10 for about August 4, and B-V ≃ +1.20 for early September. If E(B-V) ≃ 0.15, the equivalent of equation (4) can be obtained with these data.

It is

$$\frac{10{,}000\ ^\circ K}{T} = 0.73(B-V) + 1.23, \qquad (5)$$

where B-V has been corrected for extinction.

TABLE 3

Feature	Emission or Absorption	ID	λ_{rest}	λ_{meas}
7...	-	Ca II	3950	3845
7A..	-	...	...	4067
10...	-	Hγ	4340	4222
11...	+			4339
14...	-	....	...	4450
15...	-	Hβ	4861	4740
18...	+			4843
19...	-	...	...	4914
21...	-	Mg I	5175	5064
30...	-	Hα	6563	6390
31...	+			6503

The numerical coefficients are drastically different from those for 1969ℓ. This is due to the importance of changes in line intensities for 1970g. The August 4 observation shows a nearly featureless continuum near λ4400, while the September 8 scan indicates a very strong absorption feature at λ4400, which is of great importance in increasing the B magnitude.

Fortunately, the two scans of August 4 and September 8 are sufficiently separated in time that they provide enough information for a distance estimate without the use of broadband data. The angular sizes at the two dates are $\theta_1 = 0.144$ and $\theta_2 = 0.285$ in units of 10^{15} cm/Mpc.

III LINE PROFILES AND PHOTOSPHERIC VELOCITY

This section shows how the velocity of the matter at the photosphere can be obtained from a study of the observed line profiles. The work of KOPS indicates that the radiation from a supernova consists of a broad continuum, with superimposed P-Cygni line profiles. Their results suggest that the supernova envelope consists of a photosphere with a scattering atmosphere above it. The shape of the P-Cygni profiles indicates an expanding atmosphere: there is depletion of the continuum to the blue side of the line and contribution above the continuum to the red. It will be shown that the velocity of the matter at the photosphere corresponds to that velocity where the depletion of the continuum is the maximum, if the latter is sharp and well-

TABLE 4

Date		JD	V	B-V	T (10^4 K)	R/D (10^{15}/Mpc)
1969	Dec. 6	561	13.20	0.00	2.10	0.025
	Dec. 7	562	13.20	-0.05	2.50	0.021
	Dec. 8	563	13.25	+0.15	1.40	0.028
	Dec.10	565	13.20	+0.20	1.26	0.038
	Dec.11	566	13.30	+0.15	1.40	0.035
			13.20	+0.20	1.26	0.038
	Dec.16	571	13.30	+0.20	1.26	0.039
	Dec.26	581	13.35	+0.40	0.90	0.060
	Dec.27	582	13.25	+0.55	0.74	0.087
	Dec.29	584	13.45	+0.50	0.79	0.071
1970	Jan. 1	587	13.40	+0.65	0.66	0.102
	Jan. 2	588	13.35	+0.70	0.63	0.115
	Jan. 7	594	13.35	+0.75	0.60	0.129
	Jan.25	612	13.40	+0.75	0.60	0.126
	Jan.27	614	13.35	+0.75	0.60	0.129

defined, or if the latter exhibits a flat trough, to the velocity at the red edge of the depletion trough.

The following simple model of the photosphere and scattering atmosphere is considered: all the matter ejected from the supernova is assumed to be expanding radially and freely from a central point of explosion. Then the matter with velocity v travels a distance from the center R = vt, where t is the time since the explosion. The effective photosphere is located at the depth at which the continuum optical depth approaches 1. At that depth, the matter has a certain radial velocity v_{ph}. As the expansion progresses, the continuum radiation arises from layers deeper and deeper below the surface; simply put, v_{ph} decreases with t.

The radiation from the photosphere travels out through the expanding envelope until it is scattered. The scattering process can be viewed in two steps: first the primary absorption of the continuum photons, and second, the subsequent re-emission of these photons. In the latter process the emitted photons may be absorbed again and re-emitted several times if the line opacity is large. Consider first the primary absorption of the continuum radiation along the line of sight. There will be absorption by atoms moving towards the observer with velocities ranging from zero to the maximum expansion velocity. (In this discussion the relative motion between the center of expansion and the observer is ignored, though it is considered in analyzing the actual observations). Figure 4

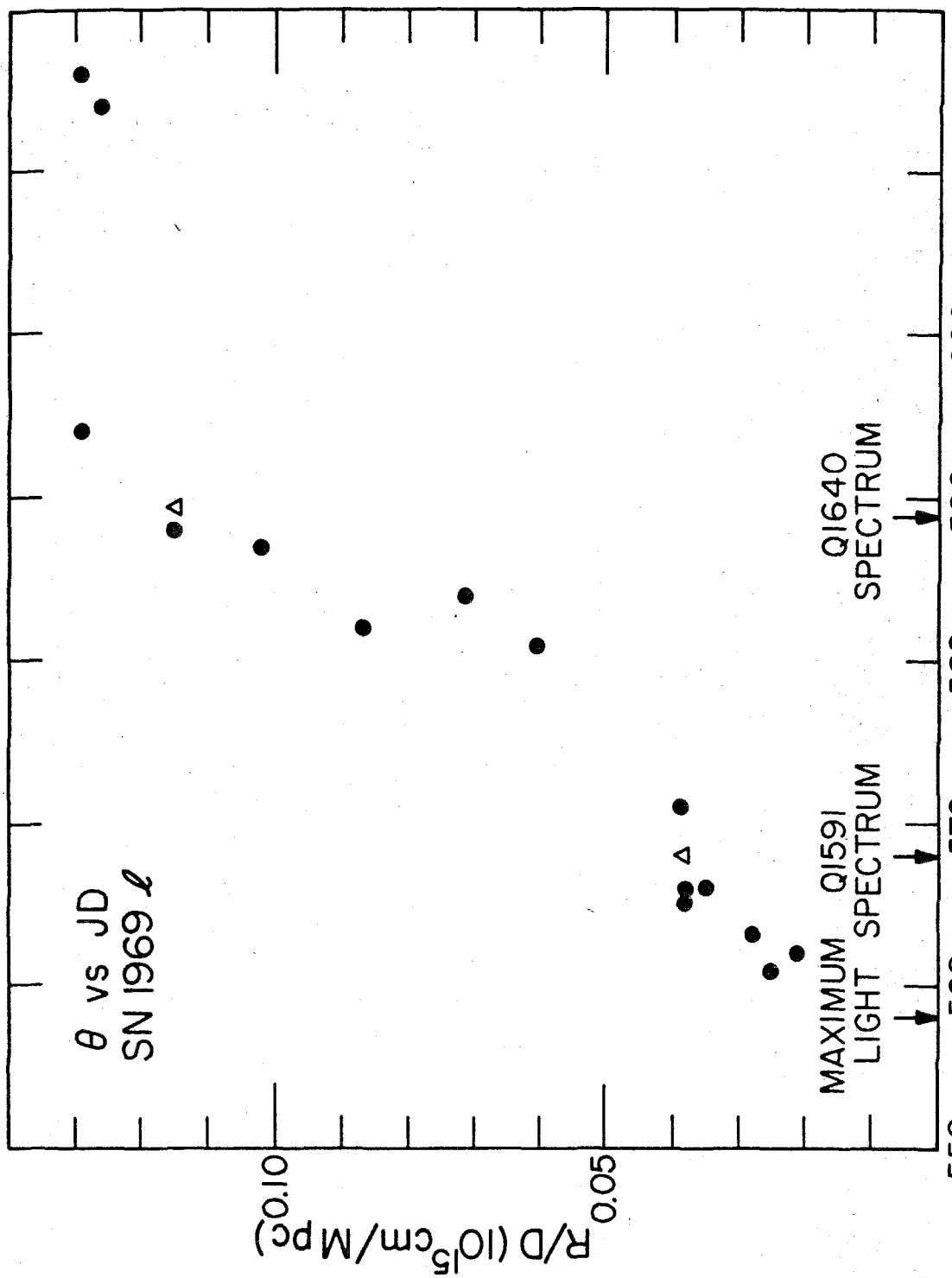

Fig. 3 -- Angular size as a function of time. The angular sizes computed from broadband observations are shown by filled circles (●), those adopted for the distance determination are shown as triangles (Δ).

shows a side view of the loci of atoms with velocities relative to the observer of v'_{obs} and v''_{obs}, where $v'_{obs} < v_{ph}$ and $v''_{obs} > v_{ph}$. In the simple case of $v \propto R$ assumed at every instant in this model, the locus is a disk perpendicular to the line of sight. At each point of the envelope, the line opacity is the same along any path and is given by

$$\tau = \frac{hc}{4\pi} BN \left(\frac{R}{v}\right) . \qquad (6)$$

Here B is the Einstein absorption coefficient and N is the number of atoms per unit volume in the lower state of the resonance line at that point in space. The number density of atoms in the upper state of the transition is much smaller and can be neglected. Equation 6 depends on the assumptions that the thermal widths are much smaller than the widths due to mass motions (Castor 1970) and that N varies slowly over a velocity range of the order of the thermal velocity. In the present case, the radial velocities are typically ≥ 3000 km sec^{-1}, while the thermal velocities of the scattering atoms are not more than ~ 10 km sec^{-1}, so that the two approximations above are clearly valid.

Although N changes slowly in one thermal velocity interval, it is a rapidly decreasing function of the expansion velocity. This can be demonstrated in two ways: first, the observed P-Cygni profiles show that

at the very blue edge of the profile, the depletion of the continuum decreases with increasing velocity. This result is possible only if N is a decreasing function of v. Second, even if the density is independent of velocity before free expansion begins, the subsequent motion would lead to a decreasing density distribution ($N \alpha v^{-2}$) at later times. In the model supernovae of Grassberg et al (1971) the density is a decreasing function of velocity when free expansion begins, and their numerical calculations of supernova luminosities and expansion velocities are in qualitative accord with the observations of KOPS.

Consider the primary absorption of the continuum photons. It is clear from Figure 4 that at observed velocities v_{obs} less than v_{ph} the amount of absorption decreases with decreasing velocity because the area of the photosphere from which absorption is possible shrinks rapidly with decreasing velocity below v_{ph}. For v_{obs} greater than v_{ph} the amount of absorption at each velocity depends on the values of τ on a surface of constant v_{obs}. With N a decreasing function of v, it is clear that, in the case when $\tau \leq 1$ at each point in the envelope, the amount of absorption decreases with increasing velocity above v_{ph}. In this case, the primary absorption of continuum photons is greatest at v_{ph}. If $\tau \geq 1$ at the inner part of the scattering envelope, the profile of the primary

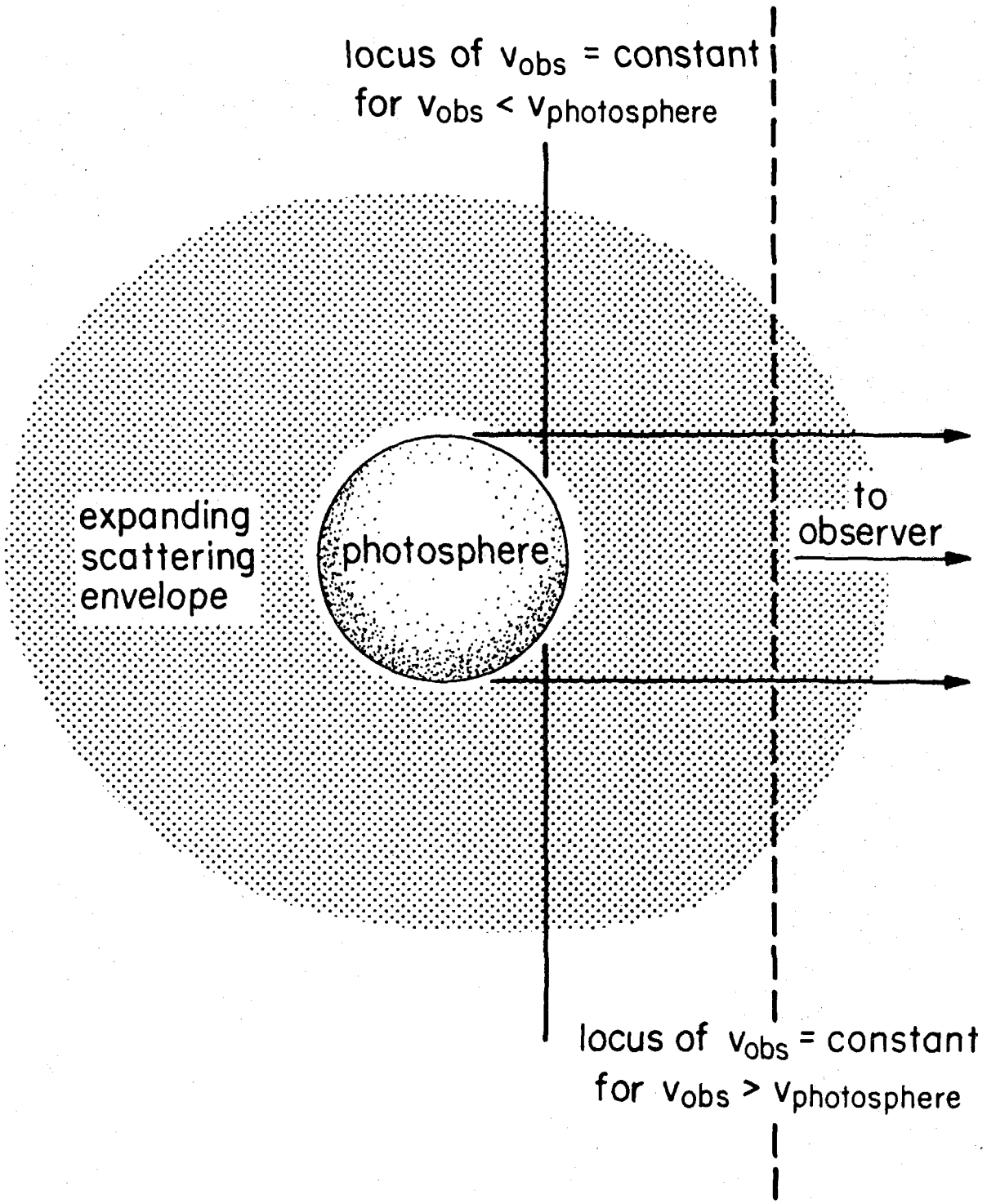

Fig. 4 -- Schematic diagram of the expanding atmosphere in which resonant scattering takes place. The loci of constant observed velocities are shown in the case where v is proportional to r.

absorption exhibits a flat trough, with the velocity at the red edge of the absorption trough equal to v_{ph}. Figure 1 provides some evidence that this change actually takes place in the line profiles for Hβ and Hγ (features 15 and 10). In the earliest spectrum Q1591, both lines have flat bottoms, while by Q1811, about 50 days later, the lines show the sharp cusps of optically thin lines

The subsequent re-emission of the absorbed photons does not alter these conclusions. In the case of $\tau \leq 1$ everywhere, it can be derived analytically that for N decreasing faster than v^{-2}, the re-emission of the absorbed photons does not shift the position of maximum depletion of the continuum as determined from the primary absorption alone. In this optically thin case, the emission profile of the re-emission peaks at $v = 0$, and decreases symmetrically with larger and smaller observed velocities (when the slight asymmetry due to occultation of the far side of the envelope by the photosphere is ignored). The superposition of this emission profile and the primary absorption profile constitutes the observed P-Cygni shape. If $\tau \gg 1$ over large parts of the envelope, the emission is no longer symmetric about $v_{obs} = 0$. More emission is observed at $v_{obs} < 0$ than at $v_{obs} > 0$, because at large optical depths, there is more back-scattered radiation than forward scattered radiation. For example, in the one-dimensional case in which radiation is only scattered forward or backward, the intensity of the back-scattered beam is $\tau/2$ times the forward scattered intensity. Caroff, Noerdlinger, and Scargle (1972) have considered the pertinent case of three-dimensional scattering in a rapidly expanding atmosphere. Their numerical results show that as the opacity is increased, there is indeed skewing of the scattered

radiation to the red. However, as τ is increased beyond about 3 - 5, they find that little additional asymmetry results. Thus in the case $\tau >> 1$ in the inner parts of the scattering envelope, the re-emission of the primary absorbed photons may cause a round-off of the depletion trough in the absorption profile. Nevertheless, in the resulting P-Cygni profile, the matter velocity at the photosphere corresponds closely to the velocity observed at the red edge of the absorption trough.

The line profiles for various distributions of matter with velocity have been calculated, in a manner similar to that of Castor (1970). In Figure 5 , two of these profiles are shown: in case A, $\tau \leq 1$ throughout the envelope. In case B , the maximum value of τ is 10, and $N\alpha v^{-4}$, but no account is taken of the preferential back-scattering, to demonstrate the maximum effect of optical depth on the absorption profile. The agreement between v_{obs} at the red edge of the observed absorption and v_{ph} is satisfactory. Also presented is an observed profile, case C. Each channel covers about 4950 km sec^{-1} in velocity, which distorts the true profile somewhat. With appropriate adjustment of parameters theoretically calculated profiles can provide a good representation of the observed data.

It has been assumed in this section that the matter velocity at the photosphere v_{ph} is well defined. This is true when the photosphere has a sharp boundary where the continuum optical depth changes rapidly with respect to the

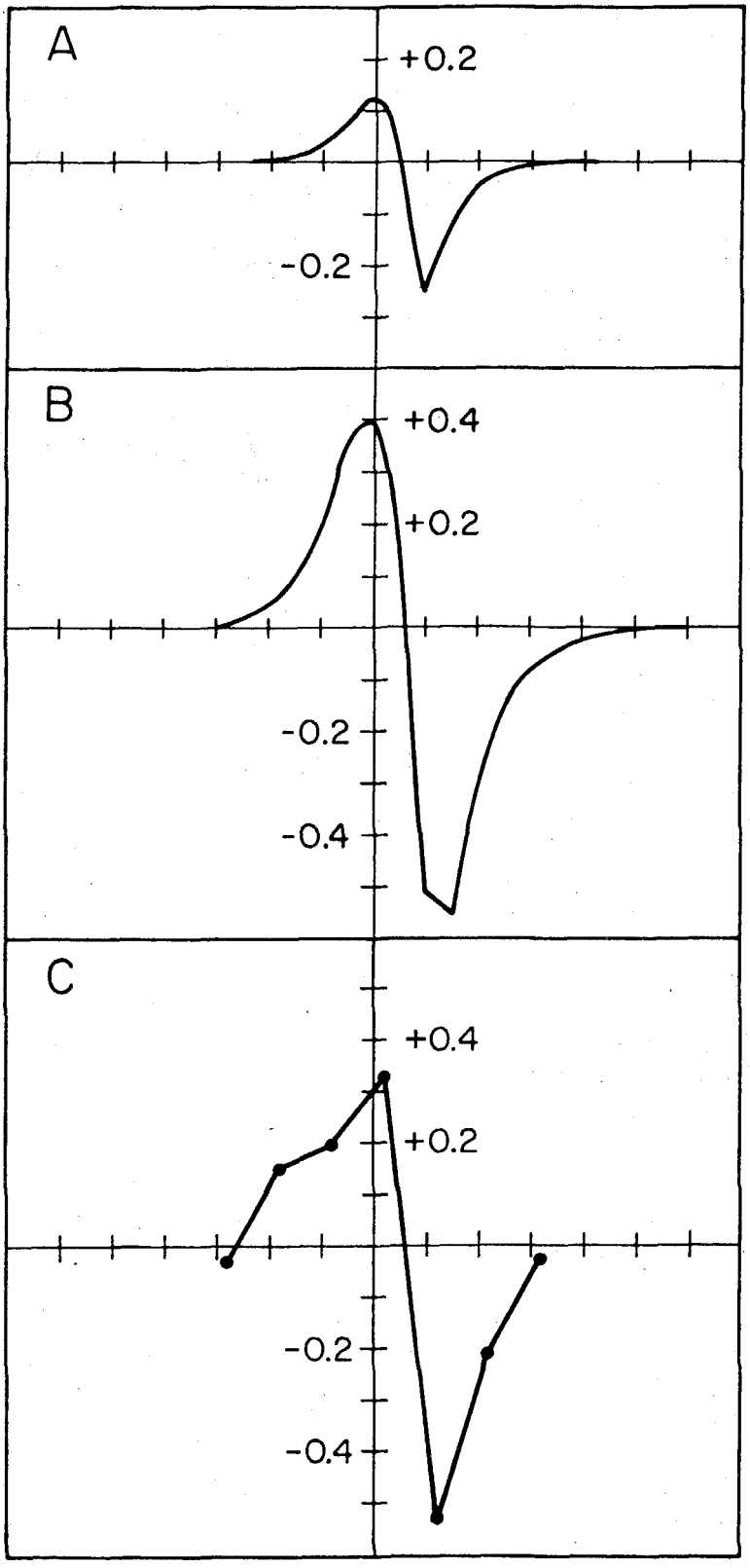

Fig. 5 -- (A) Calculated line profile for an optically thin line. The graph shows $(f_{line} - f_{continuum})/ f_{continuum}$ versus velocity, where the unit is $v_{photospheric}$. Here $v \propto r$, $N \propto v^{-4}$. (B) As in (A), but for an optically thick line $\tau \leq 10$. (C) Hβ profile from scan of SN 1969ℓ on 1970 Jan. 13. Here the velocity unit is 4950 km s^{-1}.

velocity. Figure 3 demonstrates that the calculated angular size of the photosphere increased rapidly and smoothly during the first month of expansion. The assumption of a sharp photospheric boundary is most reliable during this interval, and the values of v_{ph} used in the distance determination are all obtained during that epoch.

d. Measured Values

Although the "red edge of the absorption minimum" is a somewhat vague prescription, in practice there is little ambiguity in measuring the appropriate quantity. The Balmer lines are used because they are prominent, unequivocally identified, and have relatively unimportant hyperfine splittings. The results given in Table 5 are based on spectra for NGC 1058, and on a combination of spectra and scans for M 101.

IV DISTANCES

The distances to 1969ℓ in NGC 1058 and 1970g in M 101 can be obtained by employing the information in Table 5 in equations (2) or (3). For NGC 1058, the use of $v_{ph} = 8.6 \times 10^8$ cm sec^{-1} and $\Theta = 0.039$ on JD 568 together with $v_{ph} = 6.0 \times 10^8$ cm sec^{-1} and $\Theta = 0.11$ on JD 589 in equation (3) gives a distance D = 12 Mpc and t_o about JD 558. This t_o is close to the time of maximum light observed by Ciatti et al (1971), although errors involved in its determination are too large to infer any cause for that

TABLE 5

SN	Date*	Θ†	Plate	Hβ‡	Hγ‡	Hδ‡	Adopted‡	V_{galaxy}‡	V_{ph}‡
1969ℓ	568	0.039	Q1591	8.5	7.8	...	8.1	0.5	8.6±0.5
1969ℓ	589	0.115	Q1640	5.8	5.5	5.3	5.5	0.5	6.0±0.5
1970g	802	0.144	Q2141	7.1	7.1		7.1	0.3	7.4±0.5
1970g	837	0.285	SCAN	3.8	4.5		4.0	0.3	4.3±1.0

* Julian Date - 2,440,000

† Θ in units of 10^{15} cm Mpc^{-1}

‡ All velocities in units of 10^{8} cm sec^{-1}

coincidence. The photospheric radii implied by this distance are $R = 0.47 \times 10^{15}$ cm on JD 568 and $R = 1.4 \times 10^{15}$ cm on JD 589. The effect of an initial radius different from zero is to add 0.34 Mpc to the distance to NGC 1058 for every 0.1×10^{15} cm. Since no pre-supernova star was visible at the site of the eruption, the initial radius is likely to be smaller than 0.1×10^{15} cm, and the error introduced in the distance determination is negligible.

For M 101, using the data from Table 5 for v_{ph} and Θ, the distance to M 101 is about 6.5 Mpc. The photospheric radius on JD 837 is 1.8×10^{15} cm, and the initial time is about JD 788. This is 16 days before maximum, which indicates the uncertainty in the relation between t_o and the time of maximum light.

V DISCUSSION

a. Distances and Magnitudes

The distances derived here agree surprisingly well with the extragalactic distance scale of Sandage and Tammann (1973), who propose distances of 7.2 Mpc to the group containing M 101, and 13.9 Mpc to the group containing NGC 1058. To determine whether this agreement is mere coincidence or true convergence requires an estimate of the errors inherent in the supernova distances.

The temperatures derived from scans are probably good to 500°K, but those from broadband colors may have substantially

larger errors. The resulting values of θ may vary by 20%. The velocities are well determined in the cases where a spectrum was employed, but have significant errors where a scan was used. If the theory of Section III is reliable, the distances are only subject to about 10% uncertainty from this source when spectra are used, and about 30% when a scan is used. The effects of a non-zero R_o are less than 5%, for $R_o < 10^{14}$cm.

Considering the data actually employed, the errors incurred in the M 101 distance imply D=6±3 Mpc and for NGC 1058 D=12±3 Mpc. For the given recession velocities, these distances correspond to a mean Hubble constant of H=60±15 km sec^{-1} Mpc^{-1}.

The temperature and radius data for 1970g give clear evidence of decreasing luminosity: for JD 802, $L=4\pi R^2\sigma T^4= 4.64\times10^{42}$ erg sec^{-1}, while for JD 837 $L=1.44\times10^{42}$ erg sec^{-1}. Even though the spectrum is not really blackbody, most of the energy emitted at these epochs is observed in the band 10,000-3300 Å. This result contradicts the prediction based on a simple pulsar powered supernova, where the luminosity remains nearly constant (Ostriker and Gunn 1971).

The observed magnitude and the distance can be used to estimate the absolute magnitude near maximum light. For NGC 1058, if m_B = 13.0 and D = 12 Mpc, then M_B = -17.4 and for M 101, if $m_B \simeq$ 11.0 and D = 6 Mpc, M_B = -17.9. Thus, despite some crudeness of the estimate, the absolute magnitudes of these two Type II supernovae were quite similar.

The method described in this paper is superficially

similar to that of Branch and Patchett (1973) for Type I supernovae. The method here has some advantages in that it refers to observations made of a single object, rather than a collection of observations and extrapolations for all supernovae of a given kind. Also, somewhat arbitrary factors such as the "center to limb effects" and the ratio of "photospheric velocity" to "actual velocity of ejected material are replaced by a model of line formation. Last, the identifications of the Type II lines used here are not disputed so that the rest wavelengths are known, while the Si II line identified in Type I/Branch and Patchett by is less certain.

b. Improvements

Most of the errors inherent in this method of distance determination could be removed by carefully planned observation If the temperature and flux density were measured several times, and spectra taken on consecutive nights, the distance would be highly overdetermined, observational errors would become unimportant, and only the systematic errors would remain. This could be done with a well-equipped 2 meter telescope to magnitude 15 using conventional technology, and to a considerably fainter limit with an efficient photon-counting spectrograph.

With an ordinary photoelectric scanner, or photometer with appropriate filters, the flux could be measured in two bands which are free of lines. For example, the bands λλ7000-7500 and λλ5250-5500 would be suitable for Type II

supernovae. This color defines a temperature, and the flux would permit an estimate of θ. If spectra are available on neighboring nights, v_{ph} can be found from the red edge of absorption minima. It is important that the observations be obtained during the first month after maximum; the expansion of the photosphere is not simple at later times, as illustrated by the flattening of Figure 3.

It is not unreasonable to expect that the application of this method to supernovae in the local supercluster could provide an independent and accurate estimate of the Hubble constant, and the absolute magnitude of supernovae.

REFERENCES

Baade, W. 1926, Astron. Nachr., 228, 359.

Branch, D. and Patchett, B. 1973, MNRAS, 161, 71.

Caroff, L.J., Noerdlinger, P.D., and Scargle, J.D. 1972, Ap.J., 176, 439.

Castor, J.I. 1970, MNRAS, 149, 111.

Ciatti, F., Rosino, L., and Bertola, F. 1971, Mem. Soc. Astron. Italia, 42, 163.

Grassberg, E.K., Imshenik, V.S., and Nadyozhin, D.K. 1971, Ap. Space Sci., 10, 28.

Humason, M.L., Mayall, N.U., and Sandage, A.R. 1956, Astron. J., 61, 97.

Kirshner, R.P., Oke, J.B., Penston, M., and Searle, L. 1973, Ap.J., 185, 303.

Matthews, T.A. and Sandage, A.R. 1963, Ap.J., 138, 30.

Miller, J.S. and Mathews, W.G. 1972, Ap.J., 172, 593.

Ostriker, J.P. and Gunn, J.E. 1971, Ap.J. (Letters), 164, L95.

Sakurai, A. 1960, Communications in Pure and Applied Math. 13, 353.

Sandage, A.R. 1956, Ap.J., 125, 436.

Sandage, A.R. and Tammann, G. 1973, private communication.

Searle, L. 1971, Ap.J., 168, 327.

de Vaucouleurs, G. 1967, Astron.J., 72, 730.

Chapter 6

The Atmospheres of Type I Supernovae

I INTRODUCTION

Although Type I supernovae are readily recognized by their similarity to Minkowski's (1939) series of spectra of SN 1937c, their spectra have long eluded a really coherent explanation. This paper reports scanner observations of Type I supernovae, and in particular of the bright supernova 1972e discovered in NGC 5253 by Kowal (1972). The scans provide a quantitative spectrum over the interval 3400-11000 Å, with resolution from 20 to 360 Å.

Much of the data in this chapter, and some of the discussion have already been presented in Kirshner et al (1973a), and Kirshner et al (1973b). In this chapter, the emphasis is on unifying the presentation of the old results, and on new interpretations, therefore the discussion of the uniformity of Type I spectra, and the comparison with earlier work has not been repeated.

With the aid of the new observations, some progress in understanding the nature of Type I supernovae has been made. The continuum is shown to carry the bulk of the flux at early times, and the continuum temperature has been determined. Many lines are shown to possess P Cygni profiles characteristic of resonant scattering in an expanding envelope. Some of the strong lines have been identified with lines of Ca II, Na I, and possibly Mg I

and Fe II that also appear in Type II supernovae. The possible identification of H I in recombination leads to a measure of the electron density. The atmospheric velocities in SN I's may reach 20 000 km s^{-1}: the corresponding photospheric velocities are consistent with the kind of distance determination performed in Chapter 5.

The most puzzling problem in understanding the spectra of Type I supernovae is the behavior at late times. Observations of 1972e extend over 700 days past maximum light, and show the presence of emission features which are difficult to explain. One possibility, explored in this paper is that most of them are formed by collisional excitation of forbidden lines of Fe II, and possibly collisional excitation of permitted Fe II lines. Although this requires an unusually high abundance of iron, this does not seem impossible in the context of explosive nucleosynthesis.

II CONTINUUM MEASUREMENTS

a. Introduction

Immediately upon Kowal's (1972) discovery of SN 1972e, an intensive spectrophotometric and infrared photometric study of its development was begun at the Hale Observatories (Kirshner et al 1973a, 1973b). The overall properties of the continuous energy distribution, as determined from those studies, are discussed in this section.

We found that from 1972 May 16 (JD 2441453), the day

after discovery, to 1972 July 31 (JD 2441529), the overall shape from 4000 Å to 2.2μ could be represented by a blackbody which decreased in temperature from about 10 000°K on May 23, to 7500°K on June 5, then remained at about 7000°K until at least July 8. Observations made more than 200 days after discovery could not be represented by a blackbody, and showed only modest evidence for the presence of the continuum.

b. Observations

Observations at wavelengths shorter than 1.0μ were obtained either with the 5m Hale telescope and the multichannel spectrometer, or with the Palomar 60-inch reflector and a single channel scanner. The multichannel scans had bands 20 Å wide for $\lambda \leq$ 5950 Å and 40 Å for $\lambda \geq$ 5950 Å during the initial series of observations and were obtained in about 10 minutes. The 60-inch scans employed 40 Å bands and an S-17 cathode in the blue, and 80 Å bands with an S-1 cathode in the red. Because of the southern declination of NGC 5253 (δ=-31°), the available observing time was brief, so the single channel scans for June 15 and June 25 are the result of combining a red and a blue scan from successive nights.

Standard deviations for multichannel observations are 0.01-0.02 mag except in the far violet and near infrared. The standard deviations for single-channel observations

are much less than 0.1 mag except in the deepest absorption features, and in the vicinity of 1.0μ, where the errors maybe as large as 0.3 mag. Because the supernova was so far south, the corrections employed to account for atmospheric extinction were carefully investigated. Observations of suitable nearby stars demonstrated that extinction had been properly dealt with in the supernova, so that observations could be put on the absolute calibration scale based on α Lyr (Oke and Schild 1970). Because atmospheric water-vapor emission dominated the star's radiation between 8900 and 9600 Å these wavelengths have been deleted.

Infrared measurements were obtained by Willner, Becklin, and Neugebauer at 1.25μ (1.15-1.4μ), 1.65μ (1.5-1.8μ), and 2.2μ (2.0-2.4μ), with the 200-inch and the Mount Wilson 100-inch (2.5m), and some additional observations were obtained using the Mount Wilson 24-inch (61 cm) telescope. With only one exception, supernova magnitudes were established by comparison with the nearby star HR 5097, which was measured on several nights relative to a standard system in which the infrared magnitude of α Lyr is 0.00 in each band. The adopted magnitudes of HR 5097 are [1.25] = 5.65, [1.65] = 5.55, [2.2] = 5.62.

Figure 1 presents light curves at five wavelengths, where the flux density is represented by an AB magnitude, to facilitate comparison with broadband measurements.

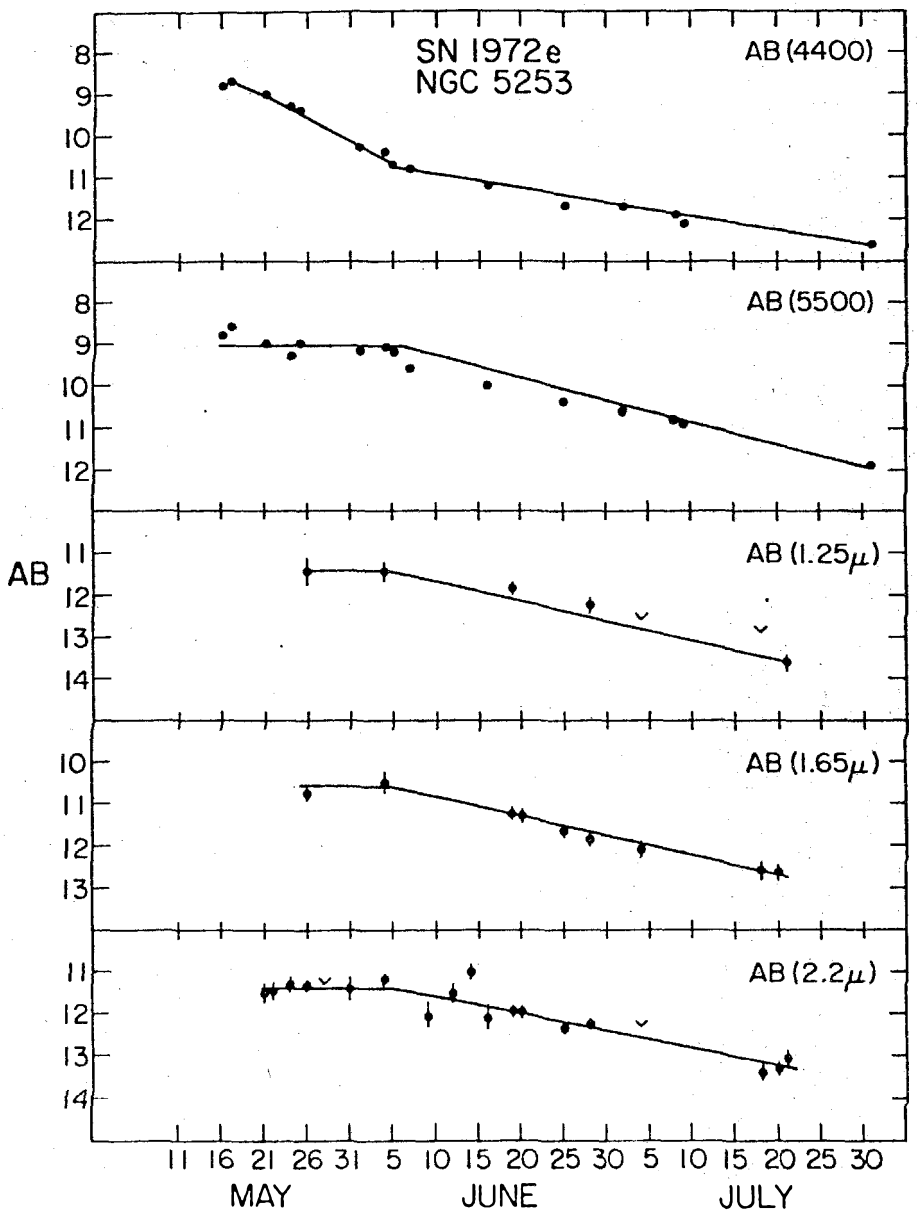

Fig. 1 -- Flux density in AB magnitudes at five wavelengths, in 1972 from May 10 to July 31 for supernova 1972e.

AB = -2.5 log f_ν-48.60 where f_ν is in units of erg $cm^{-2}s^{-1}Hz^{-1}$. AB(4400) and AB(5500) represent the flux density obtained from the scans by averaging over a 500Å band near 4400Å and 5500Å respectively. AB(5500) corresponds very closely to the standard V magnitude. Infrared measurements were converted to the same system through AB(1.25μ) = [1.25] + 0.94, AB(1.65μ) = [1.65] + 1.42, and AB(2.2μ) = [2.2] + 1.92.

All the light curves except AB(4400) show the same general behavior. The magnitudes are nearly constant from the earliest observation to about June 5, then all decline at about the same rate of 0.045 mag per day. The solid lines in figure 1 exaggerate this similarity: except for AB(4400), all the lines have the same shape. The AB(4400) curve decreases very rapidly until about June 5, then shows about the same rate of decrease as the light curves at other wavelengths. Figure 2 illustrates the long term behavior of AB(4400): the slow decline that began about June 5 (JD 472) persists for another 50 days, then a slower extremely linear decay at a rate of about +0.013 mag day^{-1} is observed for the following 640 days.

The decrease in the infrared continued through 1972 September, when a limit of (2.2μ) > 14.2 was set from 40-inch observations at Las Campanas by Becklin and Neugebauer. To increase the signal-to-noise ratio of this observation, data were taken in a broad band covering both the 1.65μ and 2.2μ bands. The flux in the 2.2μ band was derived by

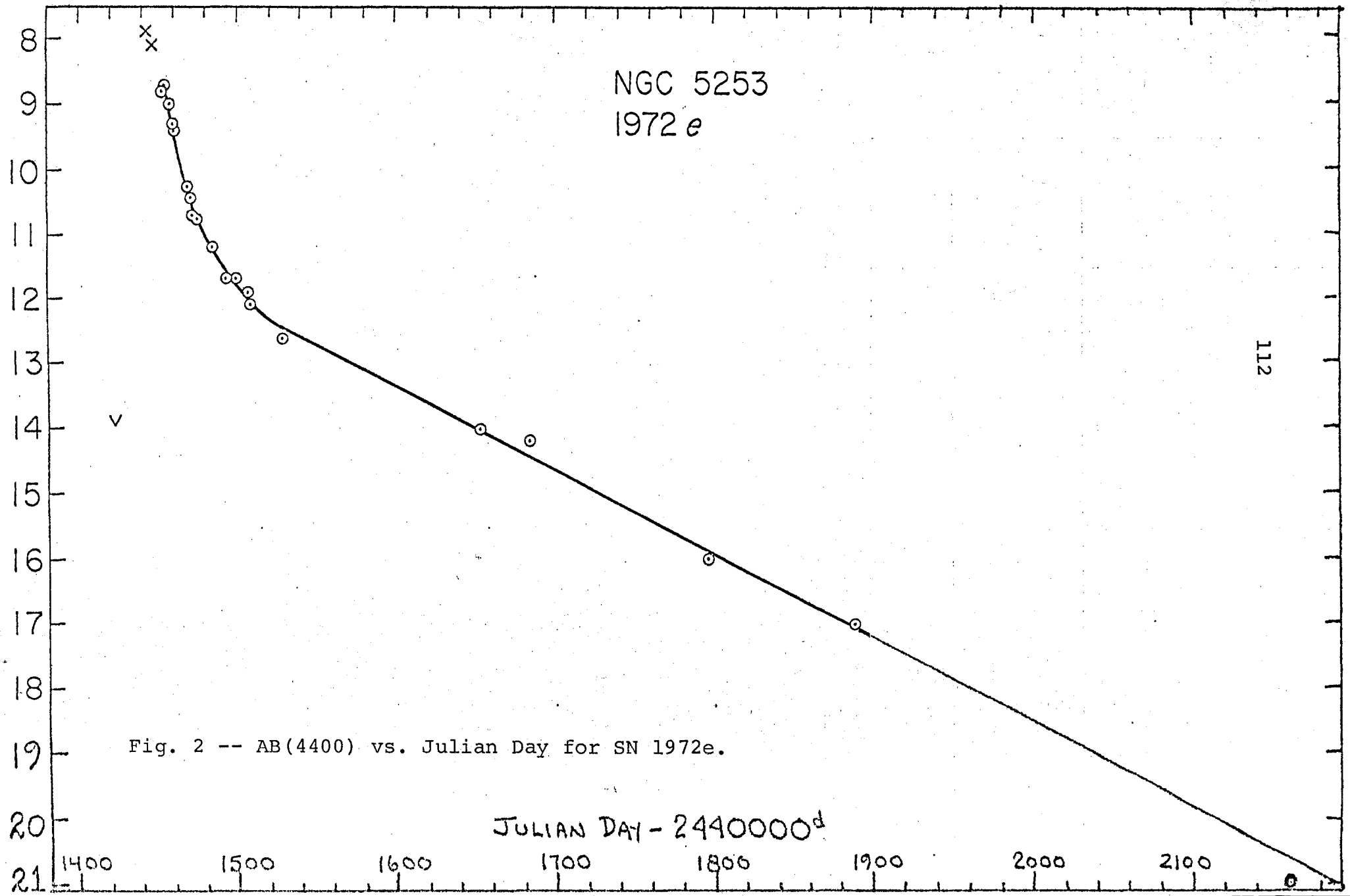

Fig. 2 -- AB(4400) vs. Julian Day for SN 1972e.

assuming the same ratio between the 1.65μ and 2.2μ flux as observed from May through July. These results disagree with those of Lee et al (1972) who reported no decrease in infrared flux between May 22 and June 29.

At longer wavelengths, upper limits to the flux were set at AB(3.5μ) > 12.27 on June 4. On June 20, AB(4.8μ) > 9.04 and AB(10.0μ) > 8.97.

c. Interpretation

The photometric behavior exhibited in figure 1 can be accounted for in terms of a simple model, analogous to the model for Type II continua. We suppose the observed effects are produced by an expanding, cooling photosphere. At first, because of cooling, the decrease in flux density is most rapid at short wavelengths, which leads to the initial decay of AB(4400) while the longer wavelengths are relatively unaffected. The subsequent decay at all wavelengths from June 5 (JD 1472) to July 31 (JD 1529) is due to the shrinking of the photospheric boundary at roughly constant temperature. The slow decay at 4400Å at later times is not closely related to the continuum.

This picture is considerably strengthened by figure 3, where a smoothed energy distribution over the entire observed wavelength range is illustrated for each night on which data were obtained at 1.2, 1.65, and 2.2μ. Each scan shown is the one made closest in time to the infrared measurements--

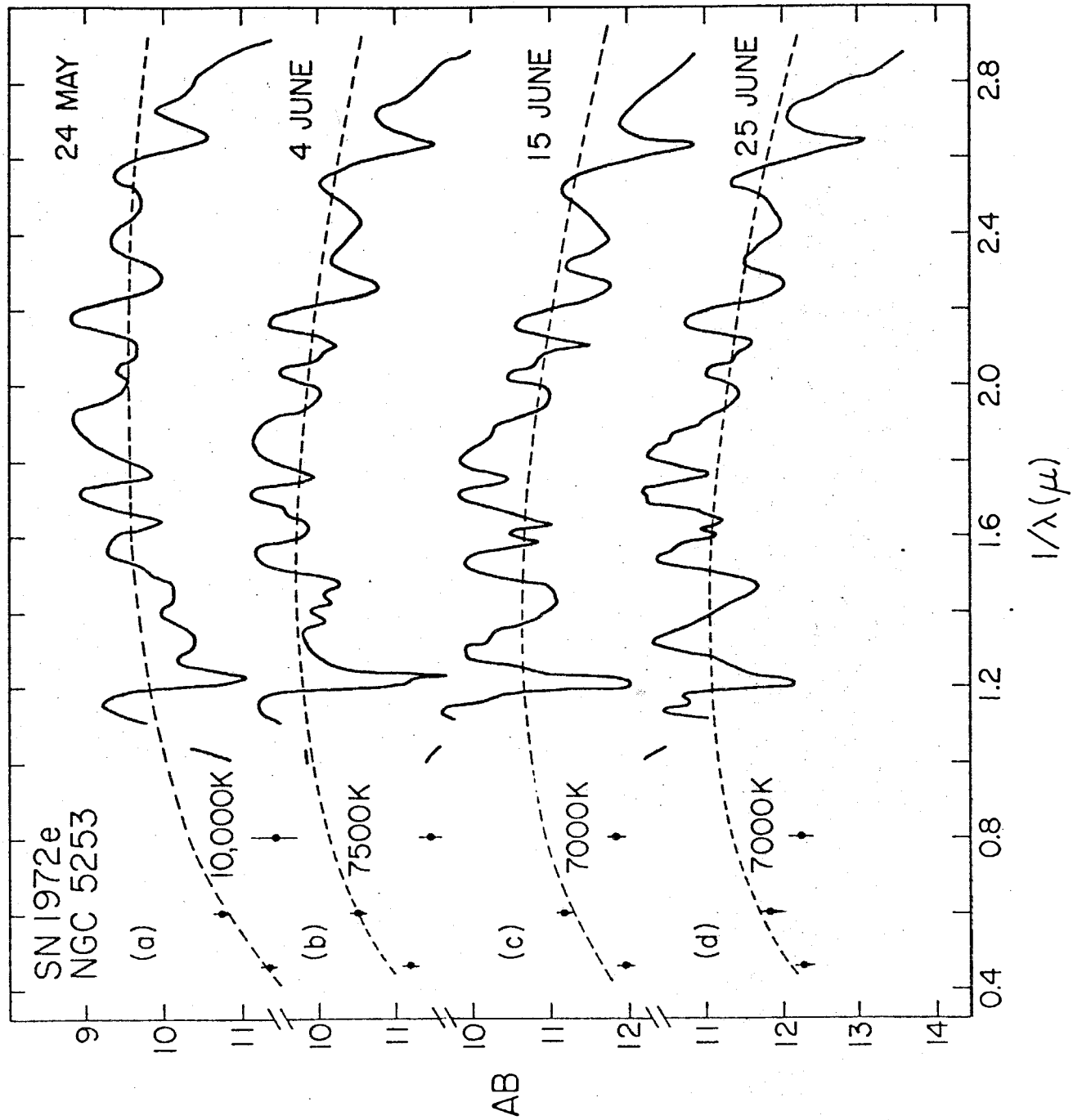

Fig. 3 -- Energy distributions for SN 1972e.

the time interval never exceeds four days. Because the 200-inch telescope was used for the infrared photometry, all the simultaneous scans shown were obtained with the 60-inch.

For each scan, a blackbody curve is illustrated which attempts to account for the overall energy distribution on the assumption that both emission and absorption features may be present. As in the blackbody fits to Type II scans, the blackbody represents the overall flux distribution reasonably well, although there appears to be a large deficit of flux in the 1.2 band, and the blackbody lies above the observations shortward of 4000Å. Table 1 summarizes the temperatures and inferred radii, if the distance to NGC 5253 is 4 Mpc (Sersic et al 1972).

The smooth and gradual change with time of the overall continuum shape is a very striking phenomenon in the first 75 days of observations. It demonstrates quite clearly that the SN I spectrum during that era is not a superposition of emission bands, but that just as for SN II's, the bulk of the energy is radiated in the continuum.

III LINE IDENTIFICATIONS

a. Line Profiles

The full, detailed scanner observations are shown in figures 4, 5, 6 and 7, which plot log f_ν vs. logν. The spectra are clearly much more complex than those of SN II's

TABLE 1

Date	JD-2440000	T (°K)	r(ph) (cm)	v(ph) (cm s^{-1})	t (s)	vt (cm)
1972 May 24	1461	10000	1.1+15	1.4+9	7.8+5	1.1+15
1972 June 4	1472	7500	1.6+15	1.1+9	1.7+6	1.9+15
1972 June 15	1483	7000	1.1+15	1.0+9	2.7+6	2.7+15
1972 June 25	1493	7000	1.0+15	1.0+9	3.5+6	3.5+15

but certain strong similarities are present. In figure 8, scans of 1972e at the earliest observation and at age one month are compared with scans of 1970g, a SN II, at the same stages. Even casual inspection of this figure reveals certain similarities between the two types. In particular, the features near 3900Å and 8600Å which were identified in Type II spectra with Ca II lines are prominent in Type I spectra in the two months following maximum light, and are present beyond.

Because the fundamental conditions of a differentially expanding atmosphere around a source of continuum emission are met, we expect resonance lines in Type I envelopes to produce P Cygni profiles. The features at 3900 and 8600Å seem to show the required shape. Reference to figure 4 of chapter 4, where a linear flux scale is employed, shows that despite some irregularity the 8600Å line does have a characteristic P Cygni profile. Though the line is blended, the red edge of the emission peak indicates a velocity of about 20 000 km s^{-1}, while the blue edge of the absorption, though very poorly defined, shows a shift of about the same magnitude.

As indicated in table 1, the velocity of the red edge of the absorption minimum for Ca II H and K has been determined roughly from the scans. For the dates JD 1461 and JD 1472, the radius of the photosphere determined from this velocity and the time is consistent with the photospheric

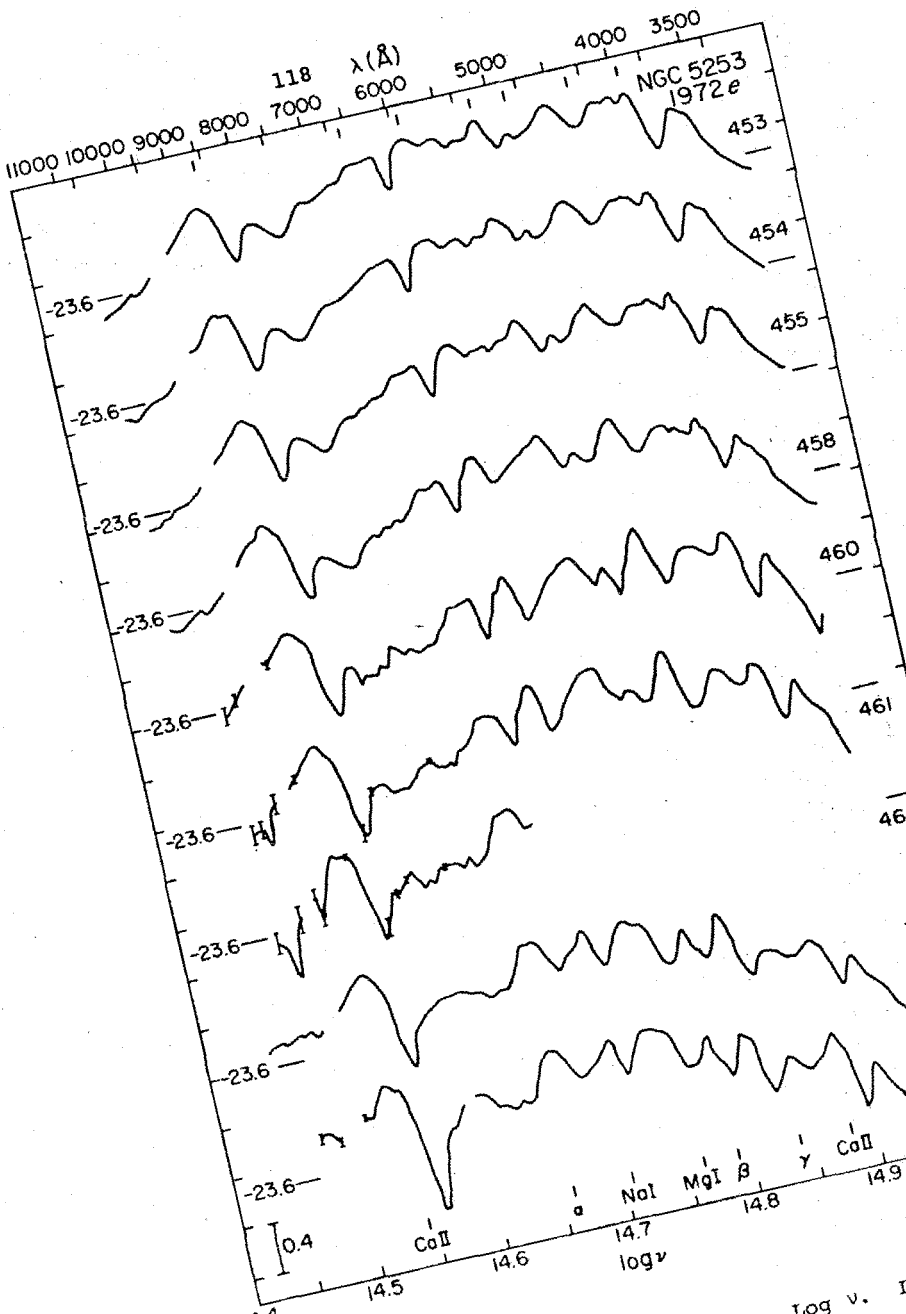

Fig. 4 -- Scans of SN 1972e. Log f_ν vs. Log ν. I
ts of JD to right of each scan.

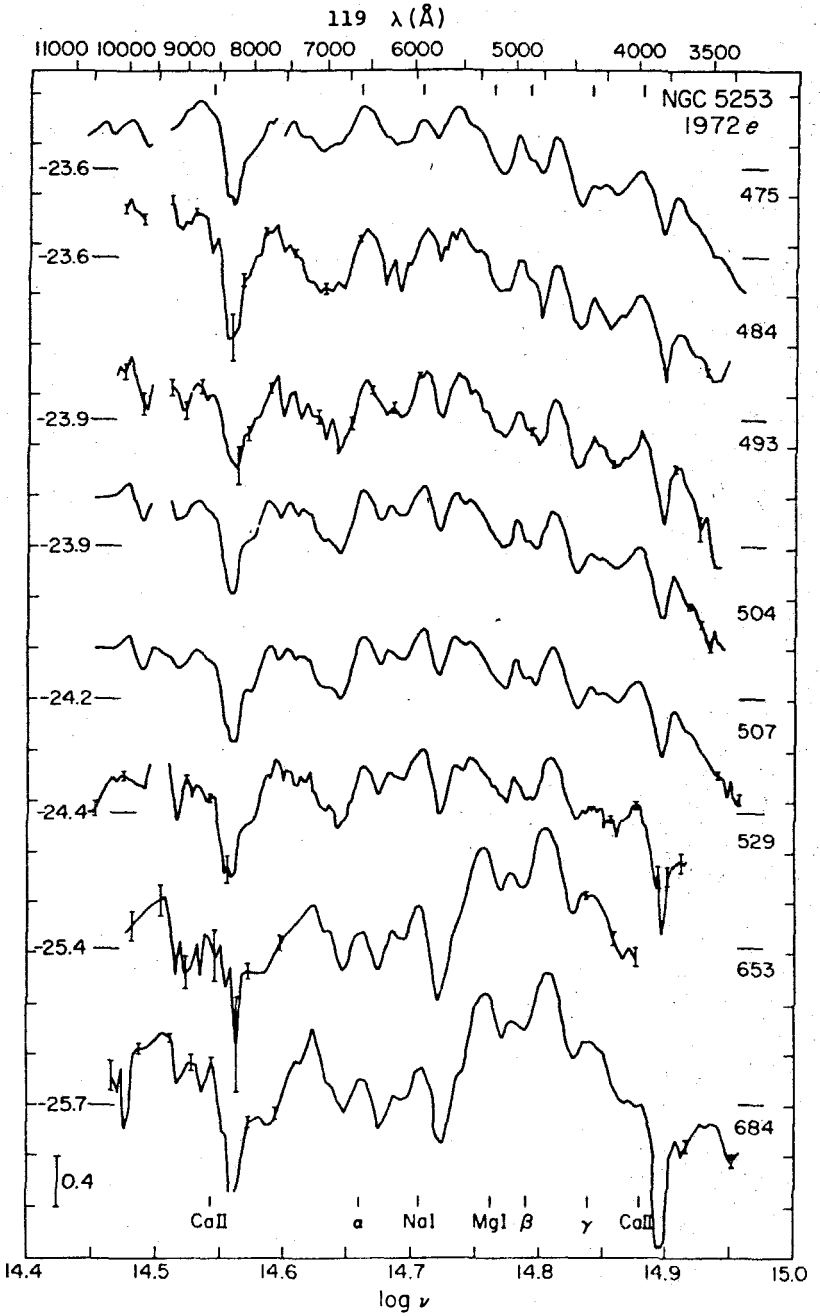

Fig. 5 -- Scans of SN 1972e. Log f_ν vs. Log ν. Last three digits of JD to right of each scan.

radius derived from the continuum flux density, the continuum temperature, and the assumed distance of 4 Mpc. After JD 1472, the photosphere begins to shrink, so that the photospheric radius is not equal to vt.

b. Lines seen in SN II's

The P Cygni shape of the Ca II lines recurs in many spectra. Inspection of figures 4 and 5 reveals several other pairs of emission and absorption features separated by about the same interval in logν-- corresponding to the same expansion velocity. The strongest of these have their emission peaks at $\lambda\lambda$8700, 5890, 5170, 4600, and 3970. These are the wavelengths of the strongest features, aside from the Balmer lines, in the spectra of SN II's. We suggest that they are in fact the same features. The identifications with Ca II λ8600, Na I λ5890, Mg I λ5174, the Fe II blend near λ4600, and Ca II H and K, seem sound in the Type I envelopes for the same reasons they seemed sound for the Type II. These are all strong resonance-like lines from easily populated levels of common atoms in the prevailing ionization state. Given a strong continuum, it is natural that they produce strong P Cygni profiles. However, as we shall see, the features near 5200Å may be the result of [Fe II] emission, even at early times.

Aside from these features, the Type I spectra in the first two months present a somewhat dismaying complexity. Features are transient, and blended so thoroughly that it

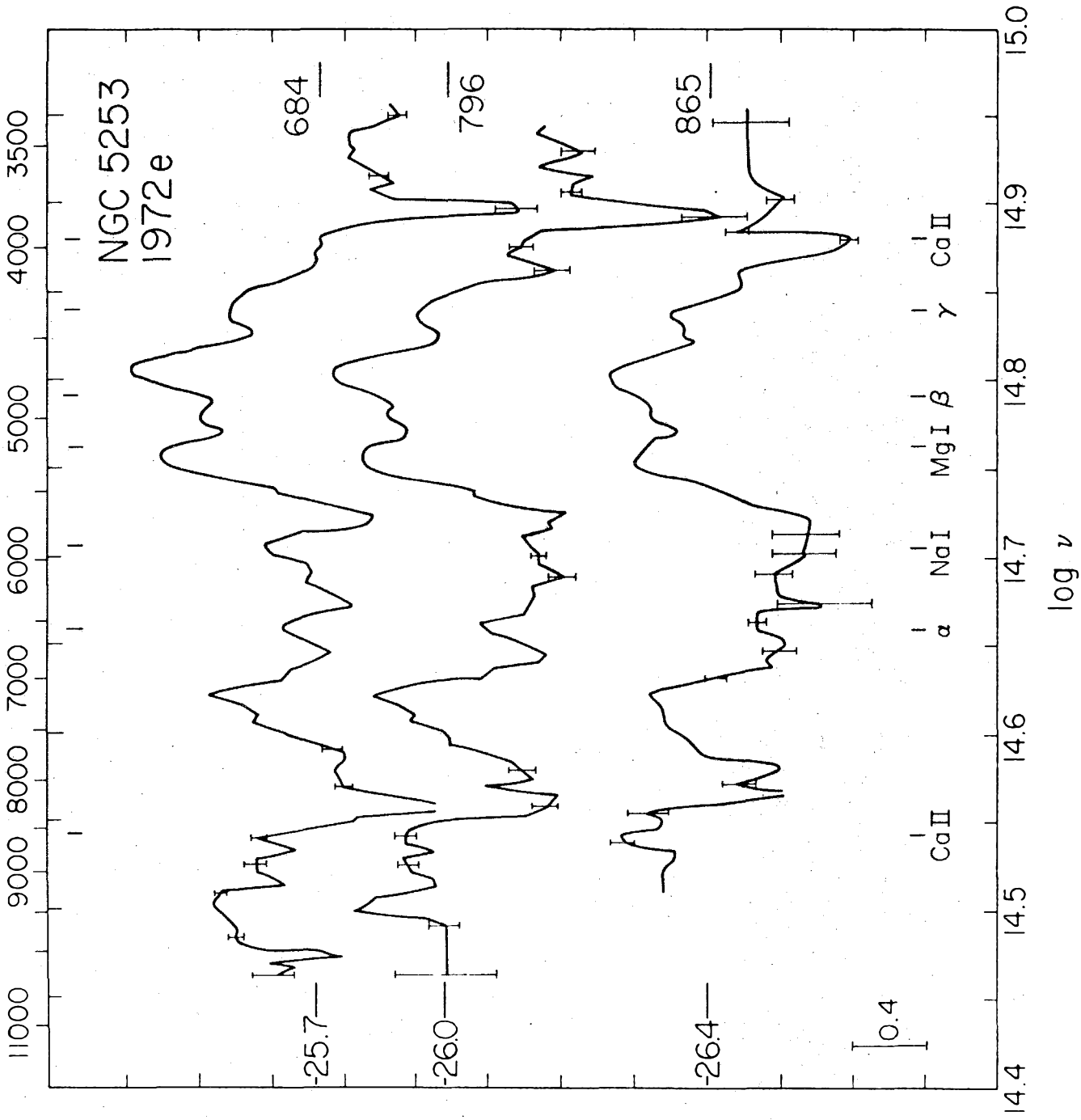

Fig. 6 -- Scans of SN 1972e. Log f_ν vs. Log ν.
Last three digits of JD to right of each scan.

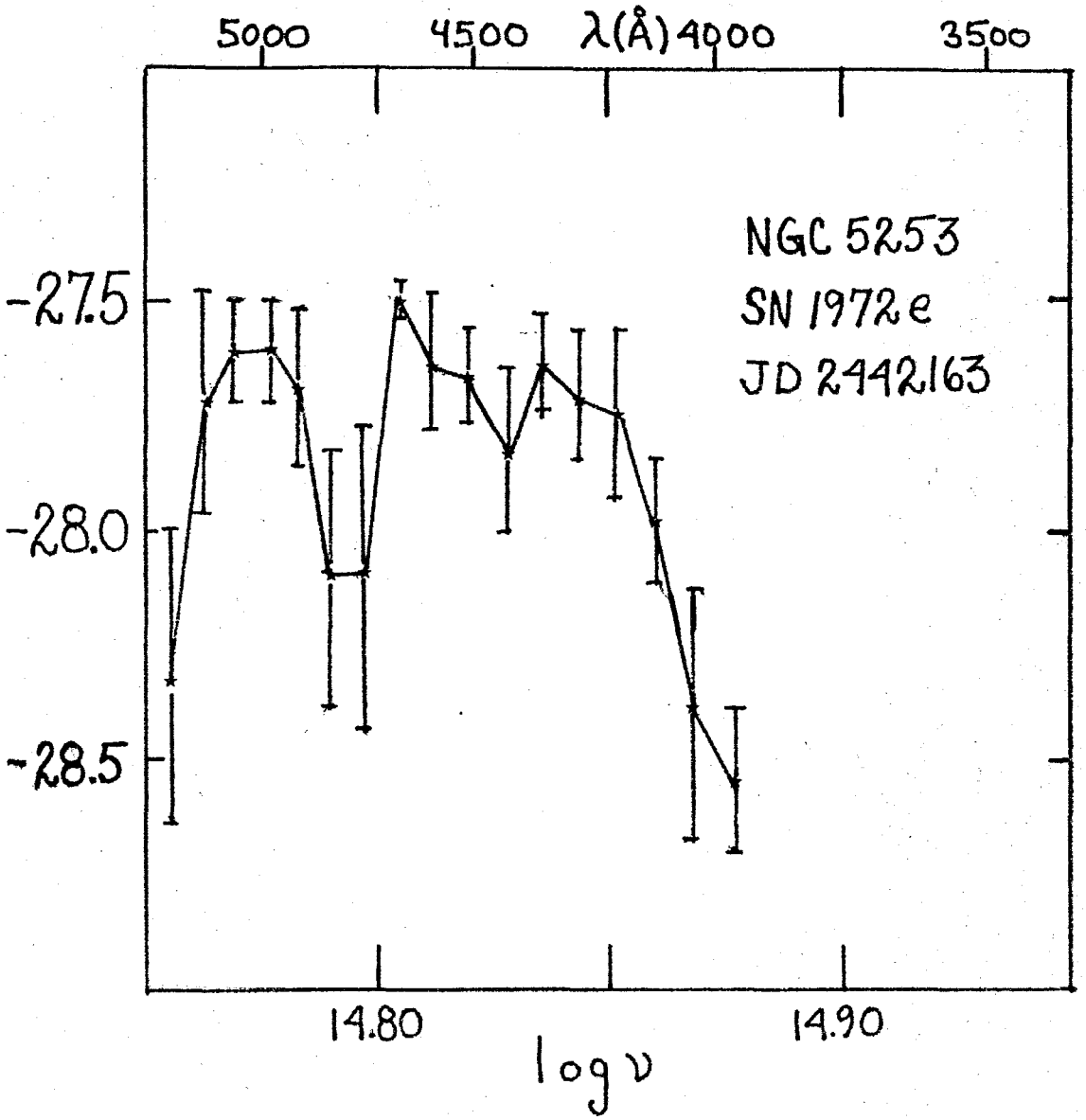

Fig. 7 -- Scan of SN 1972e more than 700 days after maximum light. Log f_ν = -27.5 is AB = 20.9.

is very difficult to specify the wavelength or even count the components. The details of the identification problem in the spectra of Type I supernovae remain of great interest and comparable difficulty.

c. Balmer Lines

One important question is whether the Balmer lines are present in the spectra of SN I's. During the first week of observation, there are no clear signs of Balmer lines, except for a broad blend near Hα. However, beginning on JD 1460, a strong emission emerges from the blend at Hα, which by JD 1484 seems to be quite clearly at the correct wavelength. At about the same time, a feature emerges at the wavelength of Hγ. Near Hβ, the spectra are complex and seriously blended, and it is not clear whether Hβ is present or not. Although some doubt lingers about the correctness of the identification, and about the exact location of the continuum, table 2 provides estimates of the Hα photon flux, and the electron density on the assumption that $n_e = n_p$.

We find that despite the relative weakness of the hydrogen features, the electron densities (10^{10}-10^7 cm^{-3}), and masses of ionized matter (about 0.1 $M_\odot$) are only somewhat smaller than the corresponding numbers for SN II's. The small Hα feature observed before JD 1460 is masked by the strong continuum at early times.

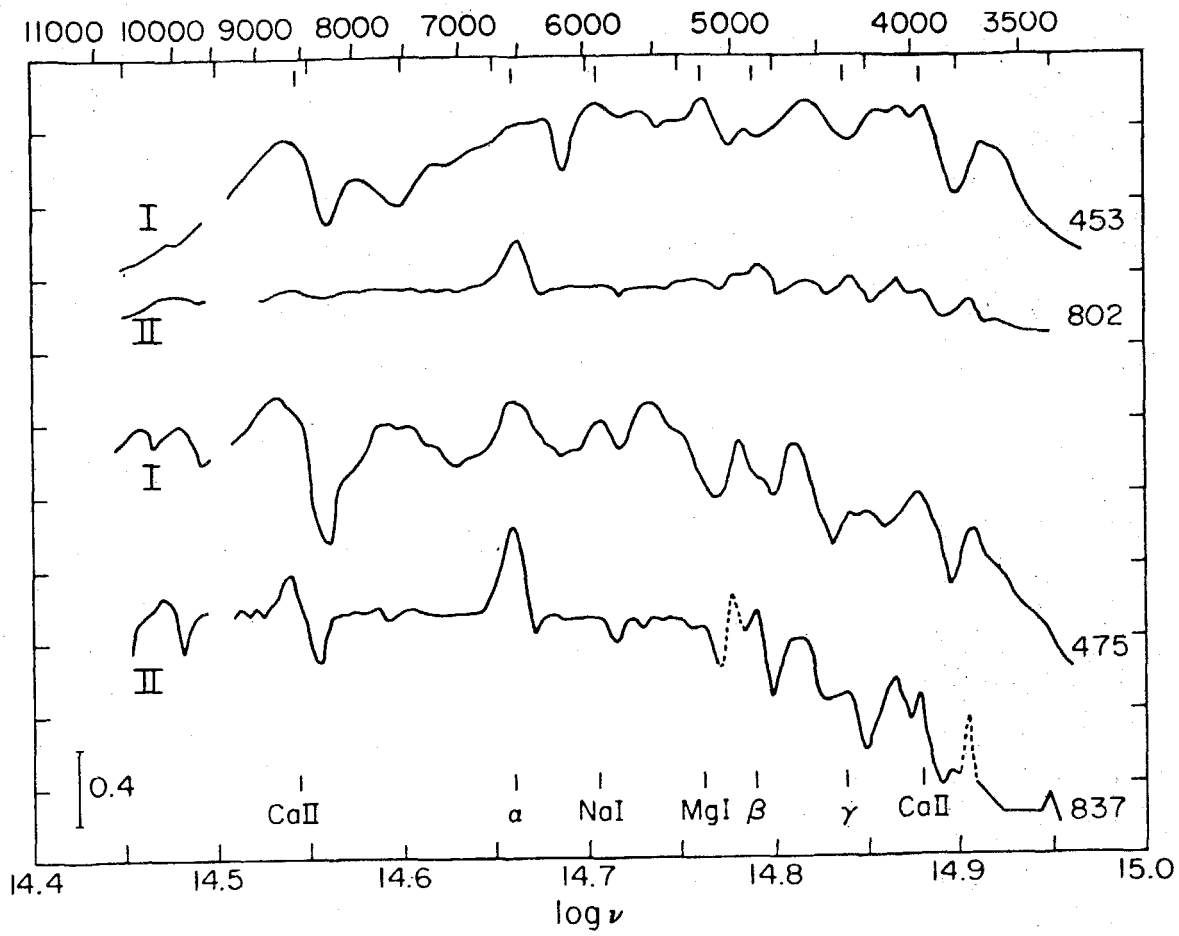

Fig. 8 -- Comparison of spectral energy distributions of Type I and Type II supernovae near maximum light and one month later. The Type I curves are from SN 1972e while those for Type II are from SN 1970g.

The problems of recombination times are similar to those for Type II described in Chapter 4. The photospheric flux of ionizing photons beyond the Balmer limit is somewhat larger than the recombination rate in the first two months of observation, so that the balancing situation described in Chapter 4 can operate.

From the mass of ionized gas and the Lyman α escape rate, we estimate that the total mass of hydrogen in the Type I envelope may be somewhat smaller than for Type II: about 1 $M_\odot$ of hydrogen is adequate. We will use this rough estimate of hydrogen to infer the relative abundance of other elements.

d. General Considerations

If the continuum behavior and line formation mechanisms are so similar for SN I's and SN II's, and if both contain substantial amounts of hydrogen, what can account for the qualitative difference between the two kinds of spectra? One possibility is that the stronger and more numerous lines in Type I supernovae are caused by the presence of more line forming ions relative to the continuum forming hydrogen and electrons. It may be that the puzzlingly complex spectra of SN I's are the result of an unusually high relative abundance of elements heavier than hydrogen. In that case, the total mass of a Type I envelope might be of order 1 $M_\odot$, with an abnormally large amount of heavy elements. If Type I

TABLE 2

JD-2440000	f(Hα) (erg cm^{-2} s^{-1})	Q(Hα)	R(atm) (cm)	V_3 (cm^3)	α(T)	n_e	$M_\odot$
1453	4-11	2+52	(8+14)	2+45	2-14	2+10	4-2
1460	2-11	1+52	(1.1+15)	6+45	2-14	1+10	5-2
1472	1-10	6+52	(1.6+15)	2+46	3-14	1+10	1-1
1484	3-11	2+52	(1.7+15)	2+46	4-14	5+9	7-2
1493	2-11	1+52	(1.8+15)	2+46	4-14	4+9	7-2
1504	2-11	1+52	(2.3+15)	5+46	5-14	2+9	9-2
1507	1-11	6+51	(2.4+15)	6+46	5-14	2+9	7-2
1529	5-12	3+51	(3.4+15)	2+47	5-14	6+8	8-2
1653	4-13	3+50	(8.5+15)	3+48	5-14	4+7	9-2
1684	2-13	1+50	(1.0+16)	4+48	5-14	3+7	8-2
1796	7-14	4+49	(1.5+16)	1+49	5-14	8+6	9-2

supernovae come from evolved stars, or if nucleosynthesis takes place during the explosion, such an enriched envelope is not an unlikely possibility.

IV LATE PHASES

a. General Features

Every effort was made by J. B. Oke, J.E. Gunn, and J.L. Greenstein to obtain multichannel scans of 1972e long after maximum light. Figures 6 and 7 illustrate the *fruits of their labors. When compared* with the last of the scans taken before the sun obscured the supernova, JD 1529, some important changes are apparent.

Most important, the continuum ceases to be the dominant feature, although it is still present. The emissions at λλ5300, 5000, 4200, and especially at λ4600 have become the outstanding features. Because the continuum lies so far below these features, it is most unlikely that they are formed by scattering photospheric photons. Indeed, the Ca II lines, and the Na I D-lines have emission peaks which lie so far below the strong emissions that the absorptions are the conspicuous features. The continued presence of these absorptions is the best evidence for the persistence of the continuum. By JD 1865, the Ca II absorptions can scarcely be distinguished from the noise, with H and K completely masked by atmospheric emission. Thus it seems fair to say

that the continuum, and the scattering lines formed from continuum photons are of much less importance in the late phases than they were at earlier times.

The blend of features between λ4000 and λ5500 deserves special attention, as most of the flux in the era JD 1653-2163 is concentrated in that blend. Table 3 lists the observed flux from each of the components of that blend, and the equivalent photon emission rate if SN 1972e is at a distance of 4 Mpc. It is a curious piece of luck that the light curve AB (4400), which is akin to the m_b and m_{pg} that have been observed for many supernovae, reflects the important physics of the supernova envelope throughout its evolution. For the first 20 days its rapid decrease reflects the change in temperature of the continuum, for the next 50 days it responds to the shrinkage of the photosphere, and in most of the late phases, during its long exponential decline, it reflects the flux in the dominant broad blend of emission lines.

b. The Strong Emission

The strong emission lines have some unusual properties which offer some insight into their possible identifications. First, the decrease in the flux from the whole blend is exponential over the entire range of observations. Second, the relative strengths of the lines change very little. And third, almost all the lines at late times are contained in the one strong blend from 5300-4000Å.

At early times, the features at λ5200 and λ4600 were identified with Mg I and Fe II P Cygni profiles. Since these are certainly not the correct identifications in the late scans, when resonant scattering is not the dominant process, we could suppose that they were correct at early times, but that some other feature, at about the same wavelength emerged at just the right moment to become part of the strong emission blend. This is not a far-fetched hypothesis, as the relative strengths and exact wavelengths of most lines are not steady, yet it is more economical to suppose that the features observed at late times account for the bumps in the early scans. The features seen at λλ4600, 5000, and 5200 at late times can be traced back to the scan on JD 1469 with some certainty, while the presence of the λ4200 feature is more doubtful. Table 3 gives the observed flux in each of the lines, and the sum for the blend over a range of time extending from JD 1469 to JD 2163. During this time interval the decrease in the flux from the combined lines is very well approximated by the equation,

$$\log F = -0.55(t/10^7) + 41.69.$$

This exponential decay of the flux is very rapid, but less rapid than the decay of the continuum. Hence these lines appear as strong emissions at late times. The physical interpretation of this exponential decay forms the basis for Morrison and Sartori's (1969) model for Type I spectra,

TABLE 3

JD-2440000	1453	1469	1529	1653	1684	1796	1865	2163
$t/10^7$(s)	.017	0.16	0.67	1.75	2.01	2.98	3.50	6.15
f(5200)	----	8-11	2-11	8-12	4-12	8-13	3-13	----
f(5000)	----	6-11	3-12	3-12	2-12	5-13	2-13	3-14
f(4600)	<2-10	7-11	2-11	2-11	1-11	2-12	6-13	4-14
f(4200)	----	----	<1-12	4-12	2-12	5-13	4-13	3-14
f(4600)/ Σf	----	0.30	0.49	0.54	0.56	0.53	0.44	0.41
ΣF (erg s^{-1})	<5+41	4+41	9+40	6+40	3+40	7+39	3+39	2+38
ΣQ (photon/s)	<1+53	9+52	2+52	1+52	8+51	2+51	6+50	4+49

but another explanation is advanced here.

The fact that the relative intensity of these four lines is constant is illustrated in table 3, where the fraction of the total blend that comes from 4600 is listed. This suggests that all the lines respond in the same way to changes in density and temperature. This could happen if all the lines arise from the same ion, and from about the same level. Alternatively, it could result from several atoms, all of which are of changing ionization, have similar energy level differences, and have the same dependence of photon production on electron density.

Because only the lines from λ5300-4000 are very strong (although there are other features in emission, especially near 7200 Å), we must check carefully that the identifications for the strong lines we do observe do not imply the presence of strong lines we do not observe.

c. Mechanisms for Line Production

At late times, when the continuum is weak compared to the strong emission features, some mechanism other than resonant scattering is required to produce the lines. In this section, general arguments are advanced to show that collisions can provide the needed excitation, and that the observed lines are likely to have low Einstein A's.

One possible way to produce emission lines is through recombination. At the late times, when the continuum lies

far below the lines, each recombination leads to the net destruction of the recombining ion, as there are insufficient ionizing photons from the continuum to replace the lost ion. The strong blend of lines between λλ4000-5300 persist for 200 days, emitting 10^{52} photons each second. If the lines are formed by recombination, this requires about 2×10^{59} ions. These ions will have a mass of about 200 solar masses if they are protons. Since they are surely more massive, the total mass becomes intolerably high. For this reason, recombination cannot be responsible for the observed emission.

Collisional excitation can be considerably more efficient. We distinguish two general cases, corresponding to high $A/n_e\gamma$ and low $A/n_e\gamma$, where γ is the collisional de-excitation rate. For high $A/n_e\gamma$, every upward collision produces a photon, so the total number of photons, Q, produced from a given mass of target atoms goes as $n_e \exp(-E/kT)$. For low $A/n_e\gamma$. the collisions establish the ratio between the lower state and the upper state at the electron temperature; we call such lines thermalized. Then $Q \propto \exp(-E/kT)$, independent of the density. Because we know both Q and n_e for a range of n_e, we can see whether $Q \propto n_e \exp(-E/kT)$ as in the high $A/n_e\gamma$ case, or $Q \propto \exp(-E/kT)$ as in the low $A/n_e\gamma$ case.

Table 4 shows $Q/\exp(-E/kT)$ and $Q/n_e(\exp(-E/kT))$, where E corresponds to 5000 Å. The temperature is chosen to be the photospheric temperature at early times, and 5000°K at late times. It is clear that the evidence favors the low

$A/\gamma n_e$ case, as the variation with density is ten times smaller. The increased flux at early times in the strong emissions is due mostly to the higher temperature rather than the increased density. The exponential decrease in the photon flux is then attributed to a linear decrease in temperature.

The de-excitation rates for forbidden lines are about $\gamma = 1 \times 10^{-7}$, so for $n_e > 10^7$, $A/\gamma n_e$ is small for $A < 1$. Thus, the circumstantial evidence points to forbidden lines.

It seems reasonable to search among the more abundant elements for forbidden lines which might contribute to the strong emission blend without producing other lines which are not observed. A list of possible ions which would be abundant under the conditions of low density and weak photoionization encountered in the expanding supernova envelope might be: He I, C I, N I, O I, Ne I, Mg I, Si I, S I, Ar I, Fe II. Of these, the only lines arising from the ground state that could contribute to the broad emission blend are N I (5200.4, 5197.9), Mg I (4571), S I (4589, 7726, 10820), and numerous Fe II forbidden lines. Chief among the iron lines are the multiplets 4287, 4359 (7F), 4416 (16F), 5159 (19F), 4815 (20F), and 4244, 4277 (21F).

The nitrogen lines have very small Einstein A's: about 1.6×10^{-5} for λ5198 and 7×10^{-6} for λ5200 (Garstang 1956). Thus these lines will be thoroughly thermalized for n_e of 10^7, and the emission rate, Q is independent of n_e. At

TABLE 4

JD-2440000	$\frac{Q}{n_e \exp(-2.88/T)}$	$\frac{Q}{\exp(-2.88/T)}$
1453	<8+43	<2+54
1469	3+44	3+54
1529	2+45	1+54
1653	9+45	4+54
1684	1+47	3+54
1796	6+46	5+53

5000°K, the expected emission in the λ5200 line of the emission blend is 2.3×10^{-7} N(N I) photon s^{-1}. With a typical line flux of 2.5×10^{51} photons s^{-1}, 1.1×10^{58} N I atoms would be required. Since this would have a mass of about 125 $M_\odot$ of N I alone, we may safely disregard N I as the source for this emission.

Similarly, the λ4571 line of Mg I has a very low A of about 2×10^{-4} , and will be completely thermalized. Then the maximum emission rate is about 3×10^{-6} photon s^{-1} per Mg I atom. The observed photon flux of about 5×10^{51} photons s^{-1} in the 4600 feature would require about 2×10^{57} Mg I atoms, whose mass would be about 30 $M_\odot$.

The S I line is an unlikely identification, because the 4589 Å line and the 7726 Å line share the same upper state, and have Einstein A's in the ratio 1:5. Thus if S I were an important contributor to the 4600 feature, we would expect a feature at 7726 which would have five times as many photons. Although there is some emission at 7700 Å, it comes nowhere near the required strength.

An examination of the multiplet table (Moore 1945) for [Fe II] reveals no less than 216 forbidden lines arising either from the ^6D ground state or the ^4F state 0.3 ev above it. Fortunately, the Einstein A for every one of these lines has been calculated by Garstang (1962). None of the A's is bigger than about 1 s^{-1} and many are smaller, so that for densities of 10^7 or greater, even the most rapidly depopulated line will have its upper state populated to

nearly the Boltzmann level. In that case, the photon flux contributed by each line is proportional to $(2J_{upper}+ 1)\ A\ e^{-E/kT}$, and the total from many lines is just a sum over such terms. The quantity (2J+1) A was calculated for each of the 105 lines with A > 0.01 and the sum for every 100 Å interval from 3000 to 10 000 Å was computed and weighted by exp(-E/k 5000°K). Figure 9 shows the log of the sum, which should be proportional to the log of the photon flux in each 100 Å band. The only region which has any significant flux over the entire observed wavelength range is the interval from λ4200-5500. Furthermore, we see a very good agreement between the relative strengths of the three lines of [Fe II] predicted by this calculation and the observed features at 5200, 4800 and 4300 Å. Even the small bump on the long wavelength side of the λ5200 peak, near λ5500 is reproduced. Only the feature at λ4600 is not predicted.

Figure 9 includes all the strong lines that would be produced by [Fe II] at low temperatures and a density of 10^7 or more. The next strongest feature, a blend at 3300 Å, would be an order of magnitude weaker than the lines shown in the figure.

Of course, more than a demonstration of possible wavelength coincidences is needed before we can be confident that the lines of [Fe II] account for three of the four strong features that dominate the late spectra of supernovae.

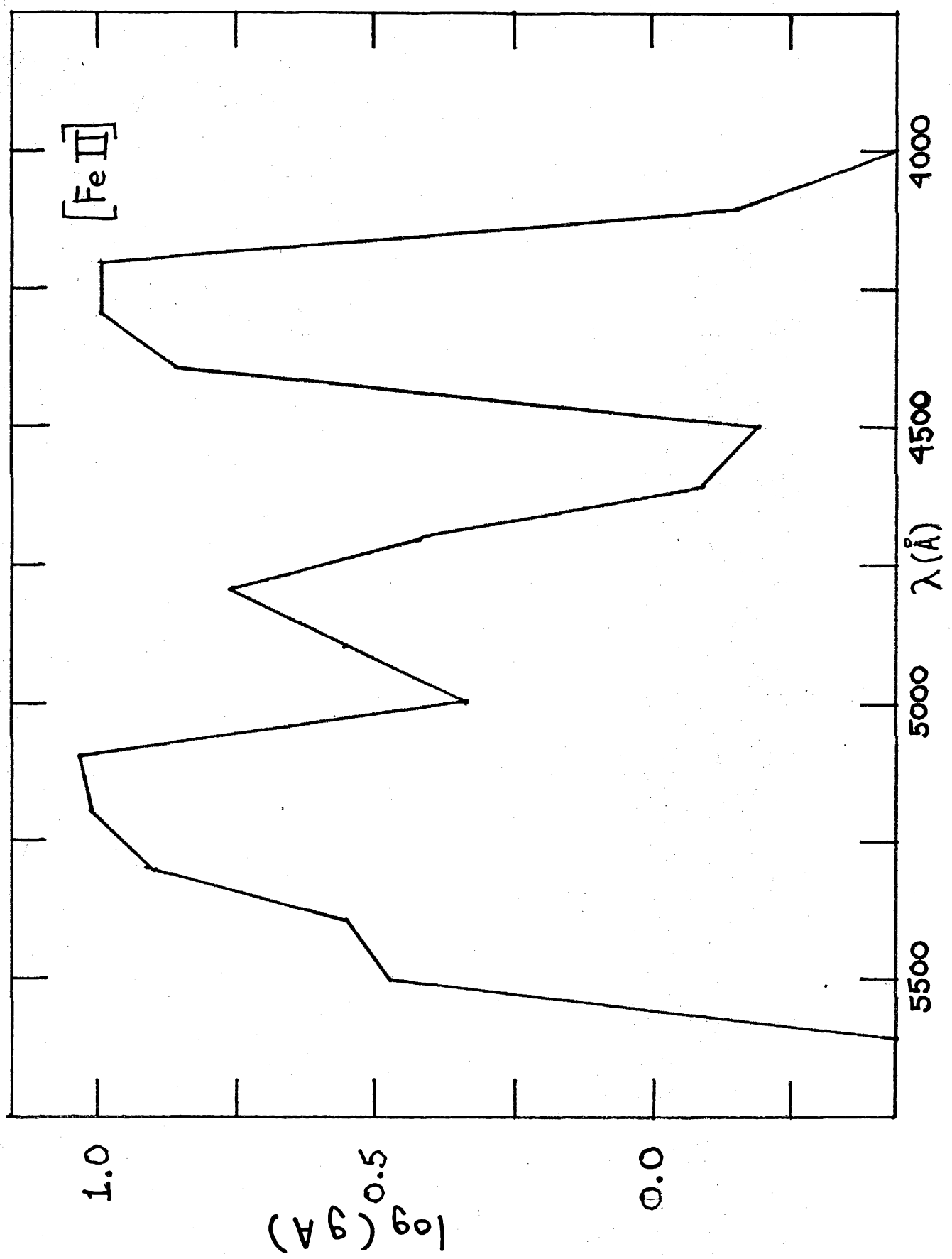

Fig. 9 -- Log $(gA)e^{-E/kT}$ for [Fe II]. The curve is normalized to $e^{-E/kT} = 1$ for $\lambda = 5000$ Å and $T = 5000°K$.

We also require that the photon flux be produced under the observed conditions. Since for Boltzmann conditions we have:

$$\frac{n_u}{n_\ell} = \frac{g_u}{g_\ell} e^{-E/kT}$$

Then the photon flux summed over all the [Fe II] lines is given by:

$$Q([\text{Fe II}]) = \int(\Sigma n_u A)\,dV = (\Sigma g_u A)\,\frac{e^{-E/kT}}{g_\ell}\int n_\ell\,dV$$

Putting in the appropriate values, we can write the total number of iron ions required to produce the observed photons.

$$N(\text{Fe II}) = \int n_\ell\,dV = \frac{Q(\text{Fe II})\; g_\ell e^{E/kT}}{\Sigma g_u A} = Q(\text{Fe II})\; 0.27\; e^{\frac{2.88\times10^4}{T}}$$

Using the photospheric temperatures through the early times when it is fairly well known, and T = 5000°K for the late times when it is not well known, N(Fe II) has been tabulated for each time in table 5. From it we see that the required amounts of iron are modest in terms of the total mass, but that the required abundance relative to hydrogen is rather high: about 20 times higher than usually regarded as the cosmic abundance (Cameron 1973).

We see that one possibility is that three of the four strong features that dominate the late phases of Type I spectra are due to collisional excitation of [Fe II], but that this requires an unusually large amount of iron relative to hydrogen.

TABLE 5

JD-2440000	Q([Fe II])	N(Fe II)	$M_{\odot}$(Fe II)
1453	<1+53	<5+53	2-2
1469	6+52	6+53	3-2
1529	1+52	2+53	8-3
1653	6+51	5+53	2-2
1684	4+51	3+53	1-2
1796	8+50	6+52	3-3

In the context of Type I supernovae, such a suggestion is made plausible by the possibility that the exploding star is a highly evolved object, and that explosive nucleosynthesis may take place during the supernova event.

The production of about $10^{-2} M_\odot$ of Fe in a supernova does not lead to an excessive mass of iron in the galaxy. If, in 10^{10} years, there are 10^8 SN I's, about 10^6 $M_\odot$ of Fe will be ejected. If the mass of our galaxy is 10^{11} $M_\odot$, the observed iron abundance of 10^{-3} exceeds the 10^6 $M_\odot$ produced by SN I's.

What are the other observable consequences of such a high iron abundance? We saw in SN II's that λ4600 and λ5000 had strong P Cygni features which we ascribed to resonant scattering from the very same metastable levels that form the upper states of the forbidden lines. For SN II's we showed that the optical depths of these lines were quite large with normal iron abundance, for SN I's, they should be several hundred times larger. It is possible that at early times, when the continuum is strong, these lines are the features at λ4600 and λ5000, and that the forbidden lines are not important contributors.

In that case, the first two or three entries in tables 3 and 4 may be irrelevant: the lines are formed by scattering and not by collisions. If that is so, then the late evolution of Q(Fe II) in table 6 is just as reasonably described by the high $A/\gamma n_e$ model as by the low $A/\gamma n_e$ model. Is it

possible that collisions produce the λ4600 feature at late times? The λ4600 feature would be due to the strong lines of multiplets 37 and 38. We can estimate whether this could possibly produce the observed emission. From Allen (1963), we find that, at 5000°K, multiplet 38 has a collisional excitation rate of about $2 \times 10^{-8} s^{-1}$. If we look at JD 1653, when $n_e = 4.4 \times 10^7$, $\gamma(up) n_e \simeq 1 s^{-1}$. The Boltzmann population in the lower state of multiplet 38 is about 2×10^{-3} of the ground state, so if the total iron number is 5×10^{53}, as inferred from the forbidden lines we expect about 1×10^{51} ions in that state. Thus we expect about 1×10^{51} photons s^{-1} to be produced in this way. A similar contribution from multiplet 37 raises the expected photon flux to 2×10^{51} s^{-1}. The observed amount is about 9×10^{51}. Since the electron density, temperature, and total iron number are not well known, it may well be that the λ4600 feature in emission at late times is also due to collisional excitation of Fe II.

The lines of multiplet 42 may contribute at 5000 Å. Other possible features are multiplets 27(4233, 4351) and 28(4179, 4297).

Overall, the case for Fe II lines as the main source of the strong emission features seen at late stages of SN I's seems plausible. More detailed investigation may be able to confirm or deny this interpretation.

The most difficult problem in understanding this emission is the source of energy. This is a problem whatever the details of the emission mechanism; for collisional excitation it takes the form of keeping the electrons hot. Photospheric heating is inadequate, and the thermal energy of the gas itself would only last for about 10^4 s. Only a small fraction (10^{-3}) of the mechanical energy in the expansion of the gas is needed to heat the electrons, but it is not clear how this might come about. When the energy source is understood, some real understanding of supernova emission will have been attained.

REFERENCES

Allen, C.W. 1963, Astrophysical Quantities (London: The Athlone Press).

Cameron, A.G.W. 1973, in Explosive Nucleosynthesis, eds. D.N. Schramm and W.D. Arnett (Austin: University of Texas Press), p.3.

Garstang, R.H. 1956, in The Airglow and the Aurora, eds. E.B. Armstrong and A. Dalgarno (New York: Pergamon Press), p. 324.

Garstang, R.H. 1962, M.N.R.A.S. 124, 321.

Kirshner, R.P., Oke, J.B., Penston, M. and Searle, L. 1973a, Ap. J., 185, 303.

Kirshner, R.P., Willner, S.P., Becklin, E.E., Neugebauer, G., and Oke, J.B. 1973b, Ap. J. (Letters), 180, L97.

Kowal, C.T. 1972, I.A.U. Circ. No. 2405.

Lee, T.A., Wamsteker, W., Wishniewski, W.Z., and Wdowiak, T.J. 1972, Ap.J. (Letters), 177, L59.

Minkowski, R. 1939, Ap. J., 89, 143.

Moore, C. 1945, A Multiplet Table of Astrophysical Interest (revised edition), Princeton University Observatory Contributions, No. 20.

Morrison, P. and Sartori,L. 1969, Ap.J., 158,541.

Oke, J.B. and Schild, R.E. 1970, Ap. J., 161, 1015.

Sérsic, J.L., Carranza, G. and Pastoriza, M. 1972, Astrophys. Sp. Sci., 19, 469.